https://doi.org/10.61092/iaea.9rjy-vj8w

INDC(NDS)- 0799
Distr.G+NM+PH

IAEA
International Atomic Energy Agency

INDC International Nuclear Data Committee

Photon Strength Functions in Thermal Neutron Capture

Jiri Kopecky

JUKO Research
Alkmaar, The Netherlands

January 2020

IAEA Nuclear Data Section
Vienna International Centre, P.O. Box 100, 1400 Vienna, Austria

Selected INDC documents may be downloaded in electronic form
from *http://nds.iaea.org/publications*
or sent as an e-mail attachment.
Requests for hardcopy or e-mail transmittal should be directed to
NDS.Contact-Point@iaea.org
or to:
Nuclear Data Section
International Atomic Energy Agency
Vienna International Centre
PO Box 100
1400 Vienna
Austria

Printed by the IAEA in Austria

January 2020

INDC(NDS)- 0799
Distr.G+NM+PH

Photon Strength Functions in Thermal Neutron Capture

Jiri Kopecky

JUKO Research
Alkmaar, The Netherlands

January 2020

Contents

1. Introduction

The photon strength function (PSF) is an important quantity which describes the distribution of the gamma decay strength for excitations below the E1 Giant Resonance. This information is needed for theoretical modelling of nuclear reactions but is also relevant for many applications. It was therefore not surprising that the PSF became the subject of many investigations both theoretical as well as experimental. The neutron capture reaction was one of the first experimental tools used for such studies in the early 1970's at three laboratories, one in Canada (Chalk River) [1] and two in the USA (ANL and BNL) [2,3].

The study of properties of isolated resonances was one of the major activities in low-energy neutron physics for several decades and resulted in a huge amount of resonance parameter data being collected and stored in traditional BNL cross section books. Neutron capture on discrete resonances was an important part of this effort and was used for deriving the first PSF database from *discrete resonance capture* (DRC) [4]. The interest in PSF studies led to a new experimental activity, measurements of *the average resonance capture* (ARC), which were carried out mainly at three laboratories, ANL, BNL and IDAHO with the latter two groups being replaced eventually by the BNL/ECN collaboration. The ANL group has carried out filtered-beam average neutron capture measurements using a boron filter [2] while the BNL group carried out experiments with Sc and Fe filters [5]. This era of experimental activities ended in 1994 [6] but the interest in DRC and ARC data was recently revived by the IAEA CRP on Generating a Reference Database for Photon Strength Functions [7]. Many other experimental techniques have been developed to study the behaviour of PSFs, however neutron capture remains historically the major tool, as it is a based on a model-independent and relatively simple method of deriving the PSF.

Surprisingly, a large wealth of thermal capture data remained almost unused in PSF applications. The aim of this pilot study is to investigate the thermal capture data THC which till now have been primarily used for spectroscopic purposes, and to test the procedures for deriving PSF data. The selection of nuclides in the low and medium mass ($A < 160$) region was deliberate for two reasons. Firstly, we have a good knowledge of the PSF behaviour of medium and heavy mass targets from the ARC and DRC experiments, which are of very good quality as they benefit primarily from often an excellent averaging (especially for ARC data). Well-established systematics as well as partial data are, therefore, available for gamma ray energies 4 – 5 MeV below the neutron separation energy S_n for this mass region. For targets below $A \sim 100$, the feature of medium or low-level density makes it increasingly possible to have well-defined assignments of final states in a broad energy range using primary transitions down to low E_γ energies. In such a case, we may additionally obtain information on the E1 and M1 trends in the 0 – 5 MeV energy range, which is especially relevant for determining the M1 strength behaviour bellow the spin-flip resonance. Furthermore, the competition of non-statistical effects with the statistical models may be observed in low mass targets. All the nuclides studied in the 1st Phase of this project are given in Table 1 and the derived PSF results are discussed in the Appendix. The criteria for the data selection were based on the presence of advanced spectral procedures which enhanced the completeness of decay schemes with a solid identification of primary transitions in a broad energy range.

2. General remarks

2.1 Photon Strength Function

The photon strength function of a gamma-ray transition was introduced in the early nineteen sixties [1] to describe the gamma decay strength from highly excited states and was defined by the relation

$$<f_{XL}(E_{\gamma i})> = \Gamma_{\gamma i} / (E^{(2L+1)}{}_{\gamma i}\, D_J), \qquad (1)$$

where X defines the transition type (E or M radiation) with multipolarity L , $\Gamma_{\gamma i}$ is the partial radiative width and D_J is the spacing of the initial state (resonance) with spin J. The partial radiation width $\Gamma_{\gamma i}$ strongly fluctuates obeying the Porter-Thomas distribution [8].

In the average neutron capture measurements (DRC and ARC), the dipole radiation is dominant and the capture states are ususally s-wave resonances so Eq. (1) can be simplified as

$$<f_X(E_{\gamma i})> = <\Gamma_{\gamma i}> / (E^3{}_{\gamma i}\, D_0), \qquad (2)$$

where X = E1 or M1 and $<\Gamma_{\gamma i}>$ is the average partial radiative width and D_0 is the s-wave resonance spacing.

Note that for the DRC measurements, the initial state is a well-defined single resonance (with known orbital momentum l_n and J^π) and averaging over resonances is numerically carried out in the data processing procedure.The width $\Gamma_{\gamma i}$ is related to the relative intensity per neutron capture I_γ and the total radiation width Γ_γ of the initial state (resonance)

$$\Gamma_{\gamma I} = I_\gamma \cdot \Gamma_\gamma . \qquad (3)$$

In the ARC experiments, the averaging over a number of resonances takes place inherently in the experiment, in the filtered neutron beam window. The averaging in the ARC experiments is usually quite strong, due to the broadness of the 2 keV window with FWHM of about 900 keV and hence the Porter Thomas fluctuations are substantially supressed. However, $<\Gamma_{\gamma i}>$ is determined on a relative scale and an absolute normalization to a standard obtained from DRC data is needed. In order to increase the averaging power, a binning of PSF values is introduced, in which an unweighted mean of a number of $<f_X(E_{\gamma i})>$ values is assigned to the mean energy $<E_\gamma>$. The energy window is usually only ±1 MeV broad, in order to minimize the additional energy dependence.

2.2 Distribution of primary intensities I_γ

DRC and ARC data

It has been shown that Porter-Thomas fluctuations result in a χ^2 - distribution with one degree of freedom of primary intensities I_γ. This is true for both ARC and DRC (differential and binned) data and the observed dispersion in many average experimental data [9-11] are in a good agreement with this assumption. However, it is inherent to Porter-Thomas fluctuations that some weak transitions are not detected (detection sensitivity threshold) and in some earlier papers a correction for missing intensity has been applied. Our experience from the recent DRC and ARC data evaluations, however, indicates that the influence of missed intensities on the mean of PSF fluctuations is negligible due to the high averaging power applied. The high statistical precision together with the complete spectral response results in a very low detection threshold and the chance of missing transitions due to fluctuation bias is significantly reduced. This observation is supported by a good agreement of the PSF systematics with the D1M+QRPA calculations [7,11].

Thermal THC data

For thermal capture the situation is different and is discussed in detail in the next section.

3. Thermal capture data (THC)

3.1 Properties of the thermal capture state

The properties of the capture state can be estimated from positive (negative) resonance contributions. In the s-wave capture (dominant at thermal energies) the overlap of resonance tails generally results in an admixture α of two resonance spin states resulting from the equation

$$J_i = J_t \pm 1/2. \quad (4)$$

J_t is the target spin and J_i the spin of the thermal capture state with the energy of S_n.

The spin admixture can be estimated from resonance parameters and measured thermal cross sections (see Mughabghab's compilations [12-14]). The value of the admixture α is determined using the following equations:

$$\sigma(th) = \text{measured value} \quad (5)$$

$$\sigma(th) = \sigma(B) + \sigma(-) + \sigma(+) \text{ (from resonance parameters)}, \quad (6)$$

where $\sigma(B)$ stands for cross-section contributions from negative resonances with $J_t \pm 1/2$ spins and $\sigma(-)$ or $\sigma(+)$ from positive s-wave resonances with $J_t - 1/2$ or $J_t + 1/2$ spins, respectively. Contributions from positive resonances are calculated from experimentally determined resonance parameters found in Ref. [14]. The admixture α is defined as the ratio of $(J_t + 1/2)$ contribution to the total cross by the equation

$$\alpha = \sigma(+)/(\sigma(B) + \sigma(-) + \sigma(+)) \quad (7)$$

with values in the range $0 \leq \alpha \leq 1$. The extreme values 0 and 1 correspond to single spin values with $J_t - 1/2$ or $J_t + 1/2$, respectively. For the target nuclides with $J_t = 0$, the spin of the capture state has a unique value $J_i = 1/2$.

3.2 Experimental thermal spin admixture

The accuracy of $<\alpha>$ estimates obtained from cross sections should, however, be treated with caution, especially for nuclei with the bound region dominating the thermal cross section. The multi-parameter fit to the measured cross sections, discussed in detail in Refs. [12-14], is based on several simplifying assumptions, such as the spin-independent fitting constant Γ_γ for all negative-energy resonances. The more spin-dependent fitting constants (e.g. scattering length) are included in the multi-parameter fit, the more accurate the estimate will be. This was demonstrated for ^{45}Sc in Ref. [15].

The most accurate approach to determining $<\alpha>$ is to measure directly the partial spin admixtures α_i. This can be done by the capture or transmission of polarized/unpolarized neutrons with polarized/unpolarized targets [16] and in combination with the capture of polarized neutrons in unpolarized targets by measuring the degree of circular polarization [17,18].The anisotropic directional distribution $I(\theta)$ of emitted gamma rays is generally given by the expression [19]

$$I(\theta) \cong f(A_k^{k1k2} f(n) f_k(I) P(\cos \theta), \quad (8)$$

in which the coefficients A_k^{k1k2} (which may interfere due to overlapping resonances) depend on the capture spins and/or their admixture α_i, transition multipolarities L and final spin J_f. The neutron polarization and orientation parameters are denoted as f(n) and $f_k(I)$, respectively.

Two different experimental approaches are now further discussed:

The circular polarization experiment – In the polarized neutrons and non-oriented targets, the circular polarization is given by the nuclear coefficient A_1^{10} which depends for a given primary transition on the spins of the target and final states and the two coherently interfering entrance channel spins $J_i = J_t \pm 1/2$. The gamma-ray quadrupole admixture is assumed to be negligible. An example of the circular polarization sensitivity to the admixture α is shown in Fig. 1 taken from Ref. [18] for ^{66}Cu nuclide. Due to the interference effects, for the inner spin values $J_f = 1$ and 2 there are always two solutions for α_I, and only the outer spins $J_f = 0$ and 3 have a unique solution. As for the final spin determination, for unique spin assignments the information on the spin admixtures α_i needs to be included.

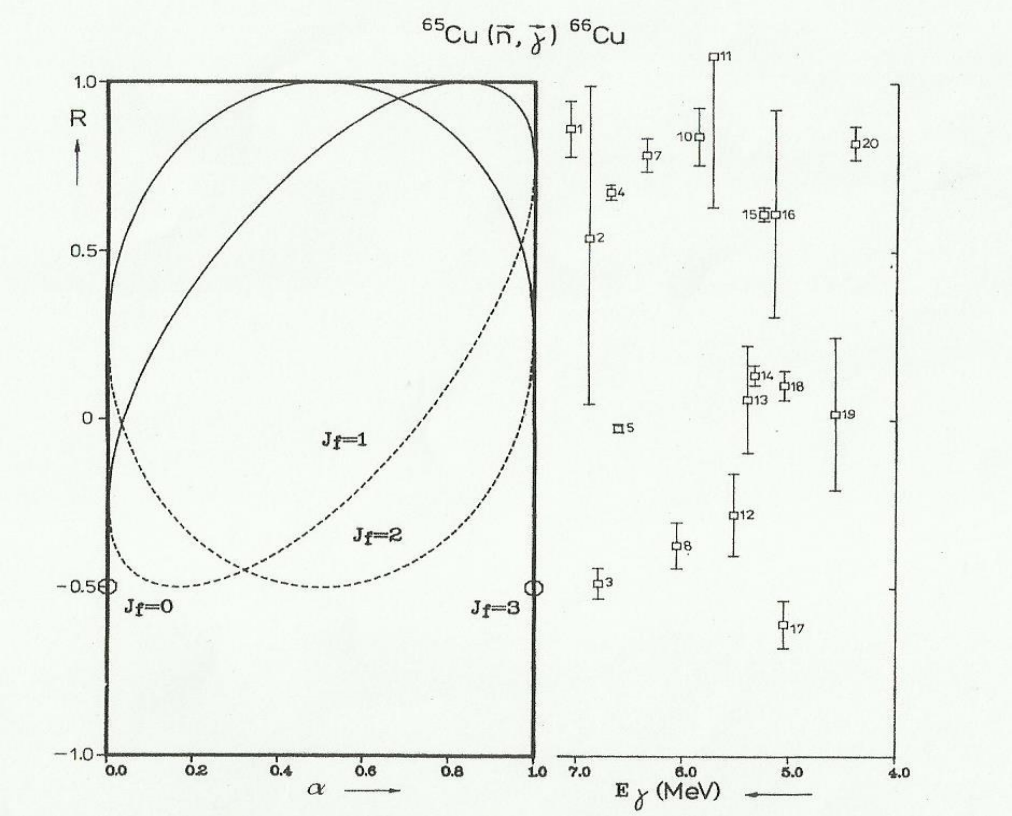

FIG. 1 *Plot of experimental A_1^{10} (called R) on the left-hand side on the spin admixture parameter α_I for final spins J_f = 0, 1, 2 and 3; on the right-hand side the measured values for analysed primaries are shown. Numbering refers to table 6 in Ref. [18]. Figure taken from Ref. [18].*

The extension of circular polarization results can be done if one includes partial admixtures α_i in the analysis coming from two separate experiments. This is shown in the next example for the ^{60}Co nucleus [17]. In this case, the A_1^{10} coefficients were determined from the circular polarization experiment (as in the previous example) while the A_0^{11} coefficients from the capture of polarized neutrons in oriented ^{59}Co nuclei measuring the anisotropy of the emitted gamma rays. The results are shown in Fig. 2 taken from Ref. [16].

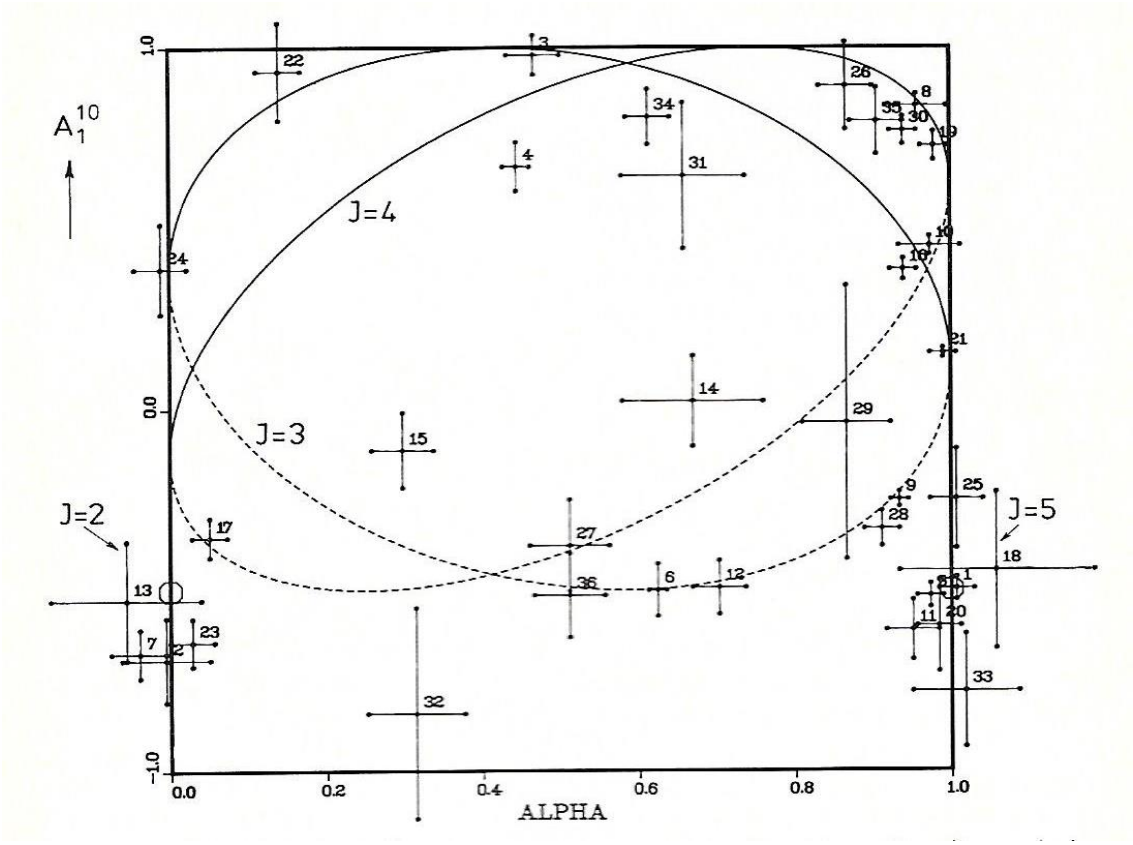

FIG. 2 *Plot of experimental A_1^{10} versus most of the observed transitions from the $^{59}Co(n_{pol},\gamma_{pol})\ ^{60}Co$ reaction. The corresponding α values have been derived from A_0^{11} values from Ref. [16]. Theoretical curves for $J_f = 3$ and 4 are shown, the dashed part is related to destructive interference. The theoretical points for $J_t = 2$ and 5 are at $A_1^{10} = -0.5$. Figure taken from Ref. [16].*

When the partial admixtures α_i are combined with the degree of circular polarization from A_1^{10} coefficients, the results (see Fig. 3) can give information on the spin assignment and the type of the interference (constructive or destructive).

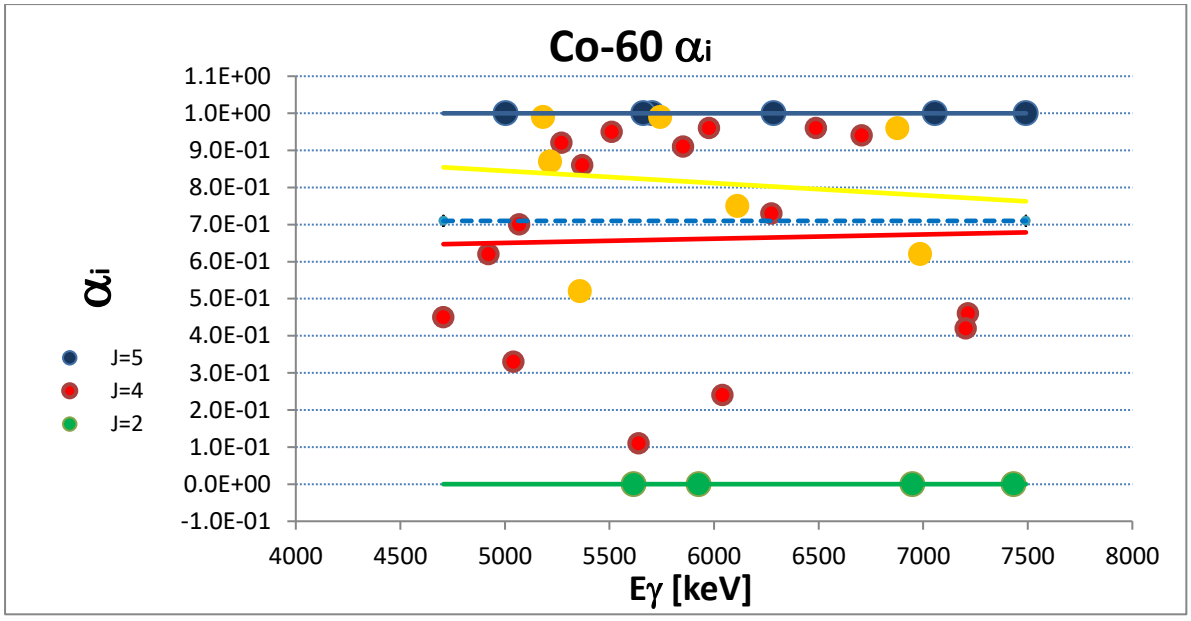

FIG. 3 *Partial α_i admixtures of capture state spins $J_i = 3^+$ and 4^+ for primary transitions from $^{59}Co(n,\gamma)^{60}Co$ reaction. Two outer final spins $J_f = 2$ and 5 have pure $\alpha_i = 0$ or 1 values, while the medium spins $J_f = 3$ and 4 follow a broad admixture distribution between 0 and 1. The plotted curves are linear trend lines, the dotted blue line is the value derived from thermal cross section components.*

Both types of experiment applied simultaneously – this is the best combination: (i) the measurement of circular polarization of primary γ-rays after the capture of polarized neutrons in non-oriented target nuclei and (ii) the angular distribution of primaries emitted by the capture on oriented nuclei. The best example of such a combined analysis yielding both final spin assignments and partial admixture parameters α_i is given in Ref. [20] for ^{46}Sc. The power of this method was enhanced by the DRC experiment to yield probably the maximum that can be achieved in this field.

The list of experiments measuring partial spin admixtures is given in Table 1. The main aim of the work performed with polarized neutrons and oriented targets in Petten, however, was to study the spectroscopy of the product nuclides; the determination of the spin admixture α was only a by-product needed for unambiguous spin assignments. The experiments at the polarized neutron facility at ECN Petten ended in 1985, during the shutdown of the HFR, and were never restarted. The range of studied nuclei in the low mass region was part of the light-nuclide spectroscopy program of the University of Utrecht.

Table 1. The list of targets with measured partial spin admixtures α_i and their mean values $<\alpha_i>$ compared with the estimate based on thermal cross sections from Ref. [14]. The value of $<\alpha_i>$ is an unweighted mean of partial values with an average uncertainty systematic limit of about 10%.

#	- number of transitions with measured α_i
ΣI_γ	- the sum of I_γ over measured transitions
α	- mean branching ratio calculated with Eq. (7)

Target	**Ref.**	**#**	**ΣI_γ**	**$<\alpha i>$**	**α**	**α(adopted)**
			%			
Na-23	[21]	9	82	0.04	0.0	
P-31	[22]	10	88	0.81	0.98	
Sc-45	[20]	28	54	0.05	(0.5)	0.1
V-51	[23]	20	82	0.23	0.28	
Mn-55	[24]	16	na	0.26	0.26	
Fe-57	[25]	11	88	0.59	0.88	
Co-59	[17]	37	67	0.65	0.71	
Cu-63	[26]	9	62	0.18	(0.5)	0.2
Cu-65	[18]	20	53	0.83	(0.51)	0.8

Results in Table 1 show, that if a reasonably large fraction of the primary strength is measured in the polarization experiment, the estimated values of $<\alpha_i>$ and α are reasonably consistent. This is a very important observation for the PSF analysis, namely that the spin admixture derived from the cross-section analysis gives a reasonably accurate average estimate of α partial interfering spin admixtures α_i. The disagreeing values, given in brackets, are cases where a strong contribution from negative resonances is present with no spin J_i assignment and the assumption of $\alpha = 0.5$ has been applied. However, the $<\alpha_i>$ values indicate which of two spins is preferable and may be used for a new adopted value in the last column. It may thus be concluded that these results indicate a possible choice for the spin admixture for such cases.

The limited number of partial α_i experiments is of no practical value for PSF/THC evaluations, however, they do help us understand the role of partial spin admixtures α_i in the total admixture α and its role in thermal capture. The results of the ^{60}Co experiment will be used to choose and validate how the thermal capture intensities are practically processed into deriving the PSF formalism.

3.3 Distribution of primary intensities I_γ in PSF experiments

The fundamental difference between initial states of isolated resonances (DRC or ARC measurements) and thermal capture has been pointed out by Bollinger in Ref. [27]. The initial state of resonance capture is an "eigenvalue" resonance state with unique spin and parity J^π parameters. The intensity of transitions (average width) is proportional to the sum of widths of resonances while in thermal neutron capture the transition intensity is determined by the sum of amplitudes of resonances involved. This implies that the distribution of primary gamma-ray

intensities in thermal capture follows only approximately the Porter-Thomas distribution with a χ^2 - distribution between one or two degrees of freedom, depending on how both spins contribute. The amplitudes interfere coherently with both signs and this results in a positive or negative interference (see the circular gamma-ray polarization results Sect. 2.2). The intensity distribution and consequently the dispersion of PSF data is therefore dependent on the size of the two spin contributions to the thermal cross section.

Four major contributions to the dispersion of primary intensities I_γ are now described with their typical uncertainties:

Statistical uncertainty of the gamma ray spectrum: primarily from the accuracy of the spectral analysis influenced also by the quality of the experimental set up. For the majority of transitions the accuracy ranges from 5% to 15%, except for the very weak transitions. This uncertainty is approximately the same for all three different ARC, DRC and THC experiments.

Uncertainty of the spacing Do and radiation width $\Gamma_{\gamma 0}$: these two experimental parameters influence significantly the absolute PSF value. These uncertainties are in general in the range 10 – 50 % and are very different for each nuclide and for the nuclides studied in this work are discussed in detail in Section 4.

The Porter-Thomas fluctuation: very much dependent on the quality of the averaging, the best being found for the ARC data due to the very high number of resonances used for the experimental averaging. Based on a crude approximation $1+ dPT = \sqrt{2}/\upsilon$, the dispersion is roughly estimated to range is from about few up to several tens %. For the DRC data, which usually have a limited number of resonances, the dispersion is larger. The THC data have no averaging and are fully PT fluctuated with uncertainties in the range 100 – 200%.

Multiple population of the inner final spins, as illustrated in Fig. 4. This affects primarily the ARC data, where the limited PT fluctuations allow the difference between single and double population to be detected. If the initial state is formed by contributions with two different spins, the population pattern is as shown in Fig. 2, with a neglect of the quadrupole radiation. This is certainly valid for primary E1 transitions and for M1 transitions because the E2 mode is very weak.

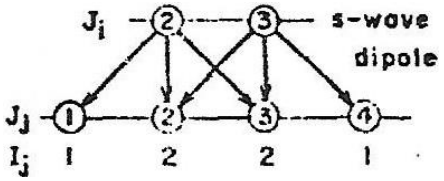

FIG. 4 *Schematic picture of double population of $J_i \pm 1/2$ final spin.*

In this case, the inner spin states are populated from two initial state spin values and the simplified correction Q may compensate for the single population of outer spins. This effect was shown by the theoretical modelling of Ref. [28] and was implemented in the processing of the ARC data and in some special cases of the DRC averaging. In a simplified approach the correction Q = 2 is a good approximation. In thermal capture, however, the factor Q is a function of the spin admixture $<\alpha>$ and in a simplified approach is given by $Q = 1/<\alpha>$ while the corrected transition intensity is $I_\gamma(cor) = I_\gamma(exp)\cdot Q$. In the absence of this correction (due to missing spin assignments) one obtains a broader data dispersion but generally the mean trend value of PSF is not affected.

3.4 Primary intensities I_γ in thermal capture PSF experiments

The relevant question is how the $I_{\gamma i}$, $\Gamma_{\gamma i}$ and $\Gamma_{\gamma 0}$ values are related. This relation can be categorized in two basic target groups, (i) those with $J_t = 0$ and/or J_i = single spin value from a dominant resonance or (ii) nuclides with two interfering spins in the capture state.

Targets with $J_t = 0$ or a single dominant resonance

The spin of the capture state has a unique value and the amplitude interference from the two spin channels is absent or negligible. The partial intensity $I_{\gamma i}$ is usually given as the intensity per neutron capture. In a pure resonance capture the relationship (8) is valid

$$\Gamma_{\gamma i} = I_{\gamma i}\, \Gamma_{\gamma 0}. \qquad (9)$$

In the thermal capture the proportionality between I_γ and Γ_γ is disturbed by the interference of transition amplitudes therefore one should instead always consider the total and partial thermal cross sections $\sigma_{\gamma 0}$ and $\sigma_{\gamma i}$

$$\sigma_{\gamma i} = I_{\gamma i}\, \sigma_{\gamma 0}. \qquad (10)$$

However, the absolute intensity I_γ is usually experimentally determined in terms of number of gamma-rays per neutron capture and then is related to the partial $\sigma_{\gamma i}$ with the help of Eq. (10).

If the interference is absent (one spin state for $I_f = 0$ targets) or a single (or dominant) resonance, then the conversion into the radiation widths $\Gamma_{\gamma i}$ is given by

$$\Gamma_{\gamma i} = (\sigma_{\gamma i}/\sigma_{\gamma 0})\, \Gamma_{\gamma 0} = I_{\gamma i}\, \Gamma_{\gamma 0}, \qquad (11)$$

which can be used in Eq. (2) to calculate the PSF. To conclude, for $J_t = 0$ targets and/or for a single resonance dominating the thermal capture, the situation is equivalent to DRC and one can use the corresponding. The case for one spin value dominance can be verified by the absence of transitions to the outer spin value from $(J_i \pm 1/2)$ when the quadrupole multipolarity is assumed to be negligible.

Targets with resonances of both spins

Spin admixtures in the capture state may result in an unequal contribution of the two spin components to the thermal cross section and to the value of the average radiative width $\langle\Gamma_\gamma\rangle_0$. The average contribution of the spin admixture $\langle\alpha\rangle$ can be estimated from partial cross sections, σ_0, $\sigma(-)$, $\sigma(+)$ and $\sigma(B)$ as shown in Section 2.1. However, because of positive or negative interferences contributing to the determination of the transition amplitude, the partial admixtures α_i per transition can have a broad distribution around the medium value of $\langle\alpha\rangle$ and Eq. (10) is not valid anymore.

The presence of these interferences, which are transition dependent, requires the use of another relationship with partial spin admixtures α_i in the admixture factor $F(\alpha_i)$

$$\Gamma_{\gamma i} = (\sigma_{\gamma i}/\sigma_{\gamma 0})\, \Gamma_{\gamma 0}\, F(\alpha_i) \;\; = I_{\gamma i}\, \Gamma_{\gamma 0}\, F(\alpha_i) \qquad (12)$$

with $F(\alpha_i) = 1 - \alpha_i$ for $J_i = J_t - 1/2$ and $F(\alpha_i) = \alpha_i$ for $J_i = J_t + 1/2$.

An example of such α_i admixtures is shown in Fig. 3 for the $^{59}Co(n_{pol},\gamma_{pol})^{60}Co$ reaction. Note the large spread of α_i admixtures for J = 3 and 4 dues to the constructive/and or destructive interference.

Using partial cross sections in Eq. (7) we get an estimate of $\langle\alpha\rangle = 0.71$, which is in reasonable agreement with the γ-ray circular polarization analysis mean value of $\langle\alpha_i\rangle = 0.80 \pm 0.10$ [17].

The limitation of this method is that only a small number of circular polarization measurements exists, namely for the targets ^{24}Na, ^{31}P, ^{45}Sc, ^{51}V, ^{55}Mn, ^{56}Fe, ^{59}Co and ^{63,65}Cu studied at the polarized neutron facility at RCN Petten. For the rest of the mass region, an approximate method is needed to simulate the partial α_i approach.

The following processing steps are discussed:

1. **Multiple population correction Q** – The use of this correction for THC data is not recommended (contrary to the ARC data), because the PT fluctuation in THC is enormous and will therefore influence the use of transitions for the absolute normalization. This also means that one should select primarily transitions to the inner spins for the absolute normalization.

2. **Absolute normalization of PSF data** – Different methods for the absolute normalization of the PSF values will be described in detail:

   2.1 *$J_t = 0$ targets* – A unique spin $J_i = 1/2$ value eliminates any interference and Eqs. (2) and (9 –11) are used with D_0 spacing for $J_t = 0$ targets.

   2.2 *Single or a dominant resonance* results in a unique or quasi-unique spin value – The simplified assumption of the absence (weakness) of the other spin and their interference is implemented. In such a case the standard Eq. (2) can be applied and the PSF values is calculated using $\Gamma_{\gamma 0}$ and D_0 parameters. This simplification, using Eqs. (9-11), gives values which slightly overestimate the mean trend but the E_γ dependence remains unchanged.

   2.3 *Non-negligible spin admixture $<\alpha>$*

   2.3.1 This approach takes in to account the spin interference which is given by the mean value of the spin admixture $<\alpha>$ obtained from the partial thermal cross section (see Eq. (7). The simplification of Eq. (12) is that the mean $<\alpha>$ value replaces partial admixtures α_i and results in the following equation

$$\Gamma_{\gamma i} = (\sigma_{\gamma i}/\sigma_{\gamma 0})\, \Gamma_{\gamma 0}\, \alpha_i = I_{\gamma i}\, \Gamma_{\gamma 0}\, F<\alpha>. \qquad (13)$$

   In Ref. [16] the fractional contribution F_J of spins $(J_t - 1/2)$ and $(J_i + 1/2)$ to the total thermal cross section has been introduced and related to the admixture α by $F_J = f(\alpha)$. The partial width $\Gamma_{\gamma i}$ then can be obtained from the measured intensity I_γ by the relation $\Gamma_{\gamma i} \cdot I_\gamma \cdot \Gamma_{\gamma 0} / F_J$, where $\Gamma_{\gamma 0}$ is the average s-wave radiative width. This procedure was applied to the ^{128}I nuclide [29] for all transitions. However, in this approach the difference between the initial state configuration for inner/outer final spins was neglected. A special situation is for $<\alpha> = 0.5$, where contributions to Γ_γ from both spin channels are equal and the interference effects are randomly distributed around the mean and their effect is averaged out.

   We tested a slightly different approach for the conversion of I_γ values into $\Gamma_{\gamma i}$, using only transitions to outer $(J_i \pm 1/2)$ spins coming from one initial spin channel. These transitions do not suffer from interference effects and therefore can be treated as single resonance cases with one initial spin and then use the spin-dependent spacing $D(J_i)$. The mean value $<I_\gamma\, \Gamma_{\gamma 0}>$ can later be used for the internal renormalization of the remaining intensities to inner $(J_i \pm 1/2)$ final states. The disadvantage of this method is the introduction of an additional uncertainty from not using the multiple population correction Q (discussed above) and from the derivation of D(J) values from D_0. A more straightforward

way is to use transitions to the inner ($J_i \pm 1/2$) spins and applying $\Gamma_{\gamma i} = I_\gamma \Gamma_{\gamma 0} <\alpha>$ and D_0 values to accounts for the interference effects. A choice of transitions, say in a 1 MeV broad energy window, can give a binned <f(E1)> value at the medium E_γ of the window which can then be used as a calibration factor for all remaining E1 and M1 transitions. However, both approaches from our point of view introduce too many additional uncertainties so we tested them only for the ^{60}Co nuclide (see further) and did not consider them in the creation of the final database.

2.3.2 A more accurate approach using partial α_i values – For nuclides with partial spin admixtures α_i, from polarization experiments, each transition with known α_i can be treated separately. In this method, Eqs. (12) and (2) can be combined in an exact formulation, namely

$$\Gamma_{\gamma i} = (\sigma_{\gamma i}/\sigma_{\gamma 0})\, \Gamma_{\gamma 0}\, \alpha_i = I_{\gamma i}\, \Gamma_{\gamma 0}\, \alpha_i \qquad <f(E_{\gamma i})> = <\Gamma_{\gamma i}>/E_{\gamma i}^3\, D \qquad (14)$$

For the spacing D either a single D(J) or mixed spins (D_0) of initial states needs to be applied. This treatment may serve as a test of the two previous approaches, because this method requires the most accurate model inputs for each transition. The robust ^{60}Co experiment will be used to test this method in Section 3. However, the availability of a limited number of such measurements with partial α_i results means this this approach cannot be used for mass THC PSF production required for the new database.

2.4 *Renormalization to f(E1) systematics* – A normalization procedure using the f_{E1}(<6.5 MeV)> E1 DRC systematics [11] can be applied to transitions to intermediate ($J_i \pm 1/2$) states. The resulting conversion factor is then extended to the remaining transitions for the complete absolute normalization. This procedure has been successfully applied to many of the ARC data. The $f_L(E_\gamma)$ dependence on the energy of initial states is in the vicinity of the neutron separation energy which is postulated to be negligible.

4. Thermal capture analysis

Three nuclides, ^{36}Cl (single resonance), ^{57}Fe (target spin $J_t = 0$) and ^{60}Co (two-spin admixture), have been selected to illustrate the processing procedures and the response of thermal data to the PSF evaluation, with a view to obtaining experience required for recommending a suitable method for further evaluations. The list of final states, accessible by dipole radiation, with and without spin and/or parity assignments, has been taken from the ENSDF compilation [www.-nds.iaea.org] and has been included as a part of the data file in EXCEL format. This file includes adopted E_γ, PSF values with statistical error and corresponding final states with J^π parameters. Excluded are states with spin values that do not comply with dipole transitions. These tables provide information on the completeness of the observed transitions and final states and also give an indication of possible missing transitions.

4.1 ^{36}Cl (single resonance)

The thermal cross section of the ^{35}Cl(n,γ) reaction is formed by a tail of a bound state at $E_n = -180$ eV with $\Gamma_\gamma = 0.542$ eV and $J_i = 2^+$ with thermal cross sections $\sigma(\text{exp}) = 43.6$ b, $\sigma(-) = 0.007$ b, $\sigma(+) = 0.06$ b and $\sigma(B) = 43.6$ b [14]. The capture process can be classified as the capture in a single negative resonance with negligible contributions from positive resonances.

For the conversion of gamma-ray intensities from Ref. [30] into partial $\Gamma_{\gamma I}$, the total s-wave radiative width $\Gamma_{\gamma 0}$ is used in $\Gamma_{\gamma i} = I_\gamma \Gamma_{\gamma 0}$. The pertinent spin values are, $J_t = 1/2^+$, $J_i = 2^+$ ($\alpha = 1$) and final states with $J_f = 1$, 2,and 3, which can be reached by the dipole radiation. The primary transitions adopted in the analysis represent $\Sigma I_\gamma = (0.94 \pm 0.05)$ of the gamma decay strength from the capture sate. A total of 64 states with $E_x \leq 7$ MeV and $J_f \leq 3$ have been extracted from the ENSDF complilation. For 13 of these the parity assignment was not available and so they have not been considered in the analysis. Only two transitions were found feeding these 13 states, for the remaining 11 states no transitions were identified and may be accounted for by weak PT fluctuations below the sensitivity threshold. However, the existence of these states may also be questioned as well.

The final list of transitions and the corresponding PSF values are given in Table 2. For the calculation of $f_L(E_\gamma)$ values, Eq. (2) has been used with partial radiative width $\Gamma_{\gamma i}$ and D(J=2) = 35.903 keV estimated from the (2J + 1) dependence of D_0 = 22.3 keV. Unused transitions or levels are printed in red and may indicate missed transitions due to the PT fluctuations.

Table 2. PSF processing for ^{36}Cl nuclide using $<\Gamma_\gamma>_0$ = 0.542 eV and D_0 (J=2) = 35.68 keV estimated from D_0 = 22.3 keV [14] using the (2J +1) spin dependence. The spin/parity unassigned states with missing transitions are printed in red in a shaded row.

Cl-36 TH ECN Petten

I_γ/100n extracted from A.M.J. Spits and J. Kopecky, Nucl.Phys. A264 (1976) 63

Sum prim. I_γ = 0.94 ± 0.05

$\Gamma_{\gamma 0}$ = 0.542 eV D_0 = 22300 eV D_0(J=2) = 35903 eV applied

Only transitions to states with assigned parity considered

E_γ	E1	M1		dE1	dM1		Ex	Jπ
8580		0.07			0.007		0	2+
7791		0.27			0.027		788	3+
7414		0.37			0.037		1165	1+
6978		0.1			0.0053		1601	1+
6628	0.24			0.0069			1951	2-
6620		0.42			0.0069		1959	2+
6111	1.3			0.0175			2468	3-
6087		0.08			0.0098		2492	2+
5903		0.08			0.0039		2676	1+
5716		0.41			0.0064		2864	3+
5586	0.04			0.0046			2994	1-2-3-
5248	0.06			0.0069			3332	2-
5110		0.02			0.003		3469	1+
5248	0.06			0.0069			3332	2-
5110		0.02			0.003		3469	1+

E_γ	E1	M1	dE1	dM1	Ex	Jπ
4980	0.43		0.0243		3559	3-
4856	0.01		0.0035		3724	4-
					3830	
4617	0.1		0.0102		3963	2-
					3997	
					4034	
4441	0.17		0.0114		4139	2-
4170		0.01		0.0055	4409	1+-3+
4083	0.15		0.0118		4496	
4054	0.12		0.015		4525	1-
4026		0.03		0.0153	4553	0+-3+
3981	0.22		0.019		4598	3-
3842					4734	
3822	0.27		0.0179		4758	3-
3750	0.09		0.0152		4829	2-3-
					4844	
3697		0.02		0.0079	4884	1+-3+
3623	0.05		0.0084		4596	π=-
3581	0.07		0.0305		4999	3- 3+
					5018	
3500	0.09		0.014		5079	1-2-3-
3429	0.3		0.0198		5151	1-2-
3375	0.19		0.0572		5205	2-
3333		0.3		0.0162	5246	1+-3+
3317	0.09		0.0164		5263	1-2-
3272	0.05		0.0228		5307	π=-
3250	0.13		0.0175		5329	2-3+
3116	0.47		0.0397		5463	2-
3062	1.84		0.1393		5518	3-
3016	0.54		0.0365		5563	2-3-
3002	0.41		0.0296		5578	1-2-
					5590	
2975		0.65		0.0456	5605	2+3+
					5627	
2877	0.36		0.0924		5703	1-2-3-
2846	0.76		0.0347		5734	2-

E_γ	E1	M1		dE1	dM1		Ex	Jπ
2802	0.4			0.0909			5777	2-3-
							5838	
2666	0.24			0.0317			5914	
2623		0.49			0.0776		5956	π=+
							5972	
2849		0.32			0.1124		6090	π=+
2311		1.34			0.081		6268	2-3+
2835	0.14			0.0351			6345	1-2-3-
2200		0.52			0.0376		6379	π=+
2092	0.58			0.1311			6487	1-2-3-
2034		1.07			0.0713		6545	1+-3+
1937	0.8			0.0826			6642	1-2+
							6951	

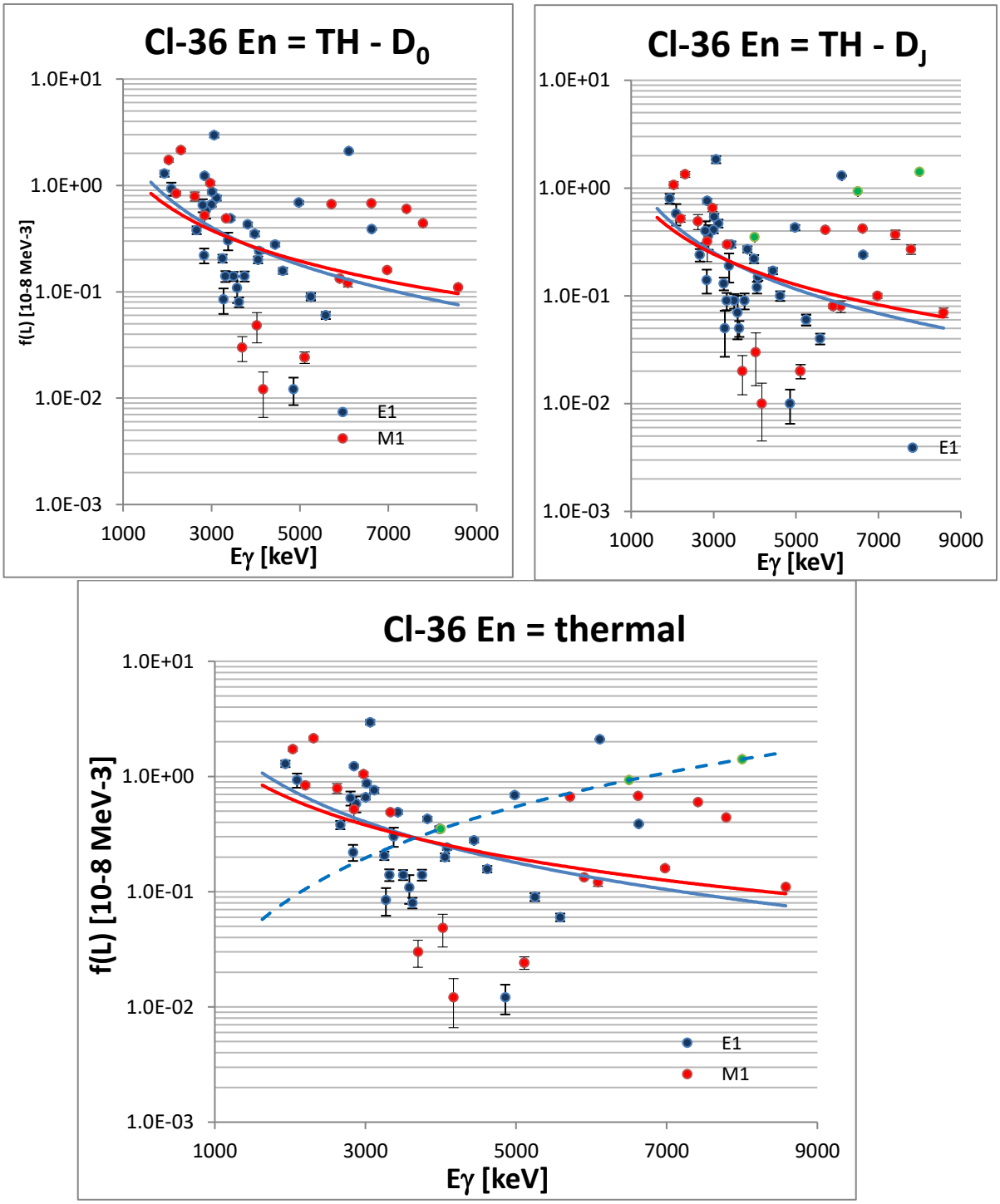

FIG. 5a *Upper panels*: *Results for two different spacing values, D_0 and D(J=2), to demostrate their influence. PSF data differ by the D_0/DJ ratio estimated to be 40%. Lower panel: PSF values from Table 2 plotted as a function of E_γ. Plotted curves are unweighted power trend fits to show the PSF behaviour as a function of E_γ. E_γ^2 dependence normalized at 6.5 MeV to <f(E1)> systematics is plotted as a dashed curve.*

The E1 trend is rather surprising, having a comparable strength with the DRC fit which however increases with decreasing gamma-ray energy. The tendancy of the E1 strength at low energies disagrees with the E1GDR model and suggests the presence of another mechanism rather then the compound nucleus model. If we remove the E1 data below 3.5 MeV which are responsible for the increase observed in Fig. 5a, then the E1 data trend changes in agreement with the E1GDR model behaviour, as shown in Fig. 5b. The data points below 3.5 MeV can be postulated to belong to different mechanisms (nonstatistical) that are relevant to the high energy region.

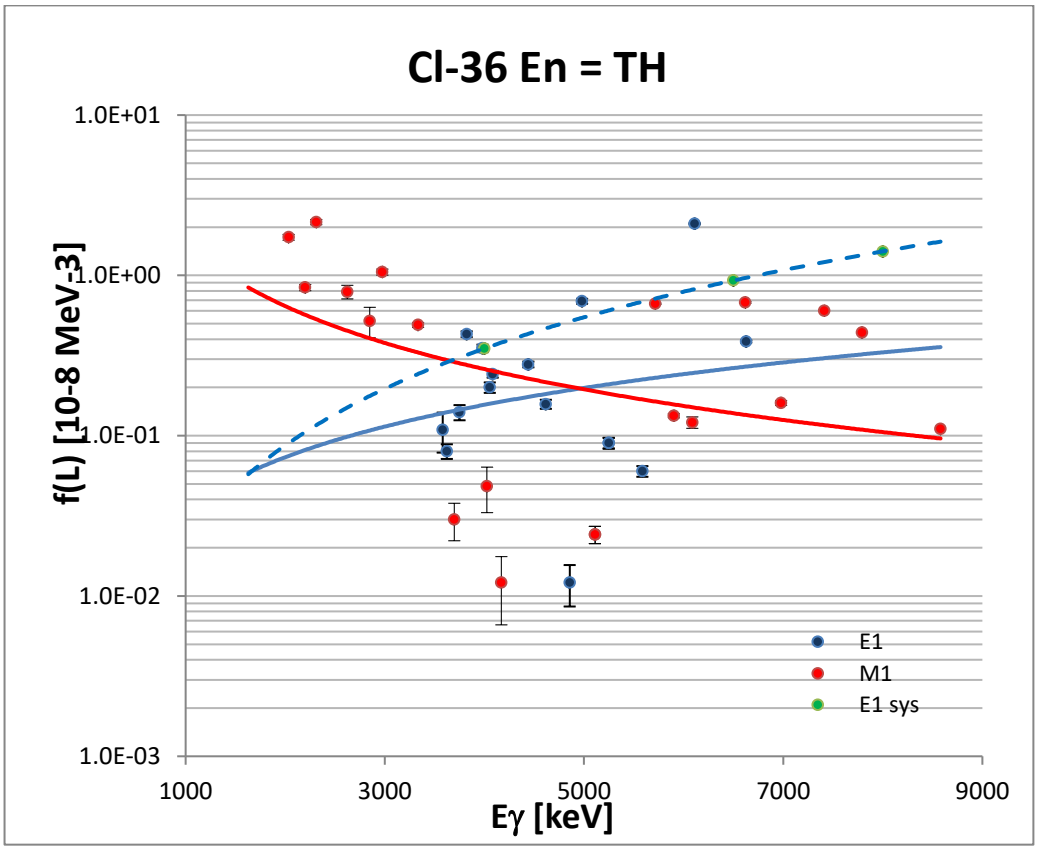

FIG. 5b *The data from Fig. 5a plotted with E1 points removed below E_γ = 3.5 MeV. Plotted full curves are again unweighted power trend fits to show the PSF behaviour as a function of E_γ. E_γ^2 dependence normalized at 6.5 MeV to <f(E1)> systematics is plotted as a dashed curve. The change of the E1 trend is obvious.*

Comparison with the available DRC data allows us to validate the present data. The DRC measurement [31] involves capture in a single p-wave resonance ($J_i = 1/2^-$) and the comparison of E1 and M1 modes between thermal and resonance capture are interchanged and are shown separately in Fig. 6.

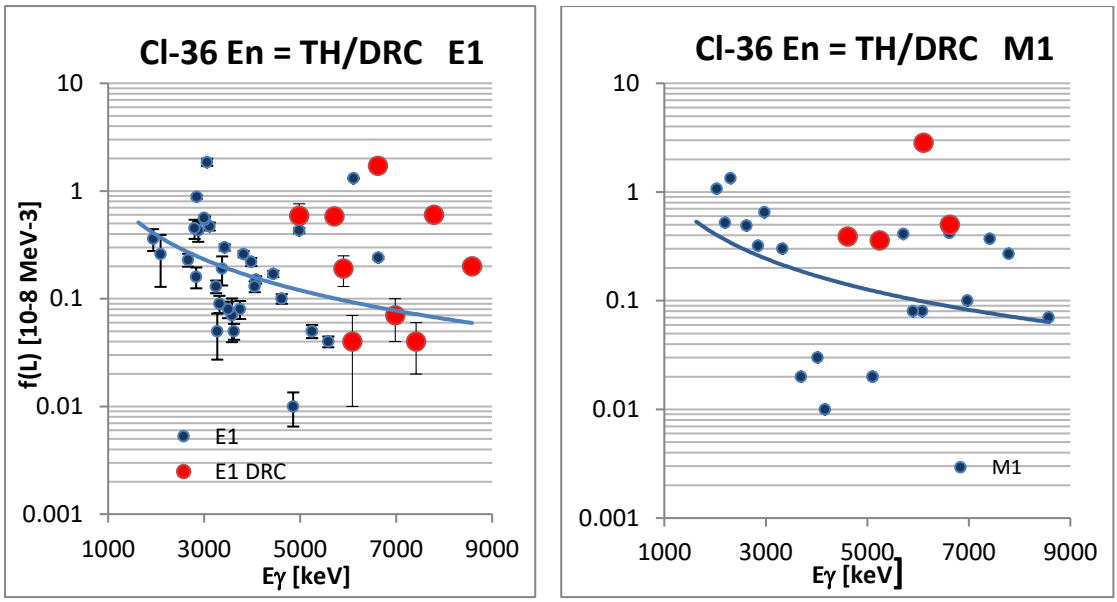

FIG. 6 *Thermal and DRC PSF data together for E1 and M1 transitions.*

A visual comparison of THC and DRC data in Fig. 6 shows that data from the two different experiments are in reasonable agreement if large fluctuations are considered. Further support comes from the comparison of average <f_L(<6.5 MeV>) values from the systematics [10] and the present data, as shown in Table 3.

Table 3. Comparison of binned data at <6.5 MeV> energy

	<f_L(<6.5 MeV>)	<f_L(<6.5 MeV>)	<f_L(<6.5 MeV>)	<f_L(<6.5 MeV>)
	10-8 MeV-3	10-8 MeV-3	10-8 MeV-3	10-8 MeV-3
	Thermal data D_0	Thermal data D_J	132 eV p-resonance	Systematics
E1	1.20(25)	0.77(16)	0.45(7)	0.93 (40)
M1	0.31(6)	0.20(4)	0.83(6)	0.69 (30)

We may conclude that the data above 5 MeV are in good agreement considering the limited number of data points. The conflict with the prediction from a compound nucleus process has been noted in Ref. [31]. A strong correlation of thermal (s-wave) and resonance (p-wave) spectra with $r = 0.84^{0.16}_{0.10}$ was observed [31] and was used to explain the M1 enhancement as a result of single particle effects. The increasing E1 strength trend at low E_γ energies is in direct violation of the E1 GRM prediction. This also demonstrated in Fig.7 in the comparison with the D1M+QRPA predictions.

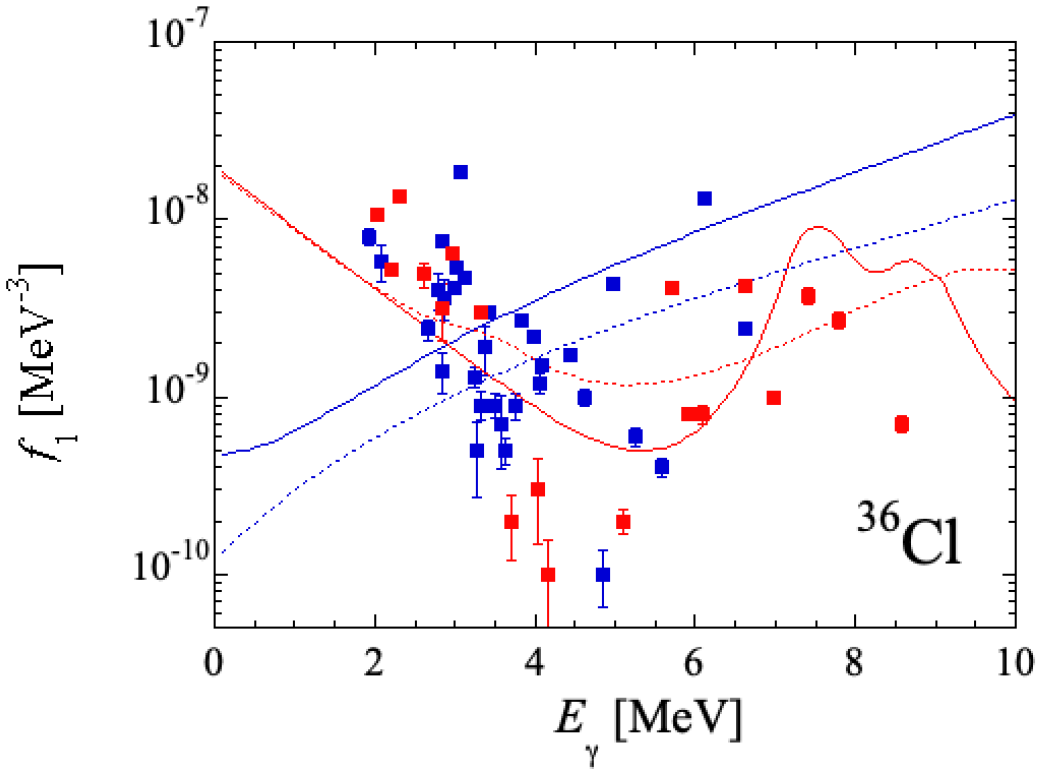

FIG. 7 *Comparison of ^{36}Cl thermal data with D1M+QRPA calculations (solid curves) and SMLO model [7,32] (dotted curves). The blue (red) data points stand for E1 (M1) transitions, respectively.*

4.2 ^{57}Fe (J_t = 0 target)

The product nuclide ^{57}Fe is an odd nucleus and therefore the initial spin of the capture state has a unique unambiguous value of $J_i = 1/2^+$ with cross sections $\sigma(\text{exp}) = 2.59$ b, $\sigma(+) = 0.09$ b and $\sigma(B) = 2.5$ b [14]. The negative resonance contribution is responsible for the thermal cross section and a strong single bound state at $E_n = -6.52$ keV is postulated with highly enhanced width $\Gamma_\gamma = 1.474$ eV against $\Gamma_{\gamma 0} = 0.90$ eV. The gamma transitions with their absolute intensities I_γ were extracted from a high-quality measurement using an advanced procedure to construct the decay scheme, supported by shell model calculations [32]. The sum of assigned primary intensities I_γ equals $\Sigma I_\gamma = (0.96 \pm 0.5)$. For the evaluation of PSF only transitions to final states with known parity were considered needed for unambiguous E1 or M1 assignments.

For the calculation of $f_L(E_\gamma)$ Eq. (2) was used with $\Gamma_{\gamma 0} = 0.9$ eV and $D_0 = 22$ keV. For the conversion of gamma-ray intensities into partial $\Gamma_{\gamma I}$, the total s-wave radiative width $\Gamma_{\gamma 0}$ from Eq. (5) is used. The calculated PSF values are plotted in Fig. 8 together with unweighted trend lines generated by a power function of E_γ. The list of adopted gamma lines and corresponding PSF values together with final states is given in Table 4. Unused transitions or levels are printed in red. Undetected transitions are shown in blue and may potentially be missed transitions due to the PT fluctuations.

Table 4. PSF data of ^{57}Fe nuclide processed with $\langle\Gamma_\gamma\rangle_0$ = 0.9 eV and D_0 = 2.2 keV. J^π with π = +, − are states with more spin proposals, where at least one of them is $J^\pi \leq 5/2$. States with no assigned transition are shaded in blue.

Fe-57 TH ECN

I_γ extracted from R. Vennink et al. Nucl. Phys. A344 (1980) 421

Sum prim. I_γ = 0.96 ± 0.05

$G_{\gamma 0}$ = 0.9 eV D_0 = 22 keV applied

Only transitions to states with assigned parity considered

E_γ	E1	M1		dE1	dM1		Ex	Jπ
7646	2.29			0.27			0	1/2-
7631	2.67			0.46			14	3/2-
7279	0.64			0.06			367	3/2-
							1139	
6380	0.17			0.02			1265	1/2-
6018	1.86			0.15			1627	3/2-
5920	1.89			0.14			1725	3/2-
							1976	π=-
							1991	1/2-3/2-
5318		0.02			0.01		2330	π=+
							2564	3/2-
							2594	3/2-5/2-
5047		0.05			0.02		2600	π=+
4948	0.29			0.03			2697	1/2-
4825		0.03			0.01		2823	π=+
4810	0.68			0.04			2836	3/2 π=?
4724	0.11			0.01			2922	1/2-3/2-
4675		0.16			0.02		2971	π=+
4659		0.04			0.01		2988	π=+
4463	0.24			0.02			3183	1/2-3/2-
4406		0.78			0.04		3240	1/2+
4324	0.06			0.02			3323	1/2-3/2-
4275	0.13			0.01			3371	3/2-
4218	2.06			0.1			3428	3/2-
3854		0.14			0.01		3792	3/2+

E_γ	E1	M1		dE1	dM1		Ex	Jπ
							3926	π=-
3663	0.11			0.01			3982	3/2-
3509		0.05			0.02		4137	5/2+?
3505		0.17			0.05		4141	π=+?
3436		1.64			0.11		4144	π=+?
							4209	(3/2)-
							4239	π=+?
3267	1.41			0.06			4379	π=-
3186	0.86			0.04			4460	π=-
							4544	1/2+
3075		0.15			0.07		4572	1/2+
3048		0.06			0.01		4598	π=+
2954		0.57			0.05		4692	π=+
							4976	3/2+
							5115	1/2+
2507		0.1			0.03		5140	π=+
2466		0.22			0.05		5179	1/2+
2424	0.17			0.06			5222	π=+- ??
2407		0.29			0.06		5238	π=+

A total of 44 states with $J_f \leq 5/2$ were adopted and only two of them have unknown parity. No transition was found for 12 states, which is a relatively large fraction of the total if the capture state decay with $\Sigma I_\gamma = (0.96 \pm 0.5)$ is taken in account.

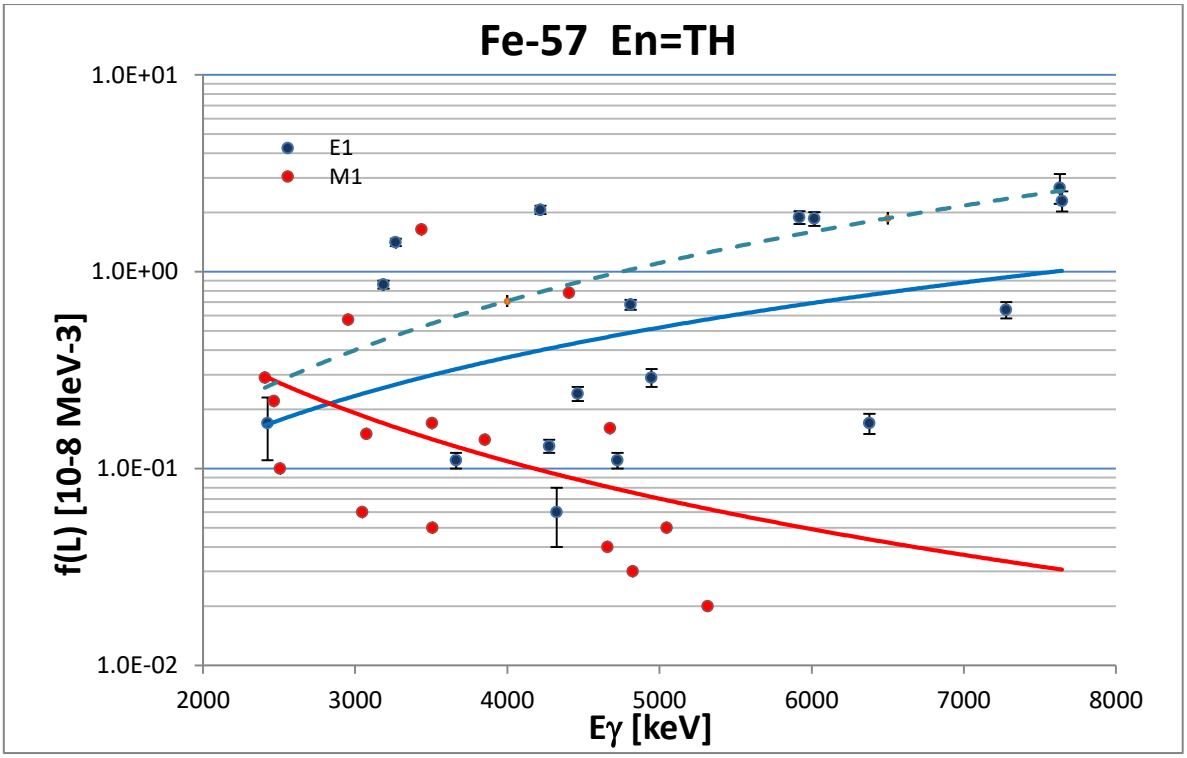

FIG. 8 *PSF values from Table 2 plotted for ^{57}Fe nuclide as a function of E_γ. Plotted full curves are unweighted fits to show the PSF behaviour as a function of E_γ. E_γ^2 dependence normalized at 6.5 MeV to <f(E1)> systematics is plotted as a dashed curve.*

The large dispersion of the data is clearly seen in Fig. 8, which demonstrates that the differential data needs to be binned to be able to provide a PSF value with a smaller uncertainty. The average <f(E1)> at <E_γ> = 6.5 ± 0.5 MeV obtained from 4 E1 transitions is equal to (1.9 ± 0.1) x 10^{-8} MeV^{-3} which is in excellent agreement with the systematic prediction of 2.0 x 10^{-8} MeV^{-3} [10] (see Table 5). The most valuable aspect of the thermal data is that the PSF behaviour may be tracked down to energies close to 2 MeV, the energy range in which the average resonance capture is far below the detection threshold limit. This is valuable information especially for M1 radiation which has several excitation modes below the spin-flip resonance energy. However, for M1 the small number of transitions or transitions with energies << 6.5 MeV does not allow for a meaningful mean estimate.

Table 5. Comparison of binned data at <6.5 MeV> energy

	<f_L(<6.5 MeV>)	<f_L(<6.5 MeV>)
	10-8 MeV-3	10-8 MeV-3
	Thermal data	Systematics
E1	1.9(1)	2.0(8)
M1	na	0.87(4)

The comparison with QRPA calculations shown in Fig. 9, kindly provided by S. Goriely, is also very supportive of the PSF results. The E1 strength is in good agreement with theoretical predictions while for the M1 mode some strength is missing especially at the lower edge (5 – 6 MeV) of the M1 spin-flip resonance.

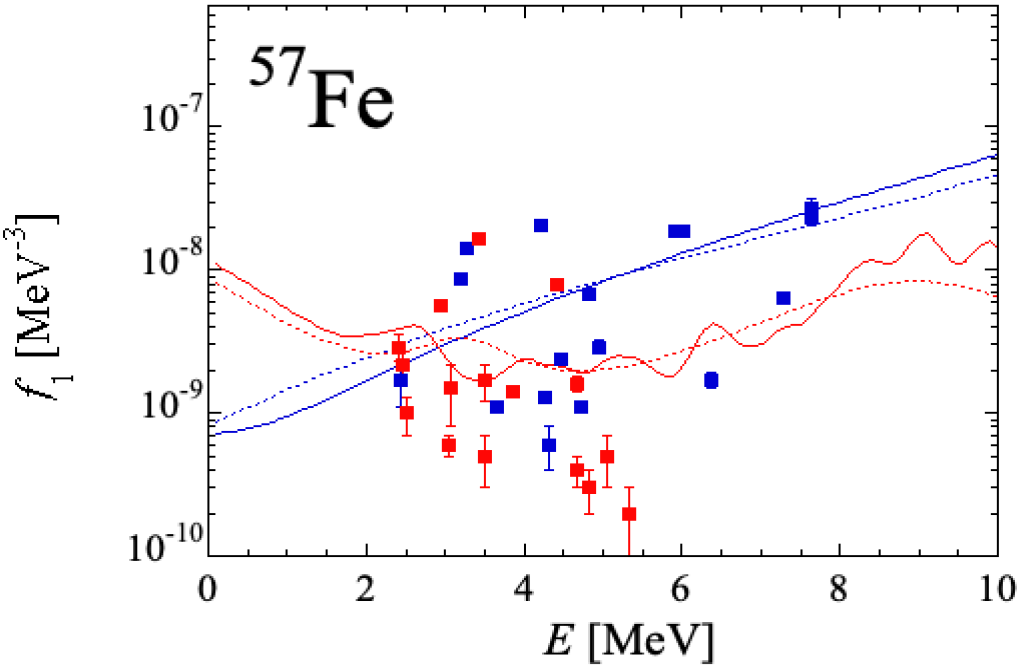

FIG. 9 *Comparison of ^{57}Fe thermal data with D1M+QRPA calculations (solid curves) and SMLO model [7,32] (dotted curves).*

Another interesting validation tool is the comparison with DRC data involving capture in a single p-wave J = 1/2⁻ resonance [34]. PSF data from these two different experimental sources are shown in Fig. 10 and agree well within data fluctuations. The energy dependence of both the E1 and M1 radiation mean strength is in a good agreement with predictions from the theoretical E1GRM model and M1 excitations at and below the spin-flip resonance (compare with Fig. 9).

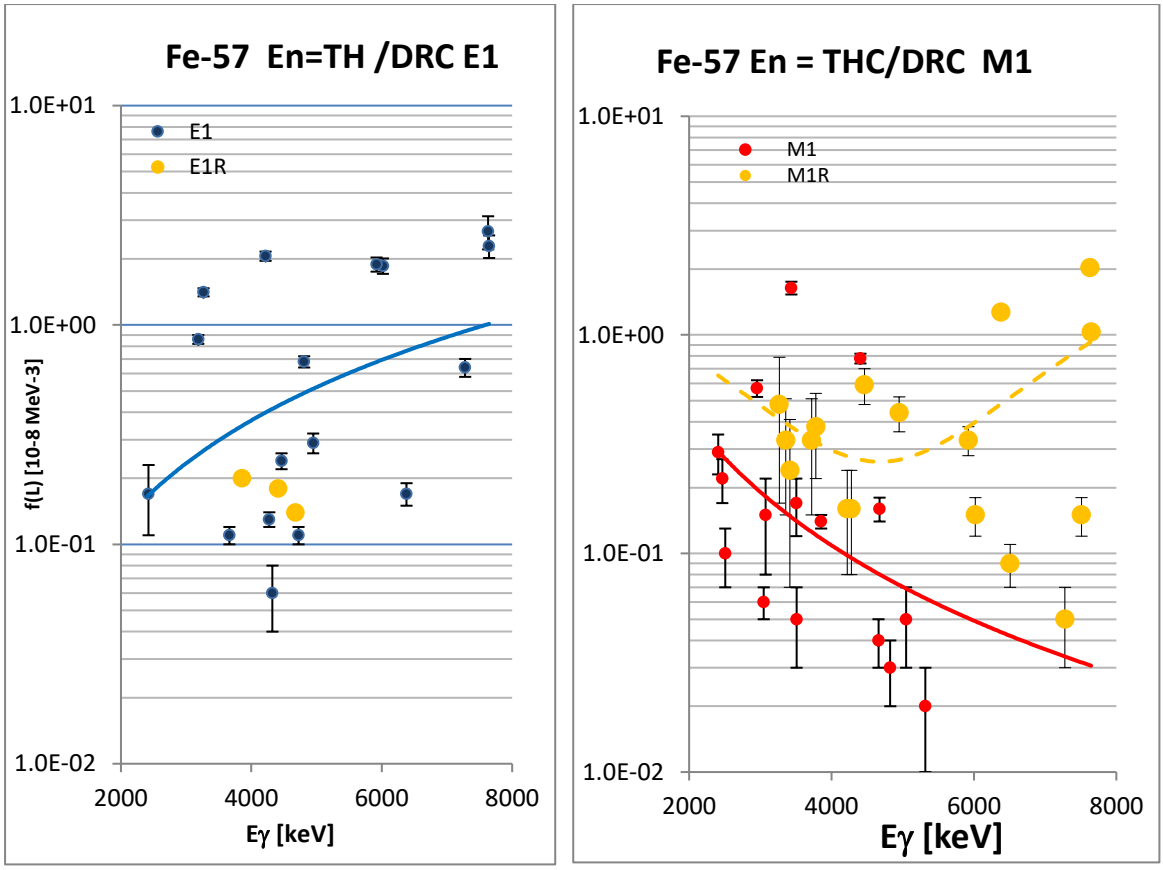

FIG. 10 *A comparison of thermal (E1 and M1 points) and DRC data (E1R and M1R points) separately for E1 and M1 transitions.*

4.3 ^{60}Co (J_i spin admixture)

The ^{60}Co nuclide was extensively studied by employing the capture of polarized, unpolarized and 24 keV neutrons [17]. From 350 observed gamma-rays, 335 could be placed in the decay scheme with 144 levels, supported also by shell model calculations. The kinematical shift between thermal and 24 keV measurements provided an additional argument for the identification of primary transitions and allowed for a fairly unambiguous selection between primary and secondary transitions. Absolute intensities of primary transitions cover (90.2 ± 0.45) % of the capture state decay strength. The integral spin admixture can be estimated from partial cross sections. The pertinent values have been extracted from Ref. [14] and are $\sigma(\text{exp}) = 37.18$ b, $\sigma(-) = 6.90$ b, $\sigma(+) = 22.66$ b and $\sigma(B) = 7.62$ b. The estimation of the spin admixture yields a value of $\alpha = 0.71$ if we arbitrarily postulate an equal participation of 3^- and 4^- for two bound states at $E_n = -4.75$ and -5.0 keV. The following subsections describe the different processing procedures and their internal tests.

4.3.1 Equal participation of spins in the capture state

Firstly, we apply the standard Eq. (2) and calculate the PSF values, using $\Gamma_{\gamma 0} = 0.540$ eV and $D_0 = 1.390$ keV values and the capture state spins $J_i = 3^-, 4^-$. In this case we neglect the spin admixture $\langle\alpha\rangle = 0.72$ and assume the spin participation as equal with $\langle\alpha\rangle = 0.50$ as is the case in the ARC averaging. In such a situation the interference effects in partial admixtures α_i are assumed to average out. The resulting PSF values are given in Table 6 and are shown in Fig. 11. Only transitions to final states with known parity have been used.

The size of the fluctuations is very large, almost three orders of magnitude for E1 radiation, but the unweighted trend lines give the expected energy dependence of the E1 and M1 strength for the compound nucleus model. The average <f(E1)> value at $\langle E_\gamma \rangle = 6.5 \pm 0.5$ MeV obtained from 10 E1 transitions is equal to $(3.72 \pm 0.4) \times 10^{-8}$ MeV^{-3} and overestimates the systematic prediction of 2.0×10^{-8} MeV^{-3} [10].

Table 6. PSF data of ^{60}Co nuclide processed with $\langle \Gamma_\gamma \rangle_0 = 0.540$ eV and $D_0 = 1.39$ keV. Ten E1 transitions printed in red form the data set for <f(E1)> at <6.5 MeV>. Blue shaded rows represent the adopted final state (printed in red) for which no primary transition was observed and the (+–) sign describes states with undetermined parity in the ENSDF compilation.

Co-60 TH ECN Petten

I_γ/100 captures extracted from J. Kopecky et al., NP A427 (1984) 413
$G_{\gamma 0}$ = 0.540 eV D_0 = 1390 eV
Sum primaries = 73.06
π = +- comes from circular polarization results

E_γ	E1	M1		dE1	dM1		Ex	Jπ
7491	2.66			0.2			0	5+
7433	0.21			0.04			59	2+
7215	3.83			0.2			277	2+
7203	0.88			0.04			288	3+
7056	1.95			0.2			436	5+
6986	3.14			0.2			506	3+
6949	0.79			0.3			543	2+
6877	10.06			0.2			615	3+
6706	9.71			0.2			786	4+
6487	8.89			0.2			1006	4+
6341	0.12			0.09			1151	(2+3+)
6284	0.95			0.3			1206	5+
6275	1.01			0.16			1217	6+,4
6150	0.78			0.28			1342	3+
6111	0.92			0.28			1381	3+
6041	0.92			0.31			1451	4+
							1508	2+3+
5976	12.56			0.2			1516	4+
5926	3.38			0.03			1566	2(+-)
5852	0.56			0.38			1640	3+4+5+
5783	0.1			0.024			1710	(+-)
5743	4.45			0.02			1749	3+
5705	0.98			0.38			1788	5(+)
							1808	4-
5661	15.29			0.02			1831	4+
5639	2.08			0.3			1853	4+
5615	2.28			0.3			1877	2(+-)
5603	2.61			0.03			1889	4+
5568	0.22			0.12			1924	π=+
5511	1.15			0.28			1981	4(+-)
							2032	2+3+

E_γ	E1	M1		dE1	dM1		Ex	Jπ
5446	0.22			0.1			2045	(+-)
5411	0.08			0.023			2081	(+-)
5370	1.25			0.1			2122	(3+4+)
5358	1.12			0.03			2133	3,4 π=-
5309	0.33			0.09			2183	2+3+
5270	2.79			0.3			2222	4+
5217	0.44			0.19			2275	π=+
5213	0.58			0.14			2280	5+
5182	7.45			0.03			2310	3(+-)
5168	0.78			0.08			2324	4(+-)
5150	0.4			0.06			2342	(+-)
5141	0.25			0.09			2352	(+-)
5128	1.38			0.3			2364	(+-)
5069	0.94			0.4			2423	4 π=+
5062		0.12			0.022		2431	3-4-
5041	0.72			0.05			2451	3,4 π=+
5003	2.25			0.3			2489	5(+-)
4963	0.61			0.06			2529	(+-)
4922	3			0.3			2570	4(+-)
							2685	3-4-
4871	0.4			0.08			2709	2,3,4(+-)
4706				0.4			2785	3,4(+-)
4666	1.34				0.05		2825	3-4-
4607				0.03			2884	5+
4607							2885	3-4-
4470		3.34		0.06			3022	3,4(+-)
4377	0.84			0.05			3114	(+-)
4307	1.62			0.81	0.008		3186	3-4-
4208		0.08		0.04			3283	3,4(+-)
							3393	3-4-
3930	5.76			0.3			3560	4+
3903	1.23			0.11			3588	3-4-
3620		1.58			0.08		3871	3-4-
3486					0.26		4005	3-4-
							4067	3-4-
3335		3.93			0.06		4156	3-4-
							4212	(+-)
3222		0.80			0.3		4270	3-4-
3126					0.11		4365	3-4-
							4390	3-4-
							4698	3-4-
2652		4.29			0.60		4800	3-4-

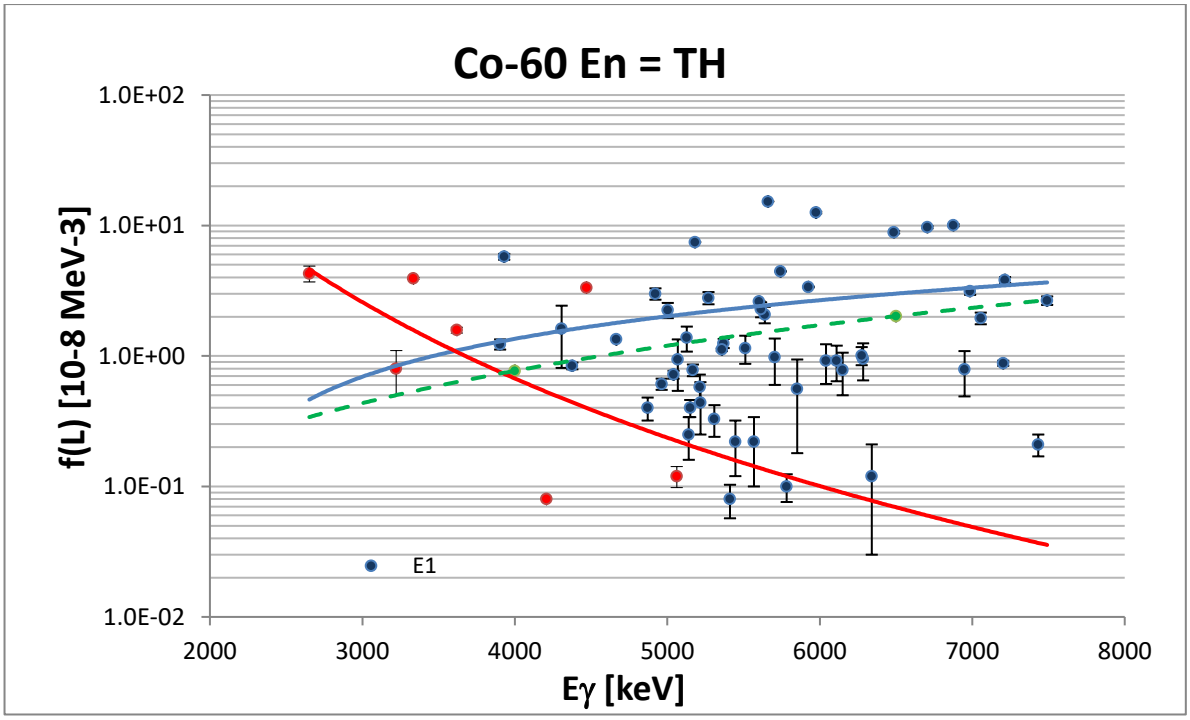

FIG. 11 *Differential PSF values of the gamma strength in ^{60}Co. Only transitions to final states with unambiguously assigned parity values are plotted. E_γ^2 dependence normalized at 6.5 MeV to <f(E1)> systematics is plotted as a dashed curve. Plotted full curves are unweighted power trend fits to show the PSF behaviour as a function of E_γ.*

Comparison with the theoretical predictions of the D1M+QRPA model is shown in Fig. 12. The calculated curve for E1 lies reasonably in the middle of the E1 data, however, the low energy M1 data below 5 MeV overestimate the theory. This overestimation may be due to the large number of missed M1 transitions (partly due to PT fluctuations and partly for experimental reasons). This can be seen in Table 6, where for a number of final states (assigned in the ENSDF compilation) no parity is given or many primary transitions are not observed. The reason for missed transitions may come from the Porter Thomas fluctuations. The decreasing spectral resolution and the diminishing detection sensitivity in this energy region may be an additional cause. This is exactly the energy range, where the low energy (0 – 2.7 MeV) and the high energy measurements (1.5 – 7.5 MeV) of the original Ref. [17] overlap. Another striking fact is that there is no M1 decay for energies above 5 MeV, because of the absence of a final state with an unambiguous assignment of a negative final spin. Several final states exist in that region with undefined parity and these states were not used.

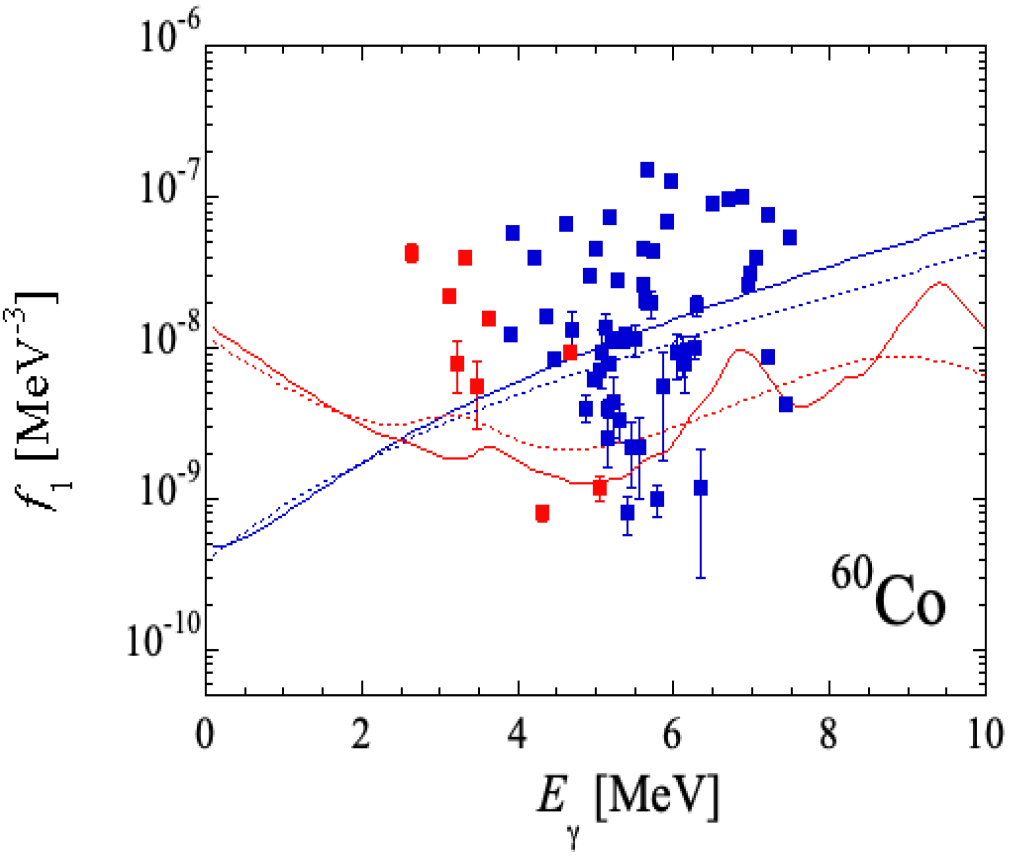

FIG. 12 *Comparison of ^{60}Co thermal data from Fig. 11 with D1M+QRPA calculations (solid curves) and SMLO model [7,32] (dotted curves).*

If we arbitrarily assume a negative parity for all these unassigned transitions, the M1 PSF data distribution and trend may be closer to the QRPA prediction (see Figs. 12 and 13) and also to the spin-flip resonance energy.

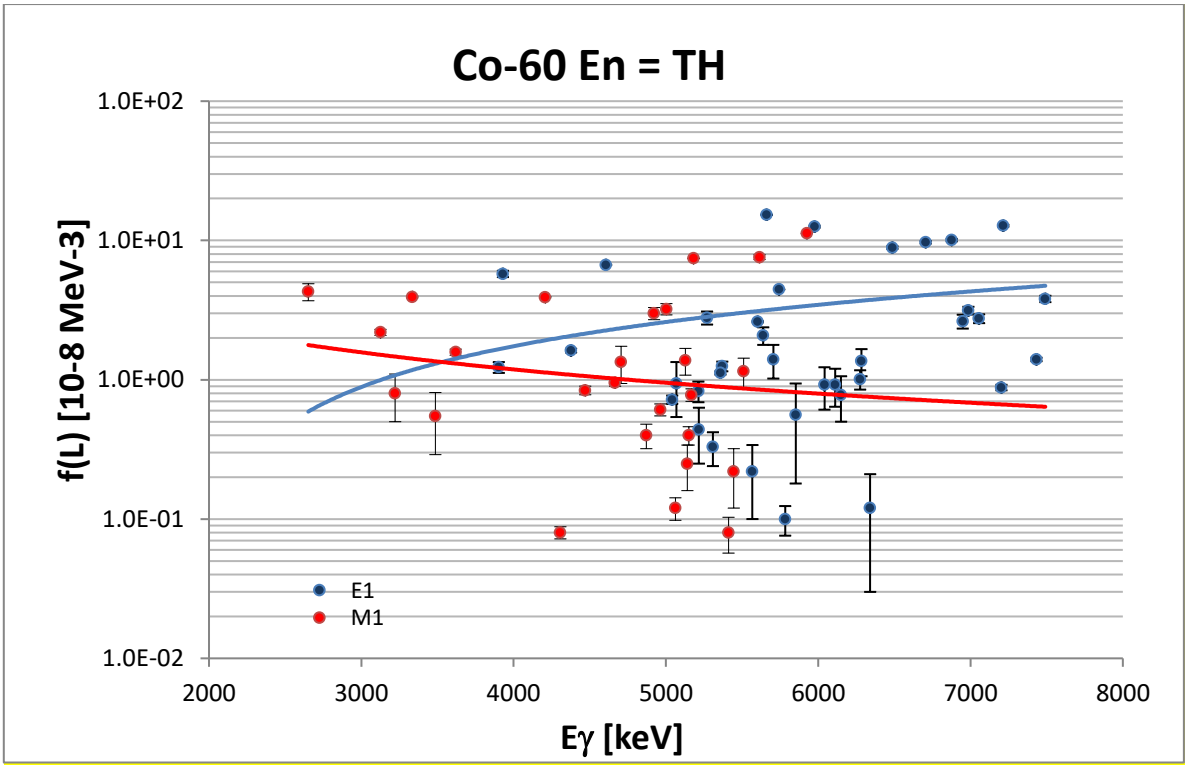

FIG. 13 *The same data as in Fig.11 but with the assumption that all the final states populated by primary transitions that have known spin but unknown parity in fact have negative parity and are therefore populated by M1 transitions.*

We therefore conclude that the completeness of the decay scheme together with the knowledge of the multipolarity of primary transitions are important factors in the interpretation of the differential PSFs obtained from thermal capture data. The same holds for DRC and ARC data, but their better averaging qualities and less dispersion allows an additional classification of E1 and M1 assignments.

4.3.2 Realistic average capture state spin admixture

The estimate of admixture from partial thermal cross sections is $<\alpha> = 0.72$ if we arbitrarily postulate an equal participation of 3^- and 4^- for the bound state. This value is in good agreement with the experimental value of (78.3 ± 1.0) % obtained from the transmission measurement of polarized monochromatic neutrons with polarized ^{59}Co nuclei [35]. This is also in agreement with the expectation the 132-eV $J_i = 4^-$ resonance dominates the thermal cross section.

The circular polarization measurement and capture by polarized target nuclei measurement reveal for each transition the degree of circular polarization and the capture spin admixture. Results from such measurements are shown in Section 3.2 and Fig. 1. Using values from Fig. 1, quoted in Table 6 of Ref. [17], the mean value $<\alpha> = 0.65$ has been obtained from transitions which exhaust a reasonably large fraction ($\Sigma I_\gamma = 67$ %) of the primary decay. This is in good agreement with previous estimates of $<\alpha>$ values. The conclusion is that approximately two thirds of the transitions come from the spin 4 capture state, and this influences the transition strength to $J_f = 2$ and 5 states. This observation requires a revision of the double population correction with the revised factors Q = 3.33 and 1.43 for $J_f = 2$ and 5, respectively.

There are two ways to perform an absolute calibration: a) by selecting well defined $J_f = 2$ or 5 states, assuming they are populated from one initial spin state and using their binned <f(E1)> to calibrate the remaining transitions, and b) by selecting a representative number of inner

states with J_f = 3 and 4, treating them as equally populated from both J_i spins and then again using their <f(E1)> to calibrate the rest of the states. Both methods have weaknesses, the first in the additional uncertainty of the D(J) estimate and the second in the assumption of equal J_i participation. We preferred to use the first procedure based on the outer spins and the results are shown in Section 3.5.

4.3.3 Partial capture state spin admixture

This is the most accurate processing of nuclides with unequal contribution from two spins in the capture state by taking in to account the partial interference effects. The measured partial α_i values from polarized neutron capture are shown in Table 7 (taken from [17]) and Fig. 3 of Section 3.

Table 7. Spin admixtures derived from circular polarization experiment. J^π assignments are based on the circular polarization results (ECN) and the ENSDF compilation.

E_γ	Ex	Jπ ENSDF	Jπ ECN	α_i
7491	0	5+	5+	1
7433	59	2+	2+	0
7215	277	2+	2+	0.46
7203	288	3+	4+	0.42
7056	436	5+	5+	1
6986	506	3+	3+	0.62
6949	543	2+	2+	0
6877	615	3+	3+	0.96
6706	786	4+	4+	0.94
6487	1006	4+	4+	0.96
6284	1206	5+	5+	1
6275	1217	6+,4	4+	0.73
6150	1342	3+	2+3+	0, 0.08
6111	1381	3+	3+	0.75
6041	1451	4+	4+	0.24
5976	1516	4+	4+	0.96
5926	1566	2	2	0
5852	1640	3+4+5+	(3)+4+5+	0.80,0.91,1
5743	1749	3+	3+	0.99
5705	1788	5(+)	5+	1
5661	1831	4+	4+	1
5639	1853	4+	4+	0.11
5615	1877	2+	2(+)	0
5603	1889	4+	4+	0
5511	1981	4	4	0.95

E_γ	Ex	Jπ ENSDF	Jπ ECN	α_i
5370	2122	(3+4+)	3(+)4(+)	0.90,0.86
5358	2133	3,4	3-(4)-	0.52,0.51
5270	2222	4	4+	0.92
5217	2275		3+4+(5)+	0.87,0.86,1
5213	2280	5+	3, (5)+	???
5182	2310	3	3	0.99
5069	2423	4+	4+	0.7
5041	2451	3,4	3+4+	0.28, 0.33
5003	2489	5	5	1
4922	2570	4	4	0.62
4706	2785	3,4	3	0.45
			$<\alpha>$ =	0.70

The method described in Sect. 2.4 employing Eq. (14) has been used to evaluate PSF values as absolute values and is shown in Table 8. Values of $\alpha_i < 0.1$ and $\alpha_i > 0.9$ were for practical use rounded off to zero or one and this is justified because the influence of these values on the spin admixture is negligible.

4.4 Renormalization to f(E1) > systematics

Another way to perform the renormalization to the absolute PSF scale is to implement the <f(E1)> systematics at <6.5 MeV>, as was done successfully for the ARC data. The correction factor is based on the ratio of $<f(E1)> = 3.7 \times 10^{-8}$ MeV^{-3} at $<E_\gamma> = 6.5 \pm 0.5$ MeV obtained from eleven E1 transitions to the systematic value of $<f(E1)>_{sys} = 2.0 \times 10^{-8}$ MeV^{-3} [10]. This renormalization results in the reduction of data from Table 5 by a factor 2.0/ 3.7 = 0.54, i.e. roughly by a factor of two. The data trend and fluctuation dispersion remain the same as in

Fig. 7.

4.5 Comparison of different PSF normalizations

The comparison of all four normalizations allows us to evaluate the results and recommend the best approach. It further provides a systematic uncertainty which can be assigned to different PSF normalization procedures. The basic common matrix of transitions to be used for the comparison was taken from the circular polarization experiment. The resulting PSF values are shown in the graphical comparison of the four normalized data sets in Fig. 14.

The four different normalizations that are compared are:

a – no spin admixture Sect. 3.1

b – normalization to systematics Sect. 3.4

c – α - rounded off admixture applied for normalization of $J_f = 2$ and 5

d – α_i applied for $0.1 < \alpha_i < 0.9$ related to $<\alpha> = 0.71$

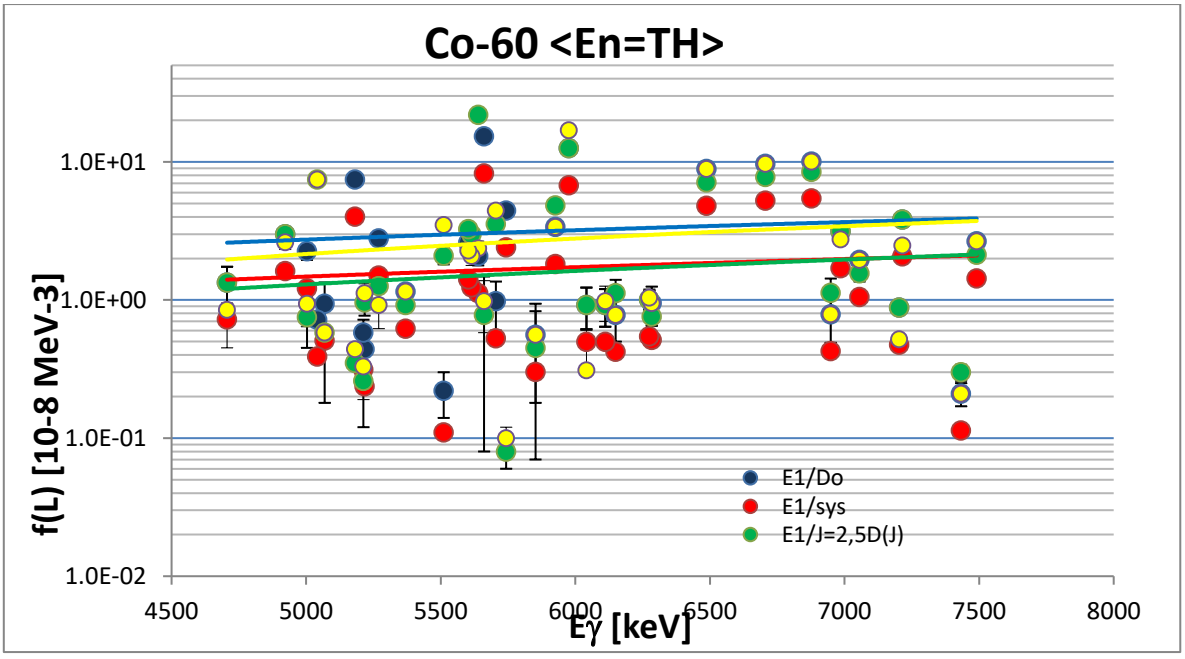

FIG. 14 *The comparison of four different normalization methods used to obtain PSFs for ^{60}Co nucleus. The plotted curves are unweighted fits and serve to guide the eye on the trends.*

To validate these different approaches firstly the binned $\langle f(E1)\rangle_{6.5MeV}$ values are compared in Table 8.

Table 8. Comparison of binned E1 data at < (6.5 ± 1) MeV> energy for all the normalization procedures a – no spin admixture as in Sect. 3.1, b – normalization to systematics as in Sect. 3.4, c – J_f = 2 and 5 used in Sect. 3. 2 and d – α_i applied in Sect. 3.3. The last column gives the systematics prediction for ^{60}Co. The quoted errors are of a pure statistical nature.

	$\langle f_L(<6.5$ MeV$>)$	$\langle f_L(<6.5$ MeV$>)$	$\langle f_L(<6.5$ MeV$>)$	$\langle f_L(<6.5$ MeV$>)$	$\langle f_L(<6.5$ MeV$>)$
	10-8 MeV-3	10-8 MeV-3	10-8 MeV-3	10-8 MeV-3	10-8MeV-3
	a– no α	b – RN sys	c – RN Jf=2;5	d – $\langle\alpha_i\rangle$ used	Systematics
E1	3.72(40)	2.01 (30)	3.24 (40)	3.63 (30)	2.0

These results are also supported by the visual comparison of data and unweighted trend curves in Fig. 14. Note that the unweighted trend curves are only a very crude representation. The simplified approach (blue curve), that treats the data with no spin admixture effect, overestimates the PSFs. Data normalized with the use of partial α_i data (yellow curve) are the most accurate because they take into account the realistic partial spin admixtures from the interference effects. The normalization to single populated J = 2 and 5 states (green curve) and the normalization using $\langle f(E1)\rangle_{6.5MeV}$ systematics (red curve) give fairly similar results. Given that the partial α_i data normalization is not generally available for all nuclides, and considering also the total systematic uncertainty involved, one can safely say that the simplified normalization, which is verified by the $\langle f(E1)\rangle_{6.5MeV}$ prediction, is the best normalization tool for nuclides with mean admixture $0 < \alpha > 1$.

4.6 Conclusions

Thermal neutron capture has been considered as a source of data for the derivation of photon strength functions. The aim of this work was to prepare and to test the processing procedures

for extracting PSFs from thermal capture data, taking in to account the specific features of the thermal neutron capture state. Four different methods for the absolute normalization of I_γ/E_γ^3 values have been proposed and tested (see Sections 2 and 3). The methods were tested for three different types of nuclides, $J_t = 0$ targets (^{57}Fe), no spin admixture with a single spin in the capture state (^{36}Cl) and a real spin admixture of both states (^{60}Co). The following conclusions and recommendations have been made, based also on the results of the validation against the <f(E1)> (6.5 MeV) systematics from DRC data:

1. For targets with $J_t = 0$ and a single spin-capture state from a dominating resonance (the spin admixture is absent or negligible), Eq. (2) can be safely used

$$<f_X(E_{\gamma i})> = <\Gamma_{\gamma i}> / E^3_{\gamma i} D_0 \ , \qquad (2)$$

   where $<\Gamma_{\gamma i}>$ is the average partial radiative width and D_0 is the s-wave resonance spacing.

2. For targets with a spin admixture of two spins, the most practical approach (supported by the partial α_i test approach) is to use Eq. (2) as a first step and then to use selected E1 transitions from the (6.5 ± 1) MeV window to renormalize against the <f(E1)> systematics $<f(E1)>_{sys} = 0.004 \cdot A^{(1.52 \pm 0.21)}$ [10]. The choice of E1 transitions to the inner ($J_i \pm ½$) spins is recommended to avoid complications with the Q correction. The comparison of these two approaches can give an estimation of the systematic uncertainty due to the simplification of the spin admixture treatment.

3. Caution is advised in the use of the correction Q of the outer spins for two capture state spins. While for the ARC data, where the PT fluctuations are significantly reduced, the Q correction is fully justified, for the thermal data the situation is different. The partial PSF values strongly fluctuate due to the PT distribution and applying the Q correction may incorrectly increase the data scatter. It is therefore recommended not to use this correction for THC data at all.

4. The non-statistical mechanism may have non-negligible contributions in low mass targets (A < 60) and may influence the distribution and magnitude of the gamma decay strength. A nice example is ^{36}Cl shown in this section. A more complex theoretical modelling is needed for these lighter nuclei.

5. Thermal capture PSF pilot database

5.1 Selected thermal capture data

The main advantage of thermal capture data is the higher statistical accuracy and a low detection threshold. These features enable us to identify primary transitions in a wide energy range down to about 1 – 2 MeV thus extending the information about the PSF behavior to lower energies. The two separate measurements of low and high energy regions allow for a complete data set of gamma transitions to be obtained. Such a data set enables the decay scheme to be built on the basis of a maximum number of primary transitions, including those with low energies, whose summed intensities ΣI_γ are close to 100%. Accurate intensity balance and absolute calibration combined with good procedures for the construction of the decay scheme are necessary conditions for selecting data that are suitable for absolute PSF processing.

The absolute I_γ calibration and the completeness of the decay scheme were among the criteria used for the selection of nuclides in this study. Selected nuclides are listed in Table 9 and include 33 targets with masses A ≤ 154. The majority of data originate from two laboratories with similar high-quality experimental procedures (RCN/ECN Petten and McMaster University) supplemented by several measurements made by the LANL and ILL Grenoble

collaboration. One of the reasons that lower mass targets have been chosen is that they were rarely studied by DRC and ARC experiments [7,11]. Low mass nuclides, furthermore, often have such a low-level density that levels up to the binding energy can be identified by primary transitions. The intensities I_γ given for the majority of the selected nuclides are absolute values, while only three nuclides (^{106}Pd, ^{146}Nd and ^{154}Eu) have recommended relative intensities I_γ only. If the absolute intensity is not determined, the absolute PSF values cannot be extracted and one needs to apply external calibration.

Table 9 also includes all the available information on thermal cross sections that is required to draw conclusions on the spin admixtures in the thermal capture state. The derived average admixture α, defined as $\alpha = \sigma(+)/\sigma(-) + \sigma(+)$ is given in the last column. If $\sigma(B)$ forms a strong or dominant contribution to $\sigma(\gamma)_0$ and the spin is not determined, the assumption of equal contribution of two spin values is adopted and is given in brackets. The derived spin admixture α is a mean value averaged over all primary transitions.

Table 9 Thermal cross sections of studied nuclides and the deduced information on the spin admixture α. Cross section values of positive and negative resonances of two spin channels are documented in Ref. [14].

I_γ	- abs = in captures/100 neutrons; rel = relative values
$\sigma(\gamma)_0$	- the measured thermal cross section
$\sigma(-)$, $\sigma(+)$ spins	- contribution from positive resonances with J_t–1/2 or J_t+1/2
$\sigma(B)$	- contributions from negative resonances together with the estimated direct capture component
$\alpha = \sigma(+)/\sigma(-) + \sigma(+)$	- the spin admixture parameter
$\alpha(B)$	- the spin admixture parameter of negative resonances; assumed 0.5 (in brackets) if both spins are present or unknown

Target	I_γ	$\sigma(\gamma)_0$	$\sigma(-)$	$\sigma(+)$	$\sigma(B)$	$\sigma(B)/\sigma(\gamma)_0$	$\alpha(B)$	α
		[b]	[b]	[b]	[b]		neg.res.	
F-19	abs	0.0095		0.0029	0.0065	0.69	1	1
Na-23	abs	0.525	0.5129	0.00001	0.012	0.02	1	0
Mg-24	abs	0.0538		0.0022	0.0516	0.96	1	1
Mg-25	abs	0.199	0.1846	0.0143	0	0		0.07
Mg-26	abs	0.0374			0.0374	1	1	1
Al-27	abs	0.231	0.0757	0.0253	0.130	0.56	1	0.67
Si-28	abs	0.177		0.0485	0.1285	0.73	1	1
Si-29	abs	0.119		0.0017	0.1173	0.99	1	1
P-31	abs	0.166	0.0009	0.0006	0.1615	0.97	1	0.98
S-32	abs	0.518		0.084	0.434	0.84	1	1

Target	I_γ	$\sigma(\gamma)_0$	$\sigma(-)$	$\sigma(+)$	$\sigma(B)$	$\sigma(B)/\sigma(\gamma)_0$	$\alpha(B)$	α
		[b]	[b]	[b]	[b]		neg.res.	
Cl-35	abs	43.6	0.007	0.06	43.6	1	1	1
Cl-37	abs	0.433	0.009	0.083	0.400	0.92	0	0.19
K-39	abs	2.1	0.015	0.005	2.08	0.99	1	0.99
Ca-40	abs	0.41		0.019	0.391	0.95	1	1
Sc-45	abs	27.2	0.36	0.53	26.33	0.97	(0.5)	0.5
Ti-48	abs	8.32		4.1	4.22	0.51	1	1
		[b]	[b]	[b]	[b]		neg.res.	
V-50	abs	45		12.7	32.3	0.72	0	0.28
V-51	abs	4.94	2.43	1.19	1.32	0.27	(0.5)	0.39
Cr-50	abs	14.7		9.34	5.36	0.38	1	1
Fe-56	abs	2.59		0.09	2.50	0.97	1	1
Fe-57	abs	2.48	0.29	0.85	1.34	0.55	1	0.88
Co-59	abs	37.18	6.90	22.66	7.62	0.21	(0.5)	0.71
Cu-63	abs	4.50	0.231	0.202	4.097	0.91	(0.5)	0.5
Cu-65	abs	2.17	0.045	0.105	2.020	0.93	(0.5)	0.51
Nb-93	abs	1.15	0.027	0.064	1.057	0.92	(0.5)	0.52
Rh-103	abs	143.5	0.05	135.55	7.92	0.06	(1)	1
Pd-105	rel	21.0	1.591	0.794	18.62	0.89	(0.5)	0.48
I-127	abs	6.15	3.59	0.39	2.20	0.36	1	0.42
Cs-133	abs	30.0	19.95	0.43	9.62	0.32	(0.5)	0.17
Ba-135	abs	5.8	1.09	1.15	3.56	0.61	1	0.81
Ba-137	abs	3.6	0.013	0.042	3.55	0.99	1	1
Nd-146	rel	50	7.75	0.3	41.9	0.84	0	0.01
Eu-154	rel	312	29.5	29.7	256.4	0.82	1	0.92

The influence of the α factor needs to be determined for each nuclide separately. The spin admixture contributes additionally to the data dispersion within the PT and statistical fluctuations.

The standard formulation of the photon strength function for E1 radiation defined in Eq. (2) was used for the analysis of all selected targets

$$f_{E1}(E_{\gamma i}) = \Gamma_{\gamma i} / E^3_{\gamma i} / D_0 ,$$

where $\Gamma_{\gamma i}$ is the partial radiative, $E_{\gamma i}$ is the transition energy and D_0 is the s-wave resonance spacing. For the conversion of gamma-ray intensities into partial $\Gamma_{\gamma i}$ the total s-wave radiative width $\Gamma_{\gamma 0}$ is used in $\Gamma_{\gamma i} = I_\gamma \Gamma_{\gamma 0}$.

Resonance parameters used in the present PSF processing are given in Table 10 (taken from Ref. [14]). The quoted errors were, however, not used in the processing and are shown only to give an estimate of the systematic uncertainty of the final PSF value. Relative uncertainties for both parameters are given in separate columns to indicate their accuracy. The mean accuracy of the D_0 spacing is pretty good (11%), while some of the $\Gamma_{\gamma 0}$ errors are close to 50% which brings the mean uncertainty to about 30% and may often form a large contribution to the systematic uncertainty.

Table 10 Resonance parameters of the studied targets used in the processing of the PSF values.

The symbol in brackets are:

(bl) - the value of the bound level used

(xres) – the value estimated as a mean from x resonances

Target	**$\Gamma_{\gamma 0}$**	**$d\Gamma_{\gamma 0}$**	**D_0**	**dD_0**
	eV	%	[keV]	%
F-19	1.5(bl)		343 (4 res)	
Na-23	0.525		122(30)	0.25
Mg-24	8 (bl)		709 (4 res)	
Mg-25	1.73 (1 res)		22 (5 res)	
Mg-26	8 (bl)		709 (4 res)	
Al-27	1.61(36)	0.22	53(7)	0.13
Si-28	0.44 (bl)		322(35)	0.11
Si-29	3 (bl)		339 (3 res)	
P-31	2. 0	na	54.9(104)	0.19
S-32	2.15(117)	0.54	179(29)	0.16
Cl-35	0.446(32)	0.07	22.3(25)	0.11
Cl-36	0.201 (bl)		27.2 (6 res)	
K-39	1.00(54)	0.54	8.0(8)	0.10
Ca-40	1.5(9)	0.6	45(4)	0.09
Sc-45	0.87(49)	0.56	1.03(5)	0.05
Ti-48	2.3(14)	0.61	20.8(25)	0.12
V-50	1.88 (bl)	na	1.76(18)	0.10
V-51	4.94(134)	0.27	3.95(27)	0.07
Cr-50	1.1(4)	0.36	34.9(32)	0.09
Fe-56	0.90(47)	0.52	22.0(17)	0.08
Fe-57	1.83(109)	0.60	7.05(70)	0.10
Co-59	0.54(4)	0.07	1.39(7)	0.05
Cu-63	0.49(3)	0.06	722(47)	0.39

Target	**$\Gamma_{\gamma 0}$**	**$d\Gamma_{\gamma 0}$**	**D_0**	**dD_0**
	eV	%	**[eV]**	%
Cu-65	0.395((40)	0.10	1520(100)	0.07
Nb-93	0.173(40)	0.23	95.6(46)	0.05
Rh-103	0.173(70)	0.40	29.8(17)	0.06
Pd-105	0.1403(290)	0.21	10.9((5)	0.05
I-127	0.110(10)	0.09	12.5(10)	0.08
Cs-133	0.12(3)	0.25	20.0(9)	0.05
Ba-135	0.121(9)	0.07	40.0(30)	0.08
Ba-137	0.100(8)	0.08	260(40)	0.15
Nd-145	0.074(3)	0.04	17.8(7)	0.04
Eu-153	0.093(2)	0.02	1.14(8)	0.07
Mean rel. error		<0.29>		<0.11>

5.2 The THC database - ATLAS_THC_f(L)_1

The resulting database has been generated in EXCEL files in the following steps.

Firstly, a data matrix of transitions is formed using the available information on spin states which can be reached by pure dipole transitions neglecting the E2 admixture in M1 transitions. These data are extracted from the ENSDF compilation. The resulting list of primary transitions is then processed to extract the PSF - after having verified the placement of the transitions. Only transitions to levels with unique spin and parity assignment are used for validation purposes.

Each evaluated data file consists of two parts, the heading and the data: E_γ, PSF data (E1, M1, E2) with associated statistical errors and E_x, $J\pi$ columns. An example of the heading of the ^{32}P nuclide data file is shown with explanations in brackets:

P-32 ILL (*laboratory*)

Ig/100 captures taken from S.Michaelsen et al., Nucl.Phys. A501 (1989) 437 (*data source*)

Gg0 = 2 eV D0 = 54.9 keV (*used resonance parameters*)

Sum Ig = 98.4% (*the sum of Ig for all primary transitions*)

α = 0.98; (*the spin admixture factor derived from thermal cross-sections*)

α_i in Table 1 of the reference (*available information on partial α_i – values*)

E(gamma) E1 M1 E2 dE1 dM1 dE2 Ex Jpi

The complete EXCEL database is available either from the author or from the IAEA-NDS. The final version of the database will be made publicly available from the online database http://www-nds.iaea.org/PSFdatabase. Examples of data file contents can also be found in Section 2.

Plots of all the evaluated data are shown in the Appendix. [Note: Before continuing to the next subsection, it is recommended to get familiar with the graphical presentation in the Appendix, because some of the plot features will be used in the validation discussion].

6. Validation of thermal capture PSF data

The DRC PSFs are the only PSF data that can be derived from neutron capture experiments directly in absolute values. The validation against DRC data, therefore, is an important verification of the absolute THC data. To compensate for the large PT dispersion, the quasi mono-energetic $<f_L<E_\gamma>>$ is further averaged over the number of primary transitions found in a narrow energy window of about $E_\gamma = (6.5 \pm 0.5)$ MeV, which is also done in the DRC data processing.

As part of the validation of thermal data, the E1 systematics $<<f_L<E_\gamma>>_{6.5\ MeV}$ from both DRC and THC measurements are compared in Table 11. Note, however, that the E1 systematics for A < 50 nuclides is uncertain due to the limited accuracy of input data caused by the small number of resonances and often also by the non-statistical behaviour of transitions. Nuclides for which the E1 transitions have energies E_γ < 5 MeV are not considered. The E_γ^2 factor correction cannot be applied to these nuclides, because reaction mechanisms other than the E1 GRM may contribute or even dominate.

Table 11. Data from DRC and THC measurements used in the comparison and the resulting THC/DRC ratio for E1 and partly M1 transitions. The three nuclides (^{106}Pd, ^{146} Nd and ^{154}Eu) without absolute I_γ values have been normalized to the systematics.

f (E1, M1) SYS	the PSF values derived from the systematics in Ref. [7,11]
$<E_\gamma>$ E1/M1	mean E_γ of the $<E_\gamma>$ window
E1# M1#	number of transitions used for averaging
f(E1) TH $^{++}$	values with '++' are corrected to 6.5 MeV by $(<6.5>/<E_\gamma>)^2$ factor if $<E_\gamma>$ is outside the 6 – 7 MeV range corrected for the E_γ dependence

Product	**<α>**	**f(E1)**	**f(M1)**	**<E_γ>E1/M1**	**E1**	**M1**	**<f(E1)>**	**<f(M1)>**	**TH/SYS**	**TH/SYS**
nuclide		SYS	SYS	MeV	#	#	THC	THC	E1	M1
F-20	1	0.38	0.52	5.2/6.1	4	2	0.09(1) $^{++}$	0.13(2)	0.24	0.25
Na-24	0	0.50	0.57	/6.0	-	5		6.4(?)		11.2
Mg-25	1	0.53	0.58	/6.5	-	2		0.11(1)		0.19
Mg-26	0.07	0.54	0.59	/6.5	-	6		0.60(7)		0.98

Product	**<α>**	**f(E1)**	**f(M1)**	**<E_γ>E1/M1**	**E1**	**M1**	**<f(E1)>**	**<f(M1)>**	**TH/SYS**	**TH/SYS**
nuclide		SYS	SYS	MeV	#	#	THC	THC	E1	M1
Mg-27	1	0.55	0.60		-	-				
Al-28	0.67	0.63	0.61	/6.3	-	5		0.136(6)		0.22
Si-29	1	0.67	0.62		-	-				
Si-30	1	0.70	0.64	/6.8	-	2		0.058(4)		0.08
P-32	0.98	0.78	0.66	/6.4	-	2		0.58(8)		0.88
S-33	1	0.81	0.67		-	-				
Cl-36	1	0.93	0.69	/6.5	2	3	0.89(9)	0.32(1)	1.05	0.46
Cl-38	0.94	1.01	0.71	5.7	2	-	0.31(5) ++		0.31	
K-40	0.99	1.09	0.73	6.3	4	-	2.42(13)		2.22	
Ca-41	1	1.13	0.74	6.2	2	1	3.31(35)		2.93	
Sc-46	0.5	1.35	0.78	6.5	14	16	3.85(13)	2.46(11)	0.35	3.15
Ti-49	1	1.48	0.81	6.5	3	-	10.44(16)		7.05	
V-51	0.31	1.58	0.82	6.5	10	-	1.34(7)		1.14	
V-52	0.28	1.62	0.83	6.3	4	-	11.60(57)		0.14	
Cr-51	1	1.58	0.82	6.2	2	-	1.70(18)		1.08	
Fe-57	1	1.87	0.87	6.2	3	-	1.9(1)		0.98	
Fe-58	0.88	1.92	0.88	6.5	5	-	4.21(46)		0.45	
Co-60	0.71	2.02	0.89	6.5	11	-	3.39(23)		0.77	
Cu-64	0.5	2.23	0.92	6.5	13	-	2.31(6)		0.97	
Cu-66	0.51	2.33	0.93	6.5	9	-	3.60(8)		0.65	
Nb-94	0.52	3.99	1.11	6.3	2	-	3.7(2)		1.1	
Rh-104	1	4.66	1.17	6.9	5	-	2.47(21)		1.89	
Pd-106	0.48	4.79	1.18	6.7	8	-	*4.79*		*1*	
I-128	0.42	6.38	1.29	6.4	9	-	9.79(41)		0.65	
Cs-134	0.17	6.84	1.32	6.4	12	-	3.70(22)		1.85	
Ba-136	0.81	7.00	1.33	6.6	2	-	3.96(16)		1.77	
Ba-138	1	7.16	1.34	5.1	2	-	8.03(34) ++		0.87	
Nd-146	0.01	7.80	1.38	6.3	2	-	*7.80*		*1*	
Eu-154	1	8.45	1.42	6.3	6	-	*8.29*		*1*	

The ratio of $\langle f(E1)\rangle_{THC}$/ $\langle f(E1)\rangle_{DRC}$ is plotted in Fig. 15 as a function of the mass A. The trend line is reasonably close to unity with one strong outlier, ^{49}Ti. The larger dispersion observed for data with A < 60 could have two reasons: firstly the <f(E1)> systematics for light nuclei is less accurate and secondly non-statistical contributions may dominate the E1 strength.

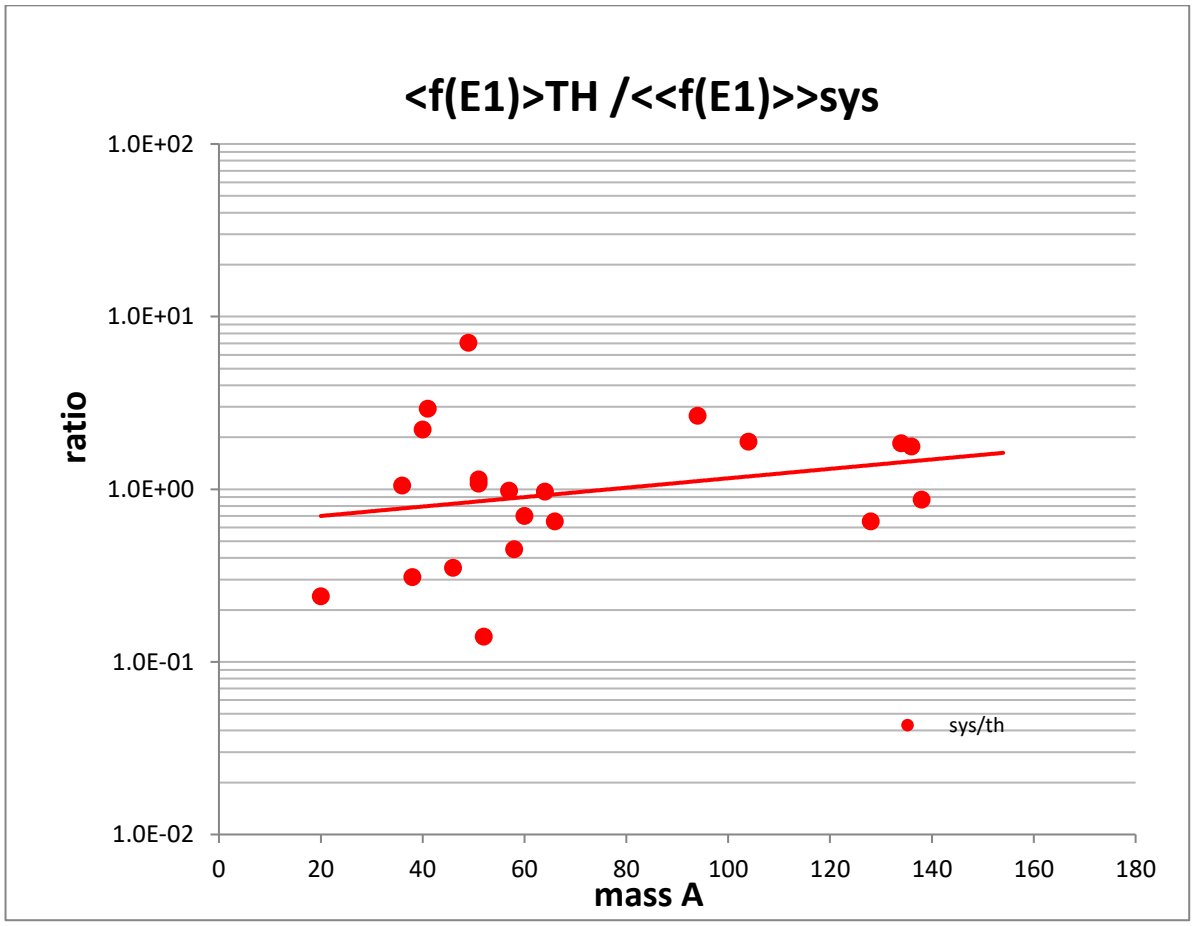

FIG. 15 *Ratio of binned <f(E1)> values from THC vs DRC are plotted for 20 nuclides with E1 transitions in the (6.5 ± 0.5) MeV energy window.*

Another way to compare the THC data with the DRC results is by a direct comparison of the <f(E1)> data as two independently processed and normalized data sets. This comparison is shown in Fig. 16 as a function of the mass A. The results show that the trends of the two data sets are rather similar, with the THC data being slightly more dispersed for low mass nuclides. It is worth noting that the general trend lines are almost identical. This is quite promising as it is additional evidence that the simplified approach adopted for THC processing generally gives PSF data compatible with the DRC results. It supports our belief that the individual systematic uncertainties in all three types of neutron capture PSF experiments do not disturb their average trend behaviour.

The additional systematic uncertainty due to the PT fluctuations is a combination of the statistical and $\Gamma_{\gamma 0}$ or D_0 errors. A conservative estimate gives a mean value of 30 – 40%. Other sources of uncertainty, difficult to quantify, may be the inner/outer final spin population (up to 100%), wrong J^{π} final spin assignments or experimentally unidentified problems.

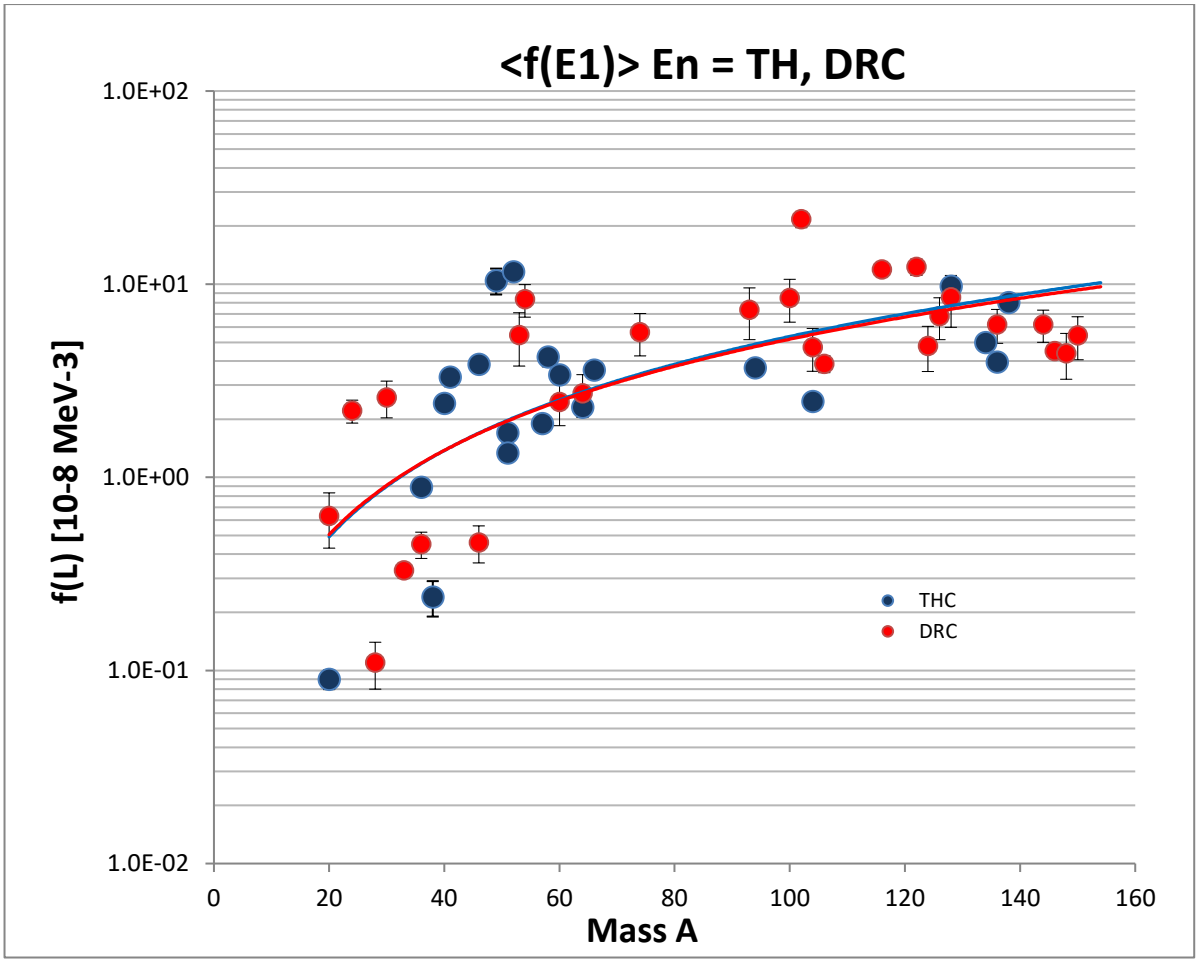

FIG. 16 *Binned <f(E1)> values from THC and DRC experiments are plotted for nuclides with E1 transitions in the (6.5 ± 0.5) MeV energy window. Note the large spread of the THC data for light nuclides.*

Several qualitative conclusions can be drawn from an inspection of the graphical representation of the derived PSF data and the fitted trend curves. Although the trend curves mainly serve as a guide to the eye, they also allow us to make some useful and relevant observations regarding the mean trend of both E1 and M1 strength distributions as a function of the transition energy E_γ.

The major observations are as follows:

1. The E1 strength of light nuclides (A < 50) disagrees with the prediction (both the strength and the energy dependence) of the E1GR model. There is a broad variation of the PSF strength among different nuclides, often much stronger than the GRM prediction. The reduced gamma-ray intensity, especially for E1 transitions, systematically enhances transitions to the high energy E_x states with decreasing E_γ energy ($E_\gamma \rightarrow 0$). This feature suggests the presence of another reaction mechanism, probably of a non-statistical nature and is discussed in detail in the conclusions and summary.
2. The distribution of the E1 PSF for nuclides with A > 50 starts to agree with predictions of the GRM (except for ^{58}Fe) and the <f(E1)> systematics prediction.
3. The energy dependence of the PSF for M1 radiation for all nuclides agrees with the general prediction of the QRPA model, increasing with decreasing energy $E_\gamma \rightarrow 0$.

   Only partial conclusions can be drawn on the absolute strength due to the broad energy

scatter of M1 data. The limited number of THC/DRC M1 ratios (see Table 11) gives $\langle f(M1)\rangle_{THC}/\langle f(M1)\rangle_{sys} = 1.93$ (60) and is derived from only 9 nuclides with $A \leq 46$, which is insufficient to make any conclusive statement. It should be noted that in light nuclides the enhancement of the M1 strength is less pronounced. This effect is discussed in the conclusions and summary section.

7. Conclusions and summary

7.1 General conclusions

The advantage of neutron thermal capture data for PSF applications is twofold. The high statistical accuracy of the measured spectra in combination with low-energy (measured with bent crystal spectrometer and single Ge(Li) crystal) and high-energy (measured with pair spectrometer) regions allows the determination of primary transitions in a very broad E_γ range from S_n down to 1 MeV. An important factor is that a complete decay scheme is formed with a maximal number of primary transitions forming ΣI_γ close to 100%. If this condition is not fulfilled, then either a number of primary transitions is missing or there is a systematic uncertainty in the absolute calibration.

The benefit of having THC data is not so much for the higher energies where the DRC and ARC measurements are by far superior due to their excellent averaging power and hence reduced PT fluctuations. It is mainly for lower excitations below 4 – 5 MeV where THC gives relevant and unique information that is not obtainable with DRC and ARC spectra due to the high detection threshold. Furthermore, thermal capture data are available for all stable isotopes and information from the binned high-energy E1 and M1 strengths can be used for those nuclides missing in the DRC+ARC Atlas.

7.2 Major observations

The PSF of 33 nuclides in the mass region $20 \leq A \leq 154$ were determined by means of a simplified processing of data, neglecting the capture state spin admixture. The results show that this omission has no influence and that a reasonable agreement with the DRC absolute normalization is achieved. The large systematic uncertainty effects are masking the spin admixture interference influence for most of the cases. The simplicity of this approach, in the way the input parameters are chosen, is a practical advantage which may help future evaluation plans.

The biggest challenge emerging from this work is to find the correct approach to determining the PSF for nuclides with $A < 50$. The enhancement of E1 transitions observed in many of the light nuclides calls for a different processing of PSFs using models other than the standard E1 GR model. The shell model may be a good candidate but also models considering the direct or semi-direct reaction mechanisms from the early seventies.

The signature feature of these latter models is the correlation between the (d,p) stripping strength $(2J+1)S_n$ and the reduced (n,γ) intensity $I_\gamma \cdot E_\gamma^{-L}$ to levels populated in both reactions. This method was used to study the ^{38}Cl nuclide in Ref. [36] where it was observed that the enhanced (n,γ) strengths for transitions to the high energy E_x levels reduce the correlation coefficient ρ from 0.95 to 0.49 for levels below and above E_x = 4.5 MeV, respectively. A marked improvement, however, was achieved by decreasing the exponent in the E1 phase space factor from E_γ^3 to $E_\gamma^{1.2}$, bringing the total correlation factor to $\rho = 0.98$. This observation formed the basis for developing the direct and semi-direct formalism with the E_γ^{-1} singularity [37,38]. It has been shown further that the large correlation ρ makes the resonance effects

negligible and gives an equal weight for the two channel spins. However, if there is a strong resonance close to the threshold it drastically affects the size of the direct component.

The M1 strength in light nuclides has been studied in Ref. [38] and was found that the semi-direct mechanism is also dominant in the case of a strong (d,p)(n,γ) intensities correlation. The M1 semi-direct strength is believed to be more important than the direct one because of the low excitation energy of the M1 (spin-flip) resonance, especially for nuclides with resonances far away from the threshold energy.

Based on all these observations, a new processing of light nuclides with A < 50 has to be developed. It seems reasonable, based on earlier studies of the (d,p)(n,γ) correlations [39-41], to postulate that the partial thermal cross section $\sigma(\gamma)_i$ is proportional to the single particle width Θ_f^2 and the sum of the non-statistical and statistical components and their interference. It is worth noting that these components have different gamma-ray energy dependences.

7.3 Future plans

We have two plans for THC data in the near future: the first one is to revisit and extend the analysis of the light nuclides as discussed above and verify the findings for different nonstatistical mechanisms from Refs. [37,38] and the general survey of Mughabghab [43]. Secondly, and very importantly, the validation of the new processing will be performed by a thorough comparison of all these data against theoretical models. Such a comparison may give us further insight into and improve our understanding of PSFs for light nuclei which may in turn lead to new ideas for further experimental or theoretical work in the future.
Besides THC data, a next step may be a continuation of the PSF analysis for heavy nuclides with A ≥ 155.

Acknowledgments

This work pays a tribute to all my former colleagues of the Neutron Nuclear Physics group at the RCN (later ECN) in Petten, for their unique and outstanding experiments with polarized thermal neutrons and polarized (aligned) targets.

Further thanks go to Stephane Goriely, for his support of the idea to look at the thermal neutron capture data for PSF applications. Many comments of Vivian Dimitriou concerning the manuscript are highly appreciated.

The IAEA NDS is thanked as a supporting institution.

References

[1] G A. Bartholomew et al., Adv. Nucl. Phys. 7 (1973) 229
[2] L.M. Bollinger and G.E. Thomas, Phys. Rev. C2 (1970) 1951
[3] L.M. Bollinger, "*Photonuclear Reactions and Applications*" Pacific Grove, California (1973) 783
[4] C.M. McCullagh, M. Stelts and R.E. Chrien, Phys. Rev. C23 (1981) 1394
[5] R. Greenwood and R. E. Chrien, Nucl. Instr. Meth. 138 (1976) 125
[6] J. Kopecky and M. Uhl, "*Present status of experimental gamma-ray strength functions*" ECN-RX-94-103, ECN (1994)
[7] S. Goriely et al., Eur. Phys. J. A 55:172 (2019)
[8] C.E. Porter and R.G. Thomas, Phys. Rev. 104 (1956) 483
[9] J. Kopecky, "*Atlas of average resonance capture data (Starter file)*", INDC(NED)- 0772 (2017)
[10] J. Kopecky, "*Revisions and Updates of Experimental Gamma-ray Strength Functions derived from the Discrete Neutron Resonance Capture*", INDC(NDS)-0738 (2018)

[11] J. Kopecky and S. Goriely, *"Strength Functions derived from the Discrete and Average Resonance capture",* INDC(NDS)-0790 (2019)
[12] S.F. Mughabghab "Atlas of Neutron Resonances" (Academic Press 1981, 1984)
[13] S.F. Mughabghab "Atlas of Neutron Resonances" (Elsevier 2006)
[14] S.F. Mughabghab "Atlas of Neutron Resonances" (Elsevier 2018)
[15] H.I. Liou et al., Nucl. Sci. Eng. 67(1978) 326
[16] J. Bosman and H. Postma, Nucl. Instr. Meth. 148 (1978) 331
[17] J. Kopecky et al., Nucl. Phys. A427 (1984) 413 *Co-60*
[18] M.G. Delfini et al., Nucl. Phys. A404 (1983) 250 *Cu-66*
[19] A.J. Ferguson, "*Angular Correlation Methods in Gamma-ray Spectroscopy*" (North-Holland Publ. Co., Amsterdam, 1965)
[20] H.I. Liou et al., Nucl. Phys. A337 (1980) 401 *Sc-46*
[21] T.A.A. Tielens et al., Nucl. Phys. A403 (1983) 13 *Na-24*
[22] J. de Boer et al., Nucl. Phys. A352 (1981) 125 45 *P-32*
[23] J.B.M. de Haas et al., Nucl. Phys. A419 (1984) 101 *V-52*
[24] P.P.J. Delheij et al., Nucl. Phys. A341 (1980) 45 *Mn-56*
[25] J. Kopecky et al., Nucl. Phys. A215 (1973) 415 *Fe-56*
[26] M.G. Delfini et al., Nucl. Phys. A404 (1983) 225 *Cu-63*
[27] L.M. Bollinger, Phys. Rev. C3 (1971) 2071
[28] M.L. Stelts, "*Nuclear Cross Sections for Technology*" (Knoxwille Conf.) Nat. Bur. of Stds.Sp.Publ.594, (1980) 936; R.E. Chrien, "*Neutron-Capture Gamma-Ray Spectroscopy and related Topics, Physics Conf. Series No 62*", (The Inst. of Phys., Bristol and London) 1982, 342
[29] M.A. Islam et al., Z. Phys. A335 (1990) 173 *I-128*
[30] A.M.J. Spits and J. Kopecky, Nucl. Phys. A264 (1976) 63 *Cl-36*
[31] R.E. Chrien and J. Kopecky, Phys. Rev. Lett. 39(1977) 911
[32] S. Goriely et al., Phys. Rev. C94 (2016) 044306
[33] R. Vennink et al., Nucl. Phys. A344 (1980) 421 *Fe-57, Fe-58*
[34] R.E. Chrien et al., Phys. Rev. C1 (1970) 973
[35] R.I. Schermer, Phys. Rev. 130 (1963) 1907
[36] A.M.J. Spits and J.A. Akkermans, Nucl. Phys. A215 (1973) 260
[37] J. Kopecky, A.M.J. Spits and A.M. Lane, Phys. Lett. 49B (1974) 323
[38] C.F. Clement, A.M. Lane and J. Kopecky, Phys. Lett. 71B (1977) 10
[39] J. Kopecky, "*Analysis of the Non-statistical Effects in the (n,γ) Reaction in the Mass Region A = 40-70*", RCN Report RCN-73-003 (1973)
[40] J. Kopecky, "*Analysis of the Non-statistical Effects in the (n,γ) Reaction in the Mass Region A = 24-80*", RCN Report RCN-73-094 (1973)
[41] J. Kopecky and A.M.J. Spits, "*Some Features of the Correlation between the (d,p) and (n,γ) reduced Widths*", RCN Report RCN-74-055 (1974)
[42] D.R. Tiley et al., Nucl. Phys. A636 (1998) 249
[43] S.F. Mughabghab, "*Non-statistical effects in neutron capture",* III. International School on Neutron Physics, Alushta (The Crimea) USSR April 19-30, 197

APPENDIX 1

ATLAS_TH data (graphical presentation)

Evaluated database

This section includes the graphical presentation of E1 and M1 strength functions from thermal capture data (for evaluated nuclides see Table 9. The standard processing, employing Eq. (2), has been applied with $\Gamma_{\gamma 0}$ and D_0 values (see Table 9). In this approach the branching ratio of capture spins for odd targets is not used as a parameter and the situation is assumed to be comparable to the ARC measurements. Each nuclide has the basic information shown in the heading, which includes the laboratory name where the measurement was taken, the source reference, values of used $\Gamma_{\gamma 0}$ and D_0 parameters and finally the fraction of included primary transition intensities ΣI_γ (%). Further the information on the state of the capture state spins and their admixture is added.

Plots have been generated in the Excel files and include unweighted trend curves in the power format. These curves only serve to guide the eye over the mean data trend and should not be considered as a quantitative result. Especially when the number of data points is small and/or scattered or concentrated in a narrow energy region, the resulting curve may be rather misleading. The <f(E1)> systematics at (6.5 ± 0.5 MeV) [7,11] are included in all the plots dotted green curves) for comparisons with the THC data. Despite the large data spread (only from Porter-Thomas fluctuations the estimate of the dispersion for a single resonance capture is $1+dPT = \sqrt{2}/\upsilon = 2.4$ which is quite large), the trend curves seem to have qualitatively the energy dependence of PSF data something that can be used to compare with different model predictions.

The author's explanatory comments to some specific data features or discrepancies are given separately below the figure captions. If the DRC measurement is available, the comparison plot includes both data for validation purposes. The DRC data are the only PSF data with absolute calibration contrary to the ARC data and that was the reason we only used them as a validation tool. Another way to validate the THC data is by comparing them with the systematics <f(E1)> curve.

Experiments with polarized neutrons and/or targets, which give information on the partial spin admixtures α_i, are included in the heading with the link to the corresponding table in the reference.

—F-20—

F-20 Los Alamos

Ig/100 captures taken from S. Raman et al. Phys.Rev. C53 (1996) 616
Gg0 = 1.5 eV (negative resonance) D0 =343 keV (estimate)
Sum Ig = 99.7 %
$\alpha = 1$

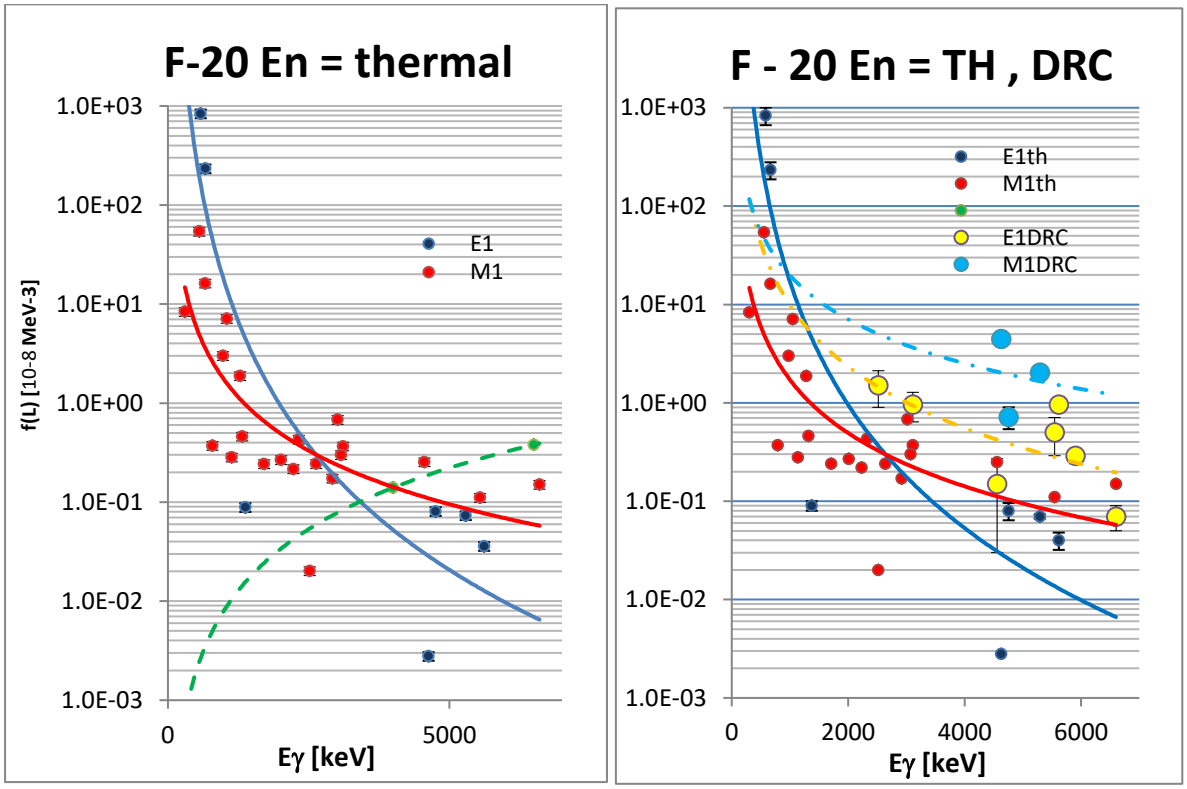

FIG. A.1 left *f(E1) and f(M1) data points (blue and red) are plotted with unweighted trend curves. The dotted green line is the <f(E1)> systematics with the assumed E_γ^2 dependence.* ***right*** *f(E1) and f(M1) data points (blue and red) are plotted with unweighted trend curves. The dash-dotted lines are E1 (blue curve/yellow points) and M1 (red curve/light blue points) trend curves to DRC experimental data.*

The DRC data originate from the p-wave capture in two resonances with a strong non statistical character for both E1 and M1 DRC data [42]. This may explain the outlying E1 and especially M1 strength against the TH capture from s-wave resonances.

——Na-24—

Na-24 ECN

Ig/100 captures taken from T.A.A. Thielens et al., Nucl.Phys. A403 (1983) 13
Gg0 = 0.34 eV (unweighted mean) D0 = 122 keV
Sum Ig = 100% based on imposed condition ΣEγIγ = 100Q
α = 0;
α_t in Table 4 of the reference

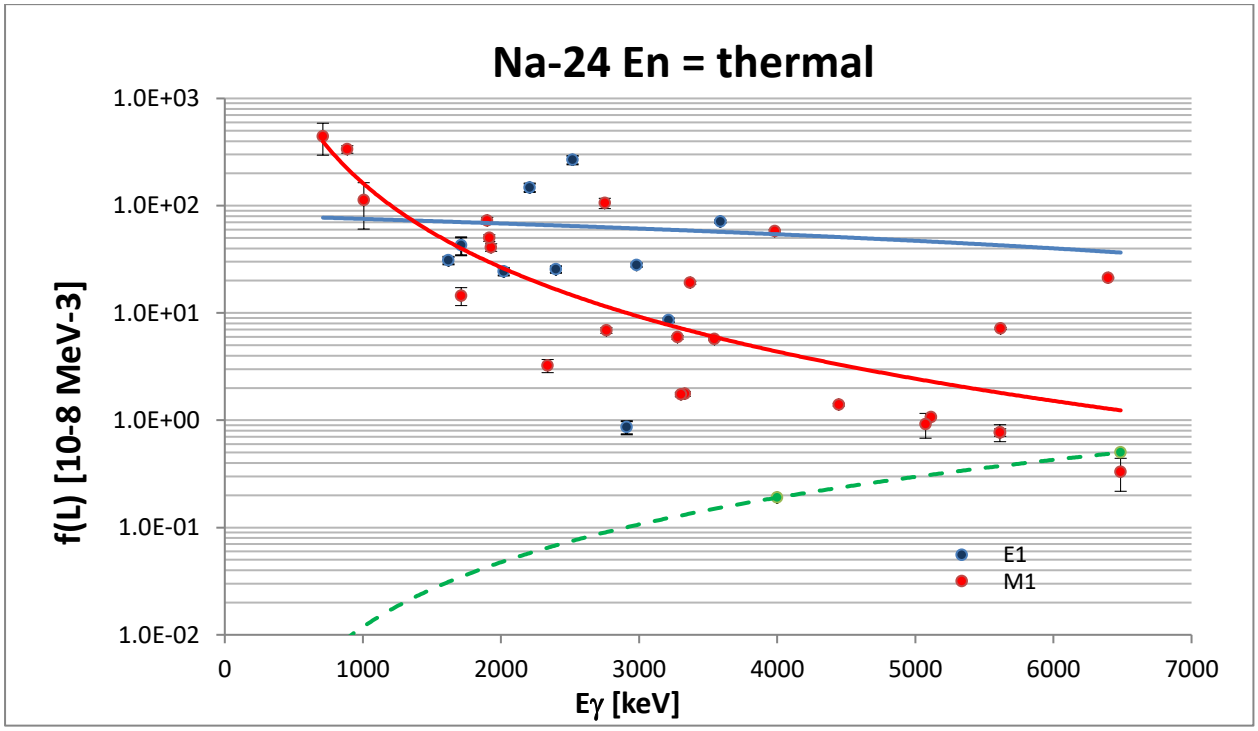

FIG. A.2 *f(E1) and f(M1) data points (blue and red) are plotted with unweighted trend curves. The dotted green line is the <f(E1)> systematics with the assumed* E_γ^2 *dependence.*

—Mg-25—

Mg-25 LANL

Ig/100 captures taken from T.A. Walkiewicz et al. Phys.Rev. C45 (1992) 1597
Gg0 = 8 eV (negative resonance) D0 = 709 keV (estimate from 4 s-wave res.)
Sum Ig = 101.3%
α = 1;

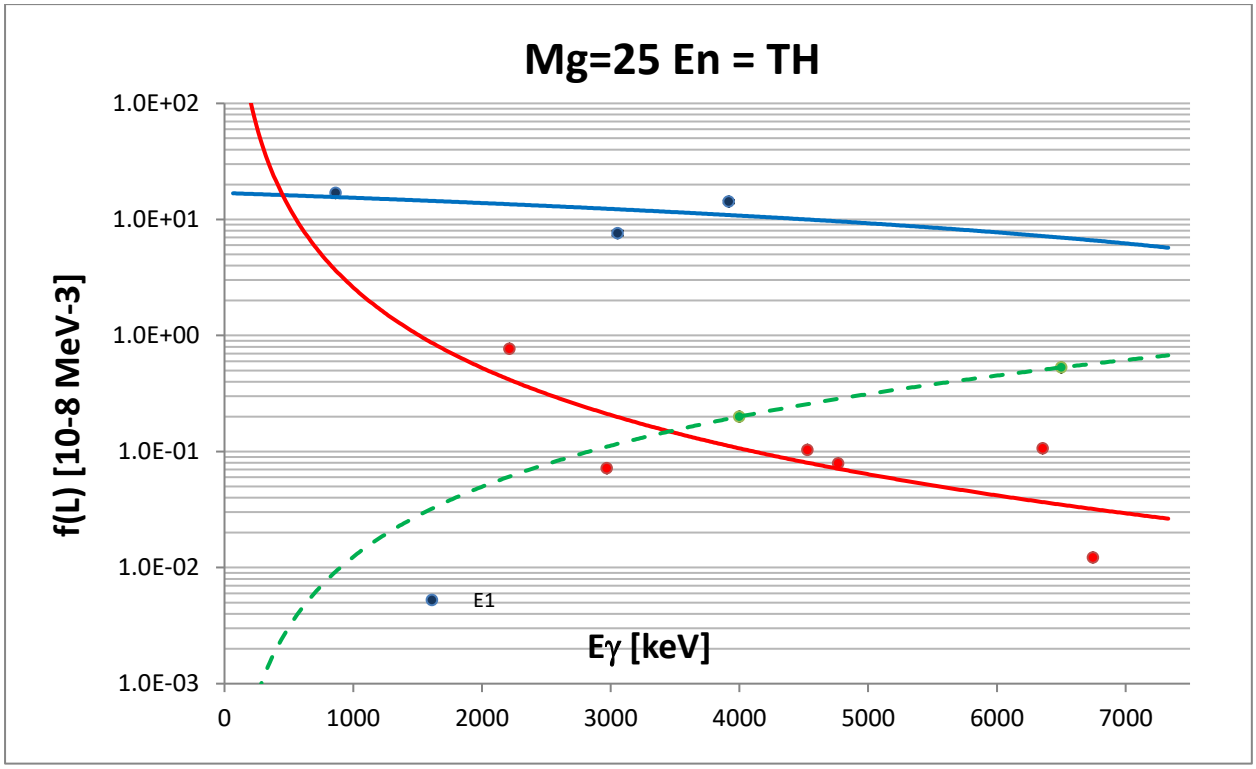

FIG. A.3 *f(E1) and f(M1) data points (blue and red) are plotted with unweighted trend curves. The dotted green line is the <f(E1)> systematics with the assumed* E_γ^2 *dependence.*

—Mg-26—

Mg-26 LANL

Ig/100 captures from T.A. Walkiewicz et al. Phys.Rev. C45 (1992) 1597
Gg0 = 1.6 eV (1. res.) D0 = 22 keV (estimate from 5 s-wave res.)
Sum Ig = 86.5%
α = 0.07;

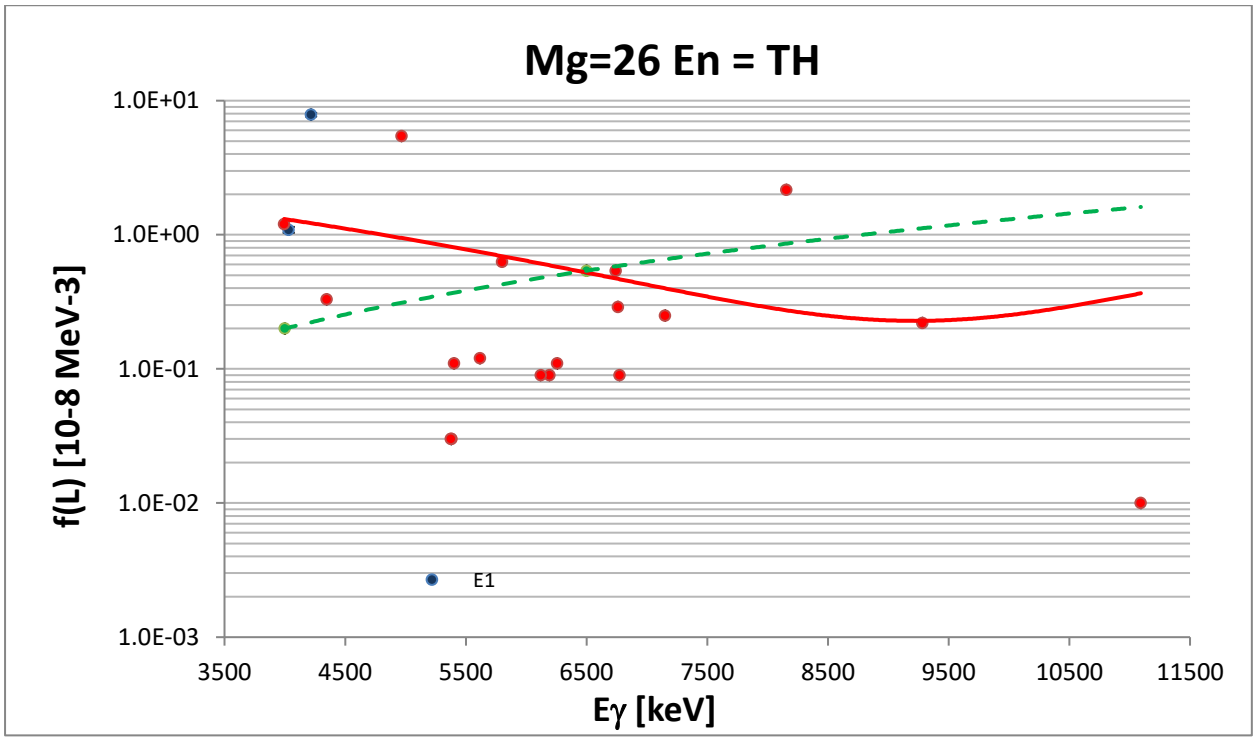

FIG. A.4 *f(E1) and f(M1) data points (blue and red) are plotted with unweighted trend curves. The dotted green line is the <f(E1)> systematics with the assumed* E_γ^2 *dependence.*

—Mg-27—

Mg-27 LANL

Ig/100 captures from from T.A. Walkiewicz et al. Phys.Rev. C45 (1992) 1597
Gg0 = 8 eV (negative resonance) D0 = 709 keV (estimate from 4 s-wave res.)
Sum Ig = 101.3%
α = 1;

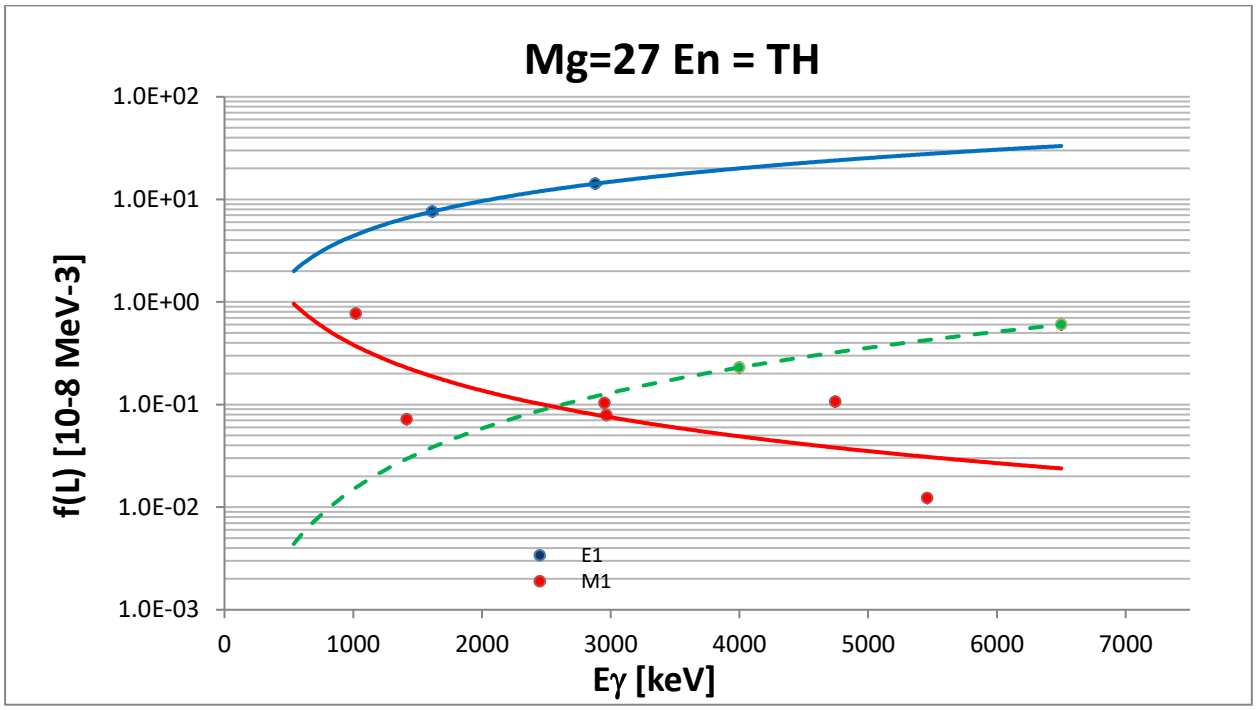

FIG. A.5 *f(E1) and f(M1) data points (blue and red) are plotted with unweighted power trend curves. The dotted green line is the <f(E1)> systematics with the assumed* E_γ^2 *dependence.*

—Al-28—

Al-28 ILL Grenoble

Ig/100 captures taken from H.H. Schmidt et al., Phys.Rev. C25 (1982) 2888

Gg0 = 1.61 eV D0 = 53000 eV

Sum Ig = 100%

α = 0.67;

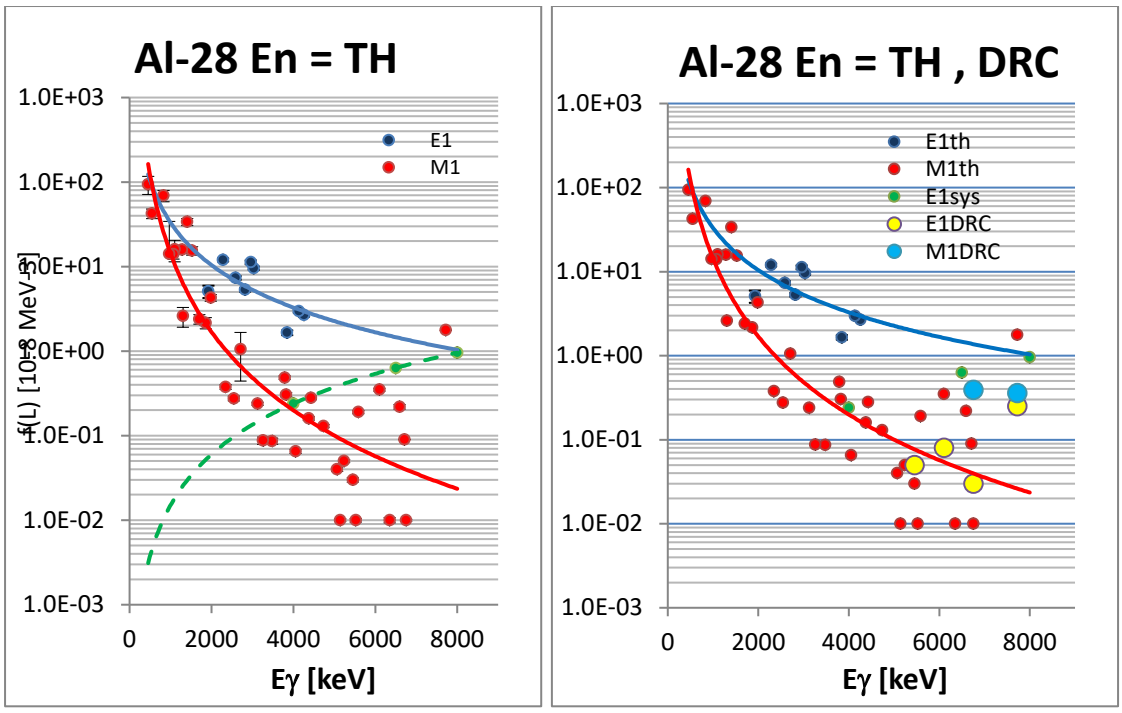

FIG. A.6 left *f(E1) and f(M1) data points (blue and red) are plotted with unweighted trend curves. The dotted green line is the <f(E1)> systematics with the assumed* E_γ^2 *dependence.* ***right*** *The DRC E1(yellow points) and M1 (light blue points) data are shown. No trend curves to DRC experimental data are plotted (E1 data are from one p-wave resonance and M1 data from one s-wave resonance).*

—Si-29—

Si-29 McMaster

Ig/100 captures taken from M.A. Islam et al. Phys.Rev. C41 (1990) 1272
Gg0 = 0.44 eV (negative resonance) D0 = 332 keV
Sum Ig = 99.3%
α = 1;

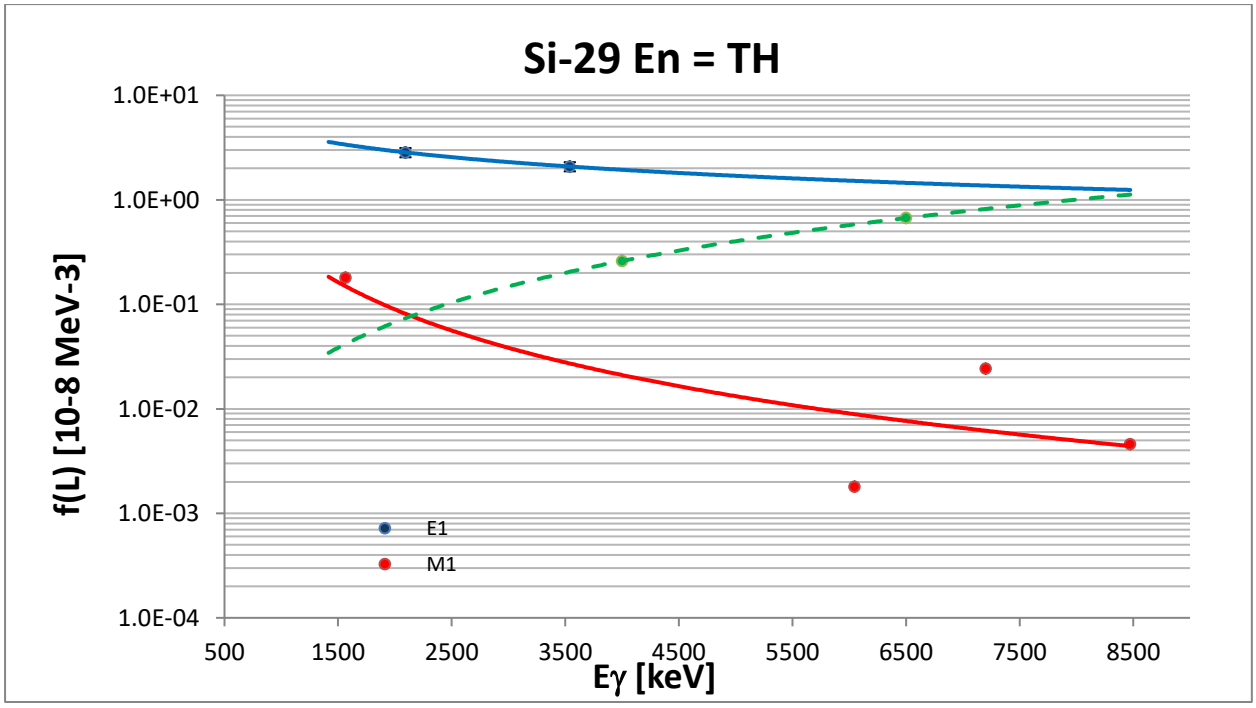

FIG. A.7 *f(E1) and f(M1) data points (blue and red) are plotted with unweighted trend lines. The dotted green line is the <f(E1)> systematics with the assumed E_γ^2 dependence.*

—Si-30—

Si-30 McMaster

Ig/100 captures taken from M.A. Islam et al. Phys.Rev. C41 (1990) 1272
Gg0 = 3 eV (negative resonance) D0 = 33s9 keV (estimate 3 s- resonances)
Sum Ig = 99.9%
α = 1;

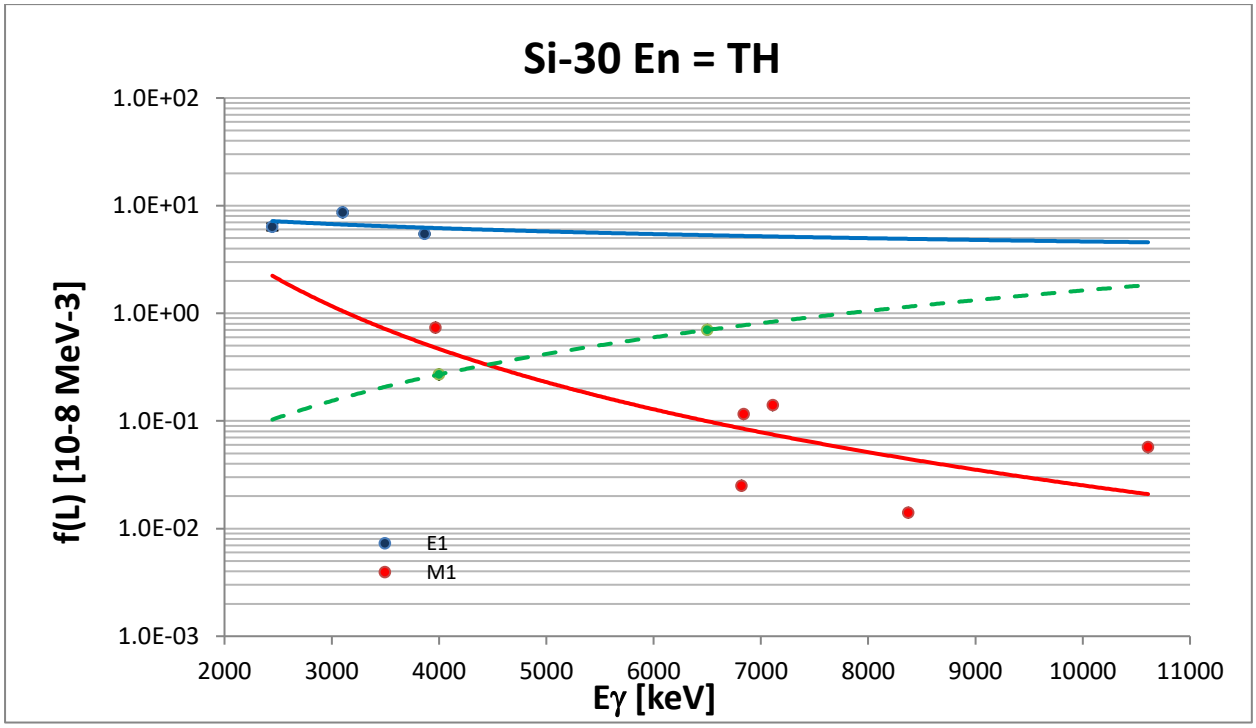

FIG. A.8 *f(E1) and f(M1) data points (blue and red) are plotted with unweighted trend lines. The dotted green line is the <f(E1)> systematics with the assumed* E_γ^2 *dependence.*

—P-32—

P-32 ILL

Ig/100 captures taken from S.Michaelsen et al., Nucl.Phys. A501 (1989) 437
Gg0 = 2 eV D0 = 54.9 keV
Sum Ig = 98.4%
α = 0.98;
α_i in Table 1 of the reference

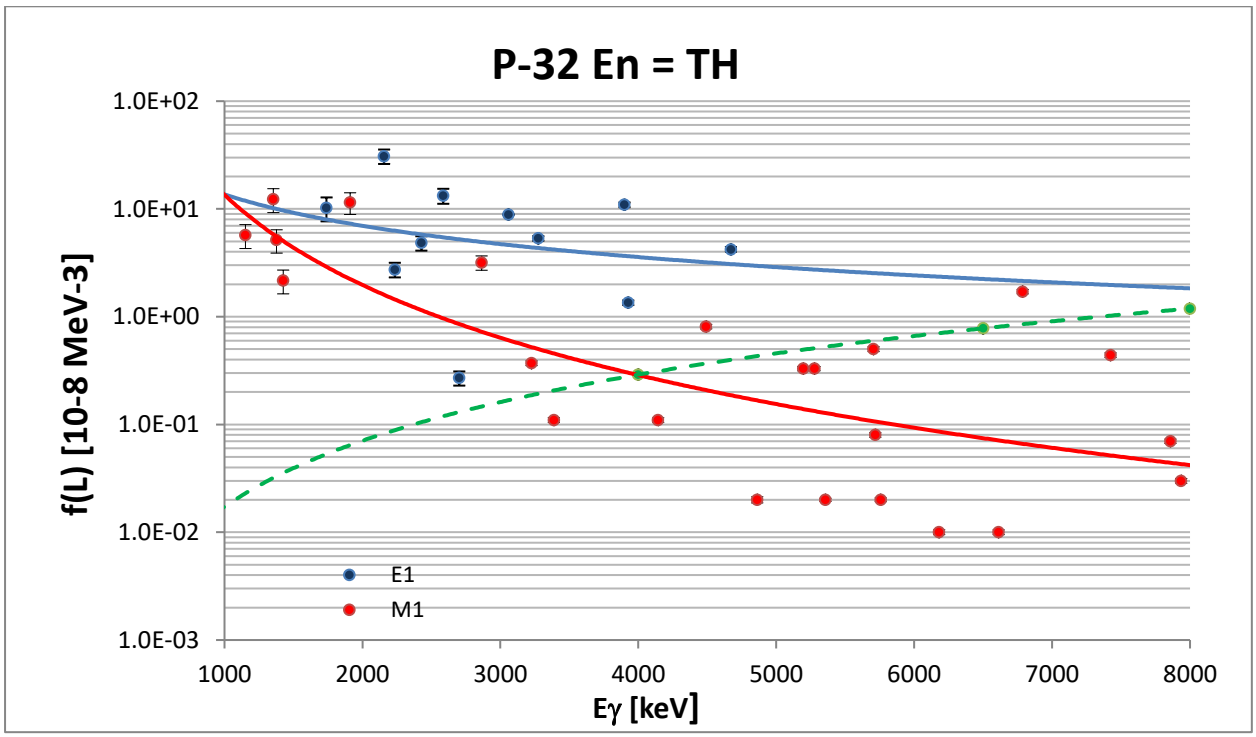

FIG. A.9 *f(E1) and f(M1) data points (blue and red) are plotted with unweighted trend curves. The dotted green line is the <f(E1)> systematics with the assumed E_γ^2 dependence.*

—S-33—

S-33 MacMaster

Ig/100 captures from J. Kennett et al. Z. Phys. A 322 (1985) 121
Gg0 = 2.15 eV D0 = 179 keV
Sum Ig = 99.2%
α = 1;

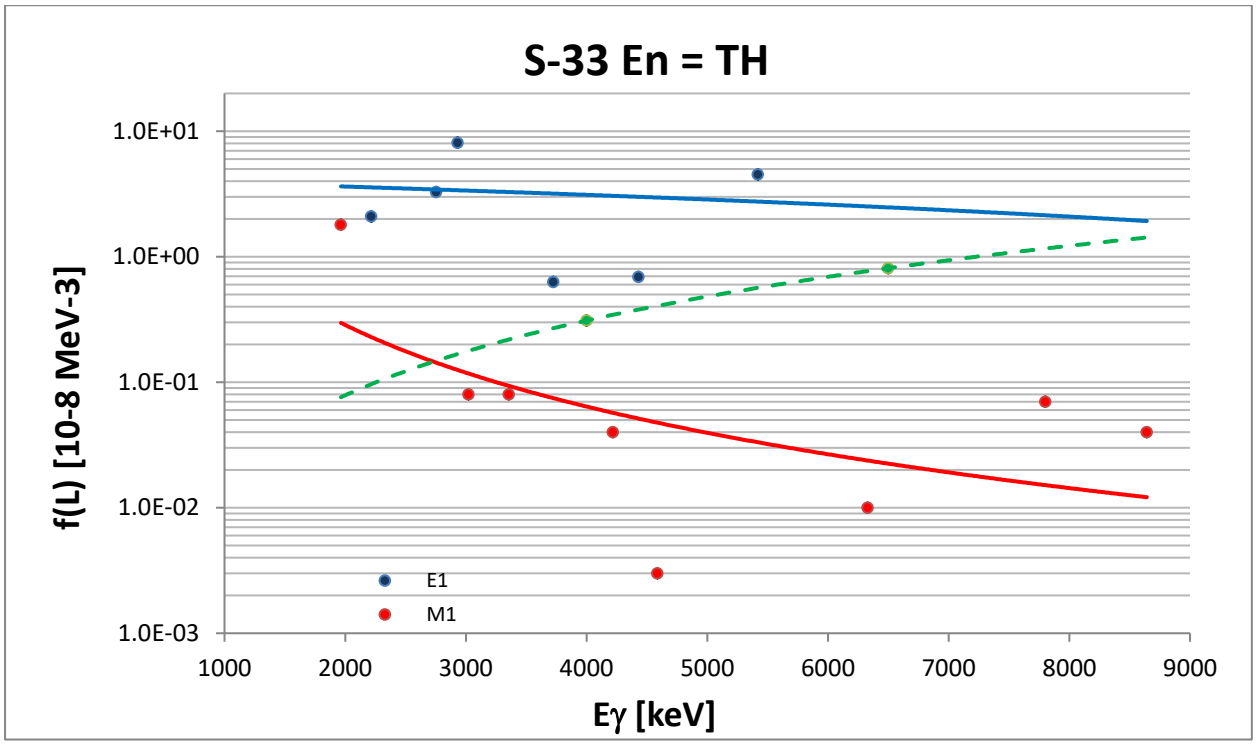

FIG. A.10 *f(E1) and f(M1) data points (blue and red) are plotted with unweighted trend curves. The dotted green line is the <f(E1)> systematics with the assumed E_γ^2 dependence.*

––Cl-36––

Cl-36 ECN

Ig/100 captures from A.M.J. Spits and J. Kopecky, Nucl.Phys. A264 (1976) 63
Gg0 = 0.542 eV D0 = 22300 eV
Sum Ig = 0.94%
α = 1;

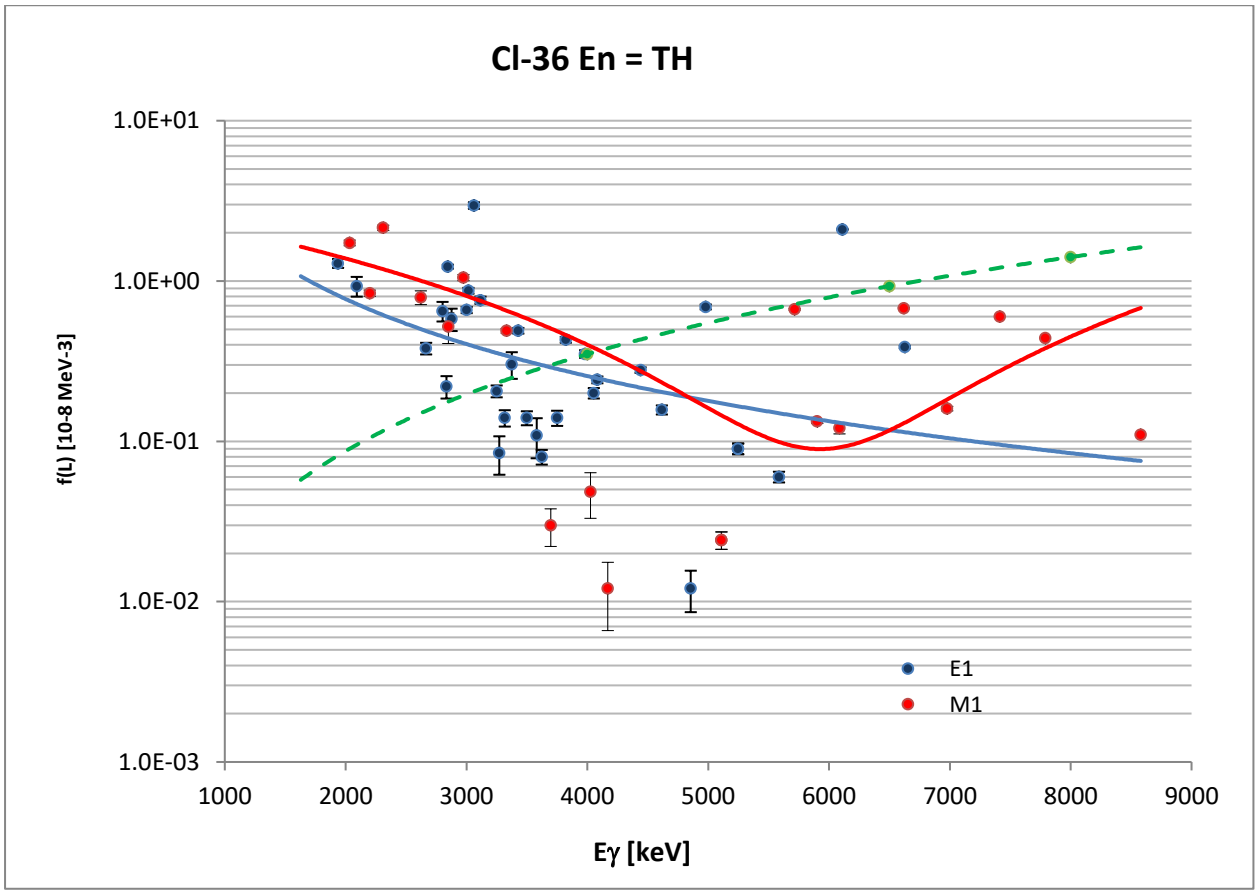

FIG. A.11 *f(E1) and f(M1) data points (blue and red) are plotted with unweighted trend curves. The dotted green line is the <f(E1)> systematics with the assumed E_γ^2 dependence.*

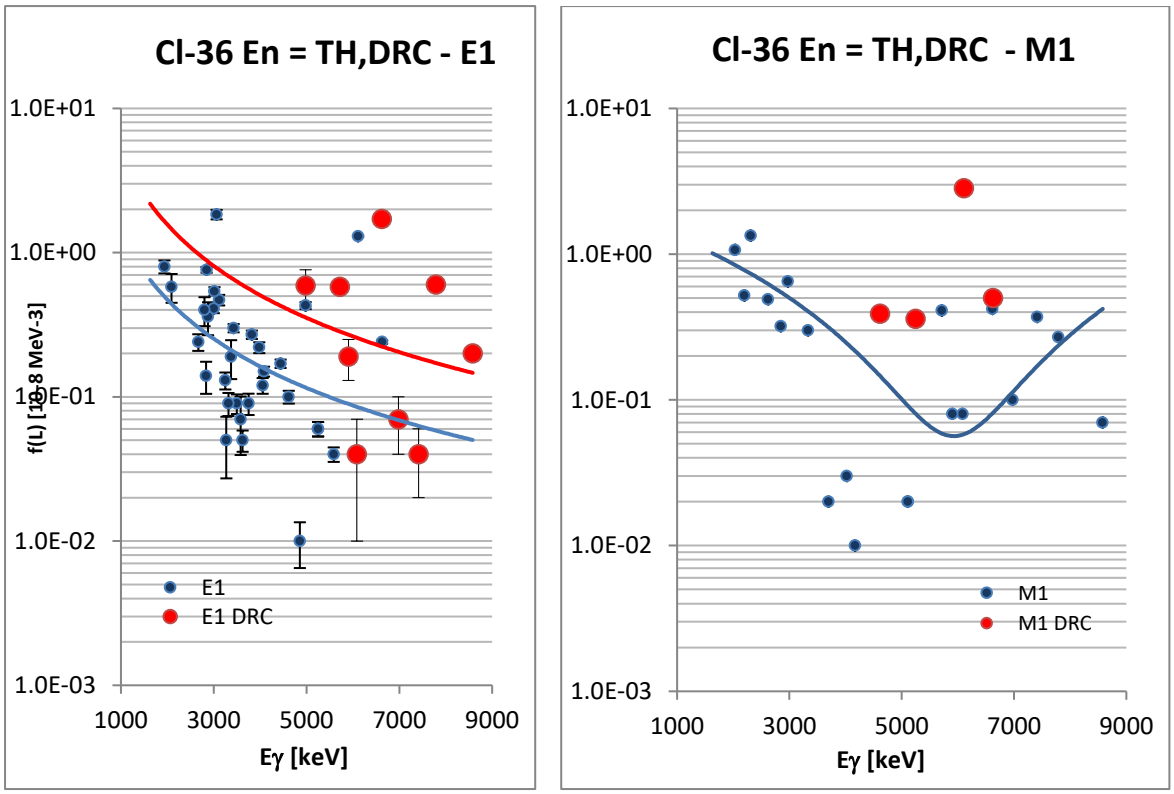

FIG. A.12 *f(E1) and f(M1) data points from THC and DRC measurements are plotted separately in two plots with unweighted trend lines. The DRC data originate from 1 p-wave resonance.*

—Cl-38—

Cl-38 ECN

Ig/100 captures from A.M.J. Spits and J.A. Akkermans Nucl.Phys. A215 (1973) 260
Gg0 = 0.201eV (neg.res.) D0 = 27.2 keV (estimate from 6 s-wave res.)
Sum Ig = 91.7%
α = 0.19

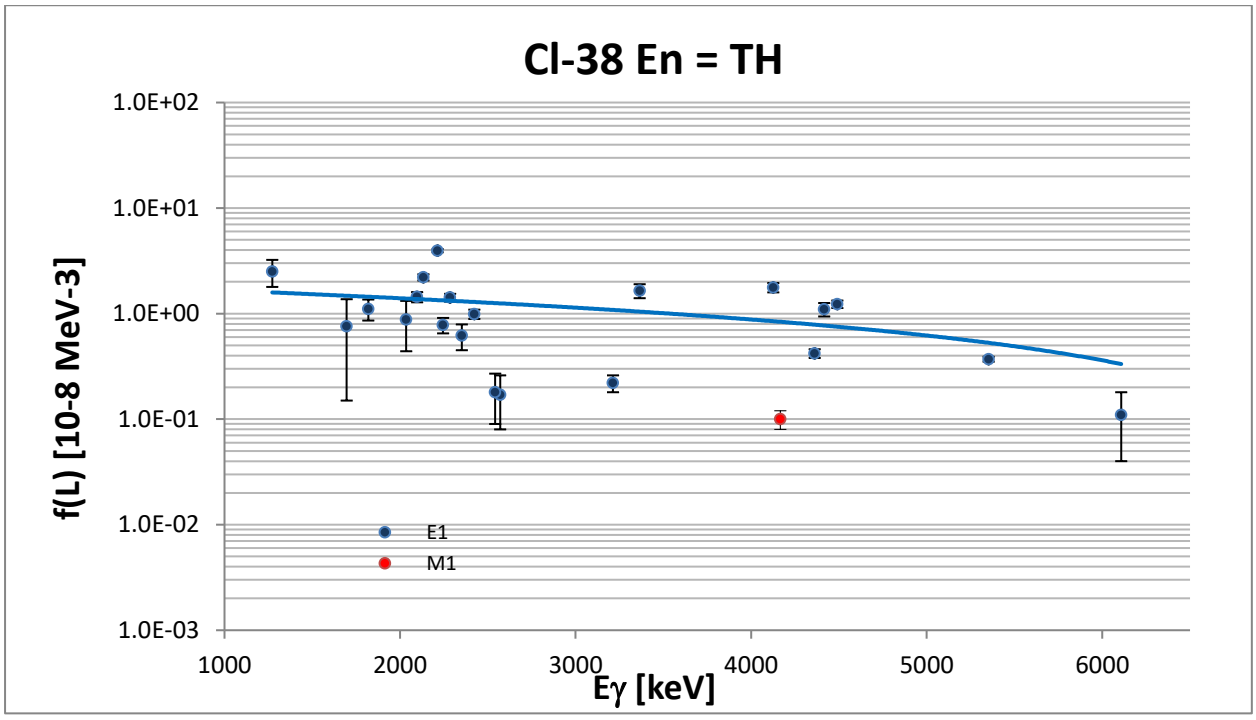

FIG. A.13 *f(E1) and f(M1) data points (blue and red) are plotted with unweighted trend lines. The dotted green line is the <f(E1)> systematics with the assumed E_γ^2 dependence.*

—K-40—

K-40 ILL

Ig/100 captures extracted from T. von Egidy et al., J. Phys. G 10 (1984) 221

Gg0 = 1.0 eV D0 = 8 keV

Sum Ig = 92.4%

α = 0.99;

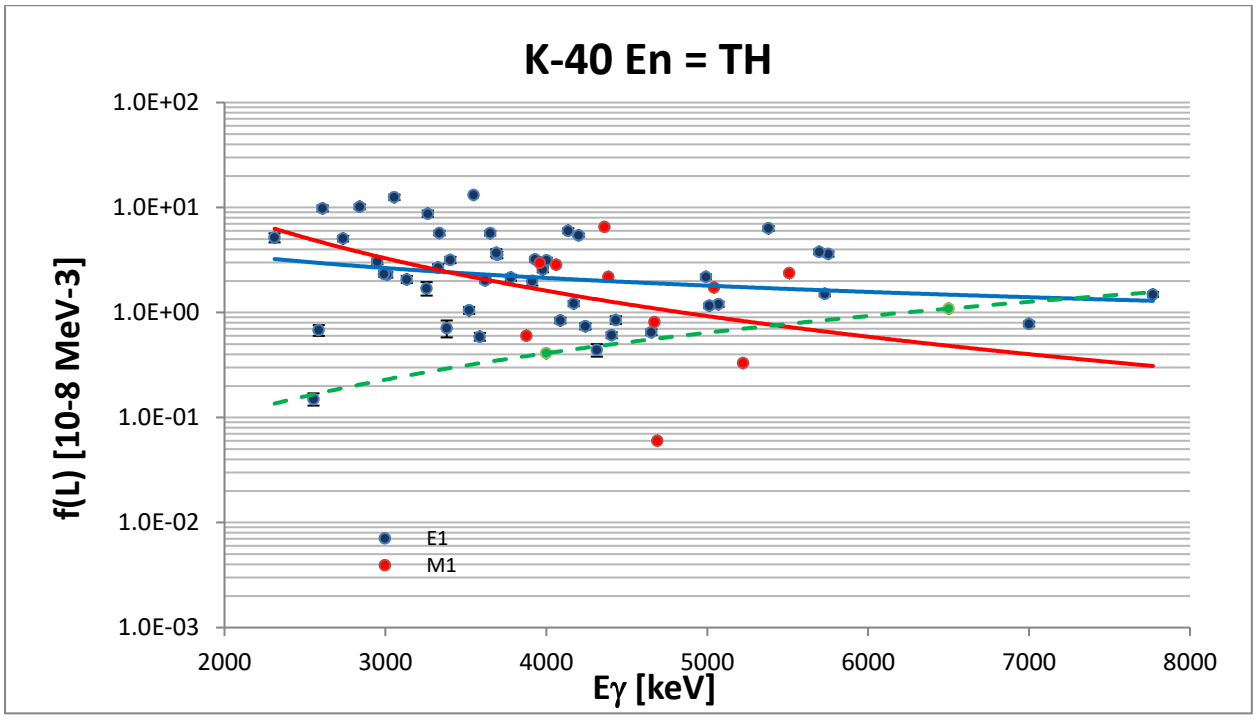

FIG. A.14 *f(E1) and f(M1) data points (blue and red) are plotted with unweighted trend lines. The dotted green line is the <f(E1)> systematics with the assumed E_γ^2 dependence.*

—Ca-41—

Ca-41 ECN

Ig/100 captures from H. Gruppelaar and P. Spiling, Nucl.Phys. A102 (1967) 226
Gg0 = 1.5 eV D0 = 45 keV
Sum Ig = 85.9%
α = 1;

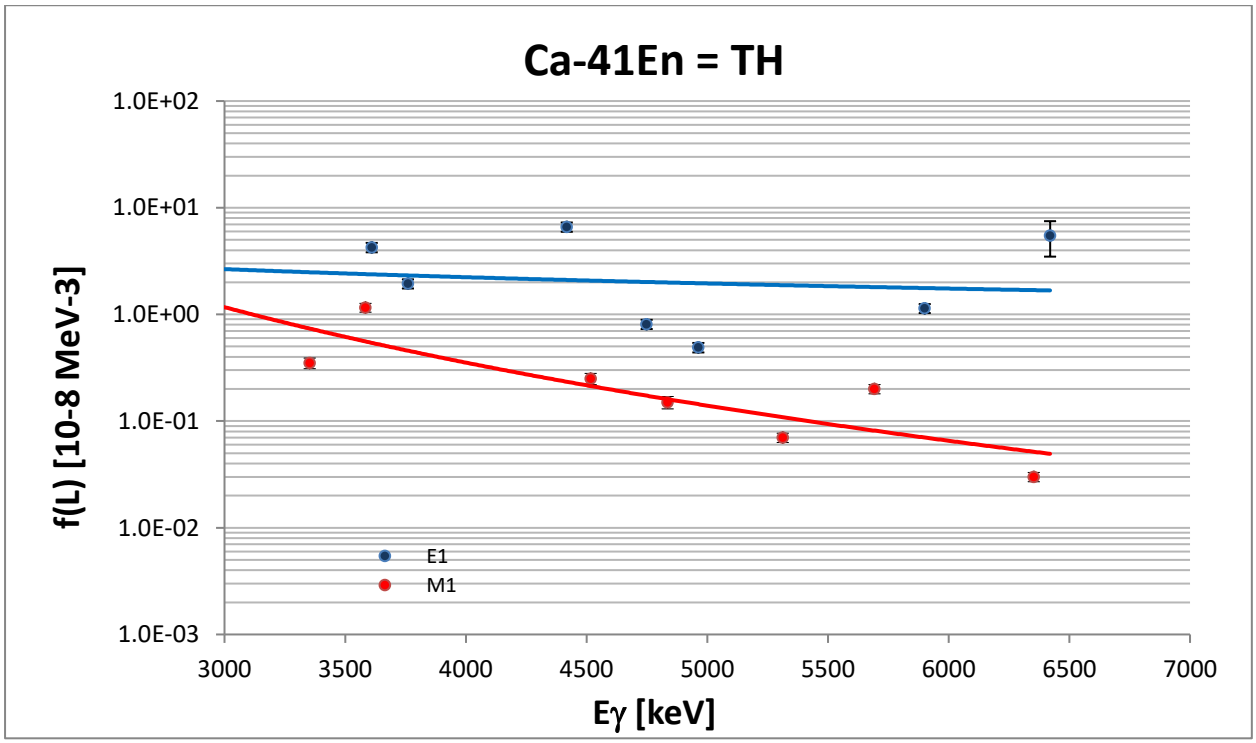

FIG. A.15 *f(E1) and f(M1) data points (blue and red) are plotted with unweighted trend lines. The dotted green line is the <f(E1)> systematics with the assumed* E_γ^2 *dependence.*

––Sc-46––

Sc-46 ECN

Ig/100 captures from T.A.A Tielens et al., Nuvl.Phys.A376 (1982) 421
Gg0 = 27.2 eV D0 = 1030 eV
Sum Ig = 100% based on imposed condition $\Sigma E\gamma I\gamma = 100Q$
α = 0.98;
α_i in Table 1 of the reference

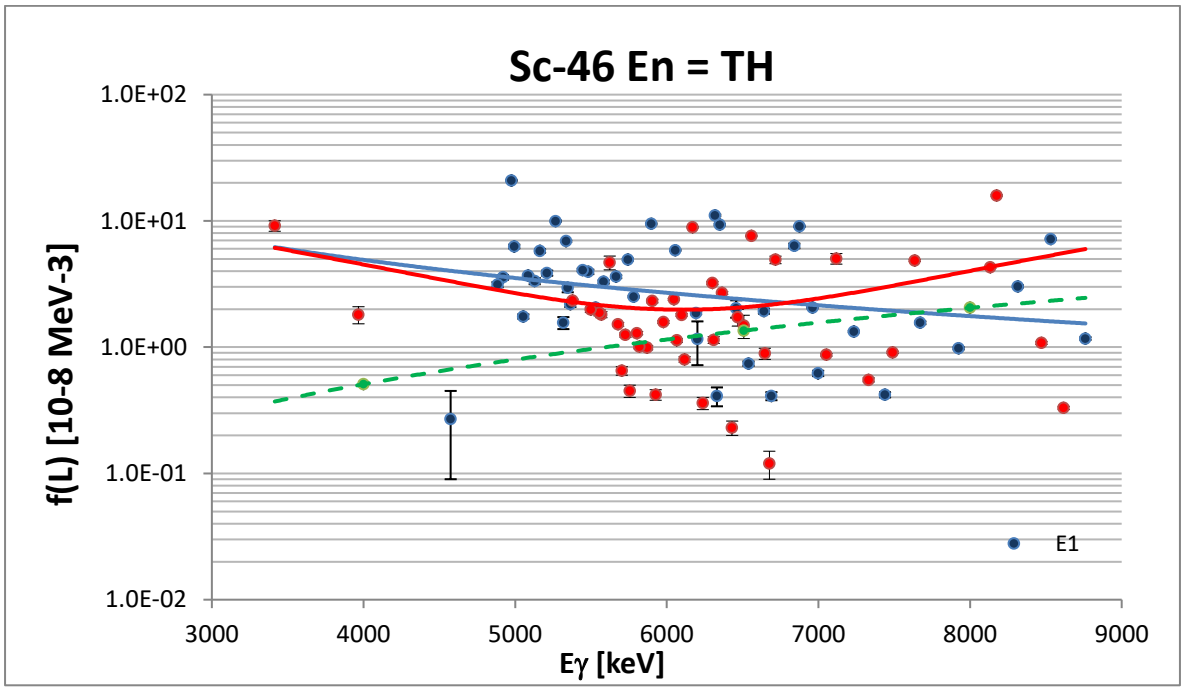

FIG. A.16 *f(E1) and f(M1) data points (blue and red) are plotted with unweighted trend lines. The dotted green line is the <f(E1)> systematics with the assumed E_γ^2 dependence.*

—Ti-49—

Ti-49 ECN

Ig/100 captures from J.F.A.G. Ruyl an P.M. Endt, Nucl. Phys. A407 (1983) 60
Gg0 = 2.3 eV D0 = 20.8 keV
Sum Ig = 99.0%
α = 1;

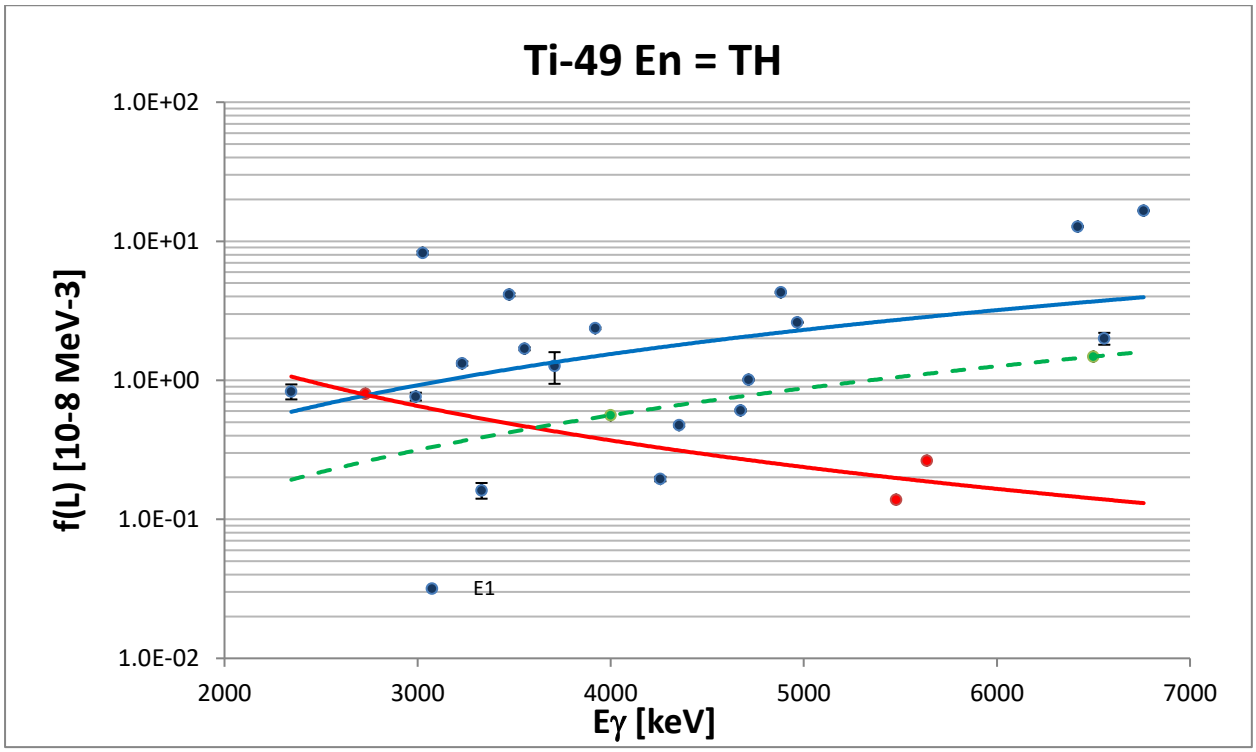

FIG. A.17 *f(E1) and f(M1) data points (blue and red) are plotted with unweighted trend lines. The dotted green line is the <f(E1)> systematics with the assumed* E_γ^2 *dependence.*

—V-51—

V-51 ILL

Ig/100 captures from S. Michaelsen et al., Z.Phys. A 338 (1991) 371
Gg0 = 0.60 eV (1.67 keV res. D0 = 1760 eV
Sum Ig = 69.5%
α = 0.28;
α_i in Table 1 of the reference

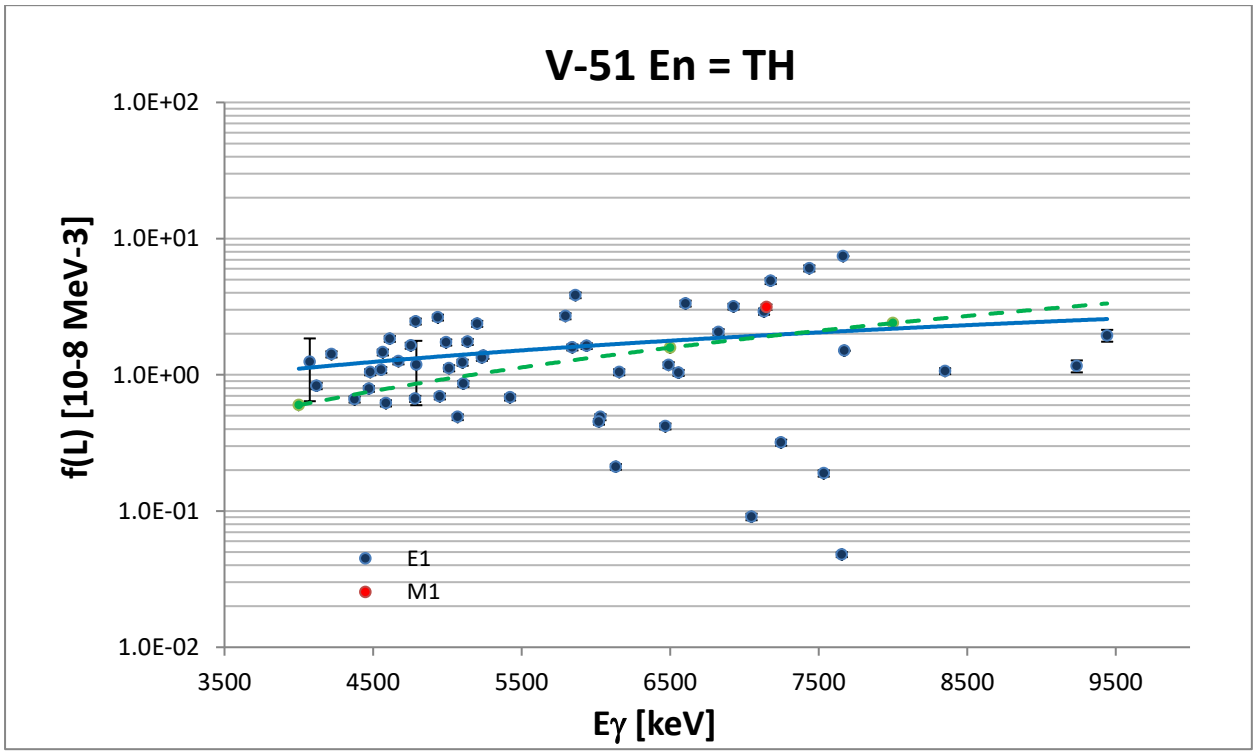

FIG. A.18 *f(E1) and f(M1) data points (blue and red) are plotted with unweighted trend lines. The dotted green line is the <f(E1)> systematics with the assumed E_γ^2 dependence.*

—Cr-51—

Cr-51 ECN

Ig/100 captures from J. Kopecky et al., Nucl.Phys. A188 (1972) 535
Gg0 = 1.1eV D0 = 14 keV
Sum Ig = 85.5%
α = 1;

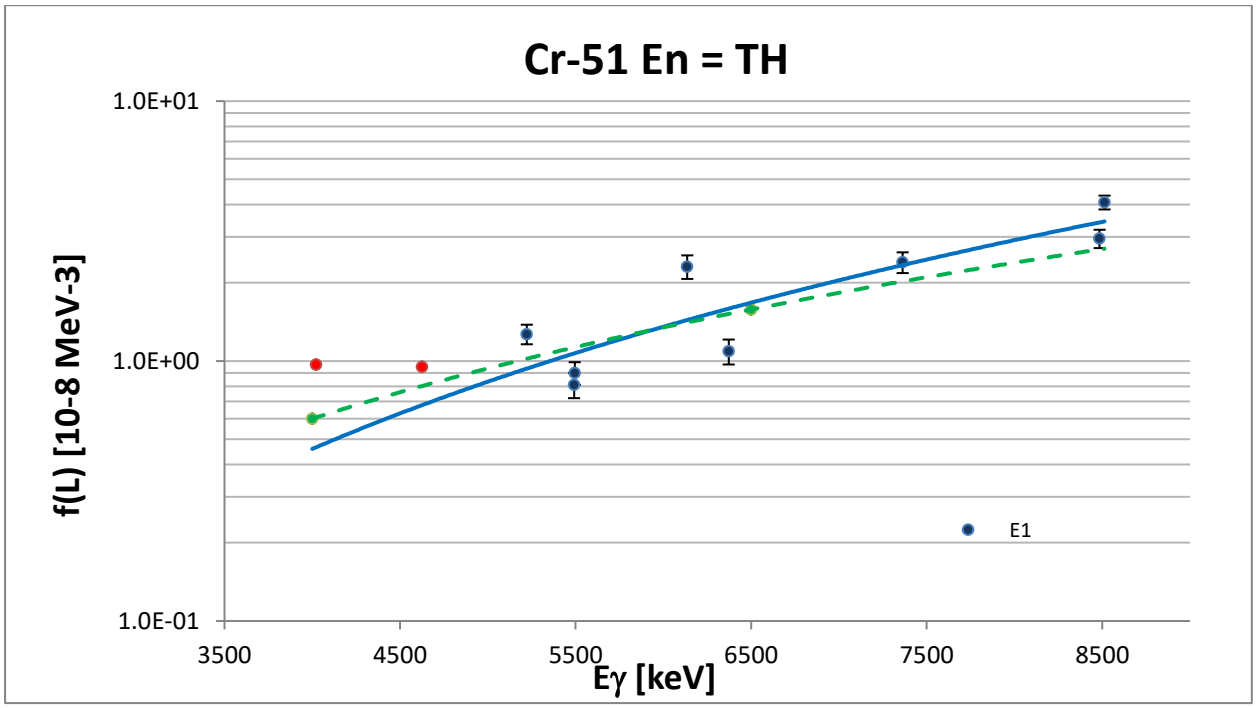

FIG. A.18 *f(E1) and f(M1) data points (blue and red) are plotted with unweighted trend lines. The dotted green line is the <f(E1)> systematics with the assumed E_γ^2 dependence.*

—V- 52—

V-52 ILL

Ig/100 captures from S. Michaelsen et al., Z.Phys. A 338 (1991) 371
Gg0 = 1.34 eV D0 = 3950 eV
Sum Ig = 96%
α = 0.39;

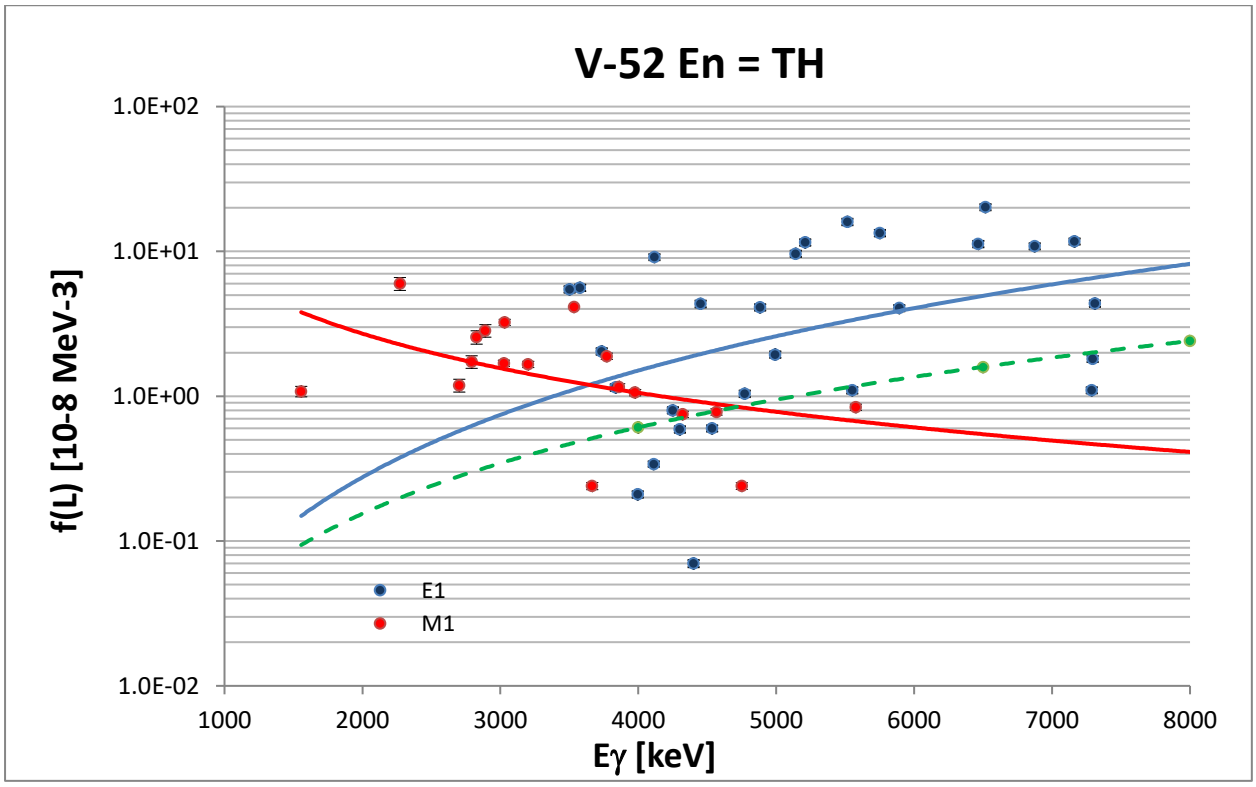

FIG. A.19 *f(E1) and f(M1) data points (blue and red) are plotted with unweighted trend lines. The dotted green line is the <f(E1)> systematics with the assumed E_γ^2 dependence.*

—Fe-57—

Fe-58 ECN

Ig/100 captures from R. Vennink et al., Nucl.Phys. A344 (1980) 421
Gg0 = 0.9 eV D0 = 22000 eV
Sum Ig = 96.2 based on imposed condition ΣEγIγ = 100Q
$\alpha = 1$;
α_i in Table 1 of the reference

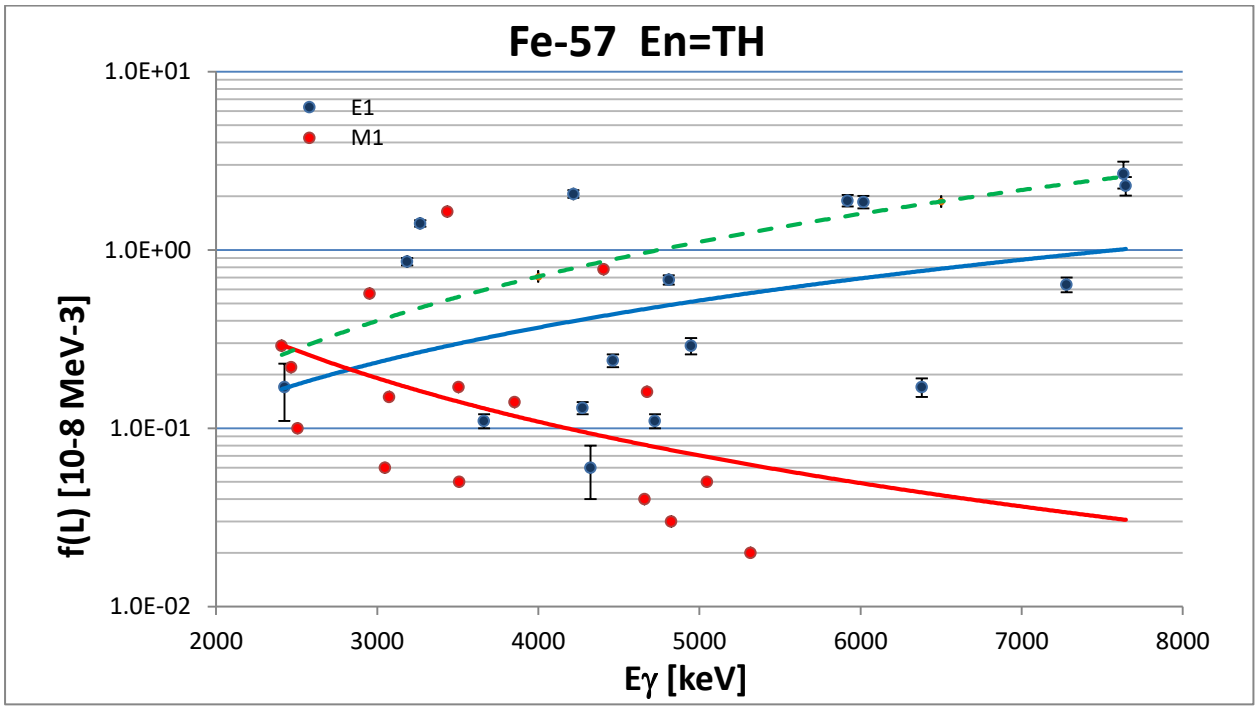

FIG. A.20 *f(E1) and f(M1) data points (blue and red) are plotted with unweighted power trend lines. The dotted green line is the <f(E1)> systematics with the assumed E_γ^2 dependence.*

—Fe-58—

Fe-58 ECN
Ig/100 captures from R. Vennink et al., Nucl.Phys. A344 (1980) 421
Gg0 = 1.83 eV D0 = 7050 eV
Sum Ig = 92.9% based on imposed condition ΣEγIγ = 100Q
α = 1;

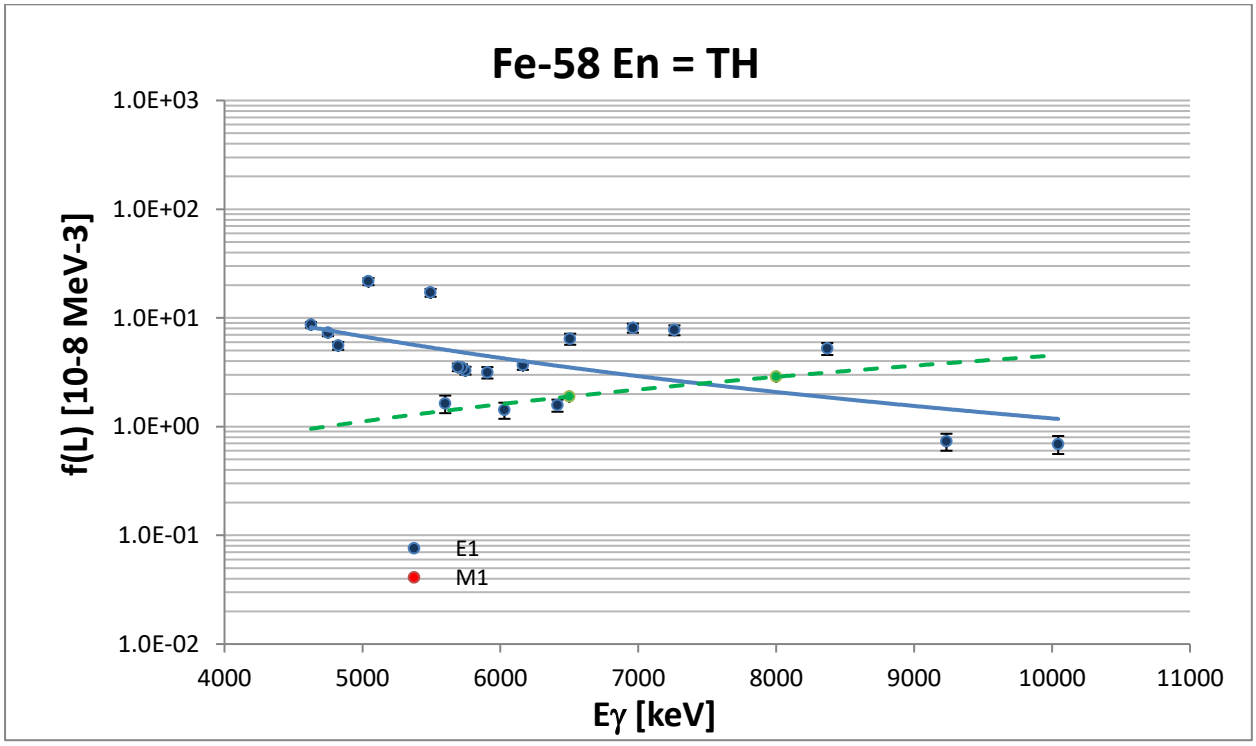

FIG. A.21 *f(E1) and f(M1) data points (blue and red) are plotted with unweighted trend lines. The dotted green line is the <f(E1)> systematics with the assumed E_γ^2 dependence.*

—Co-60—

Co-60 ECN

Ig/100 captures from J. Kopecky et al., NP A427 (1984) 413
Gg0 = 0.540 eV D0 = 1390 eV
Sum Ig = 73.1% based on imposed condition $\Sigma E\gamma I\gamma = 100Q$
α = 0.71;
α_i in Table 1 of the reference

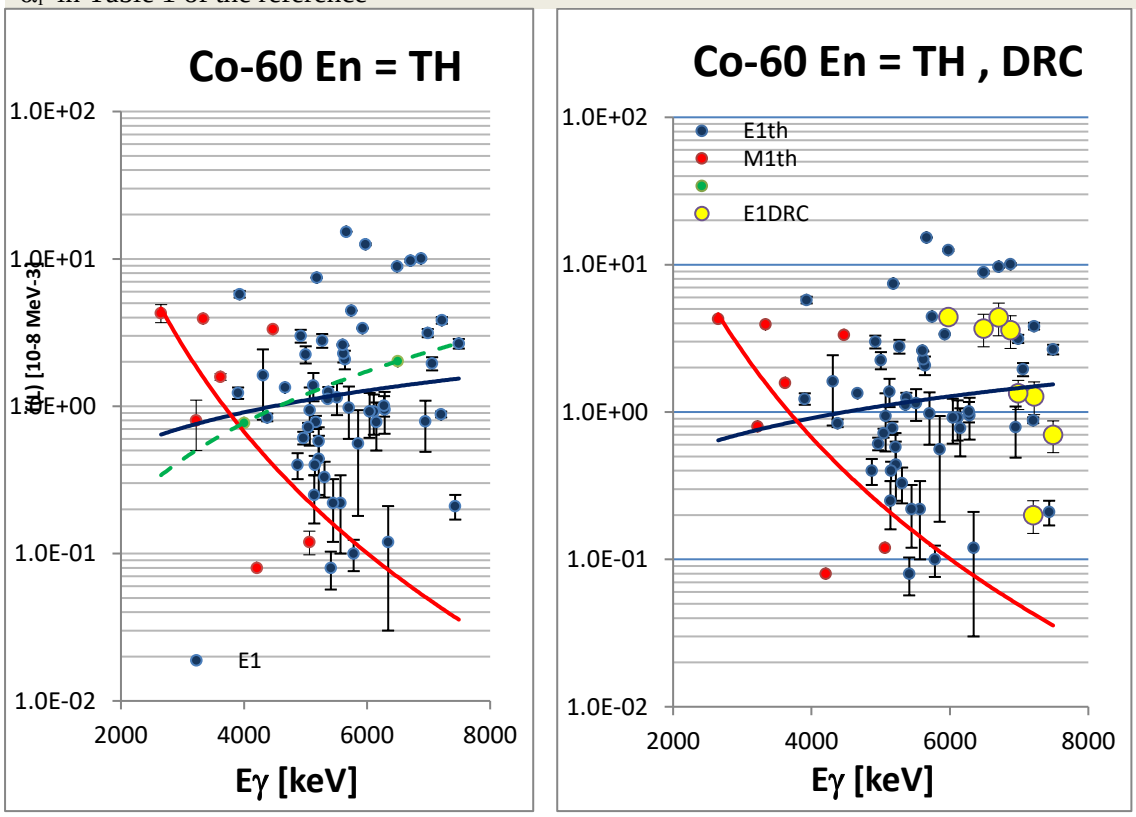

FIG. A.22 left: *f(E1) and f(M1) data points (blue and red) are plotted with unweighted trend lines. The dotted green line is the <f(E1)> systematics with the assumed E_γ^2 dependence.* ***right:*** *f(E1) DRC data (yellow points) from the capture in one s-wave resonance are plotted with no trend lines (too narrow energy range).*

—Cu-64—

Cu-64 ECN

Ig/100 captures from M.G. Delfini et al., Nucl.Phys. A404 (1983) 225
Gg0 = 0.49 eV D0 = 722 eV
Sum Ig = 78.9% based on imposed condition ΣEγIγ = 100Q
α = 0.5;
α_i in Table 6 of the reference

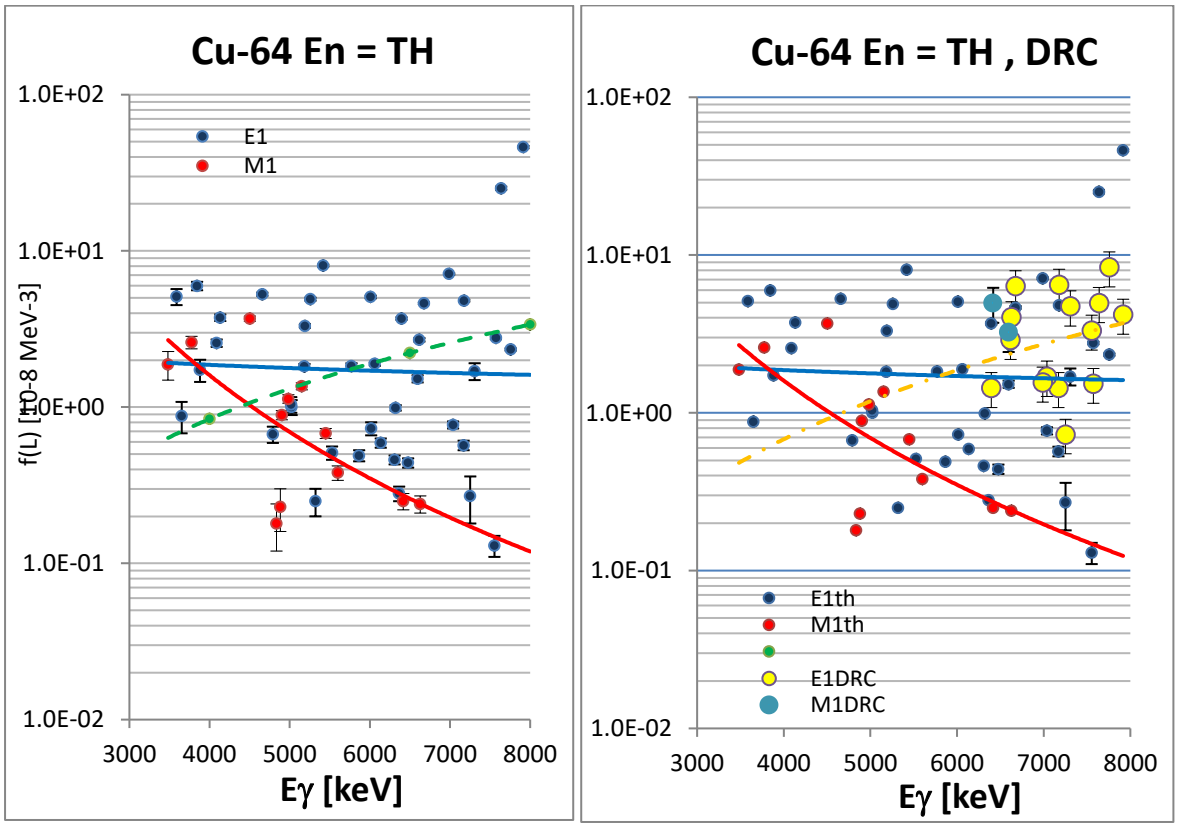

FIG. A.23 left: *f(E1) and f(M1) data points (blue and red) are plotted with unweighted trend lines. The dotted green line is the <f(E1)> systematics with the assumed* E_γ^2 *dependence.* ***right:*** *f(E1) and f(M1) DRC data points (yellow and light blue) red) are plotted with unweighted power trend line for E1 (dash-dotted yellow curve).*

––Cu-66––

Cu-66 ECN

Ig/100 captures from G.M. Delfini et al., Nucl.Phys. A404 (1983) 250
Gg0 = 0.395 eV D0 = 1520 eV
Sum Ig = 80% based on imposed condition $\Sigma E\gamma I\gamma = 100Q$
$\alpha = 0.51$;

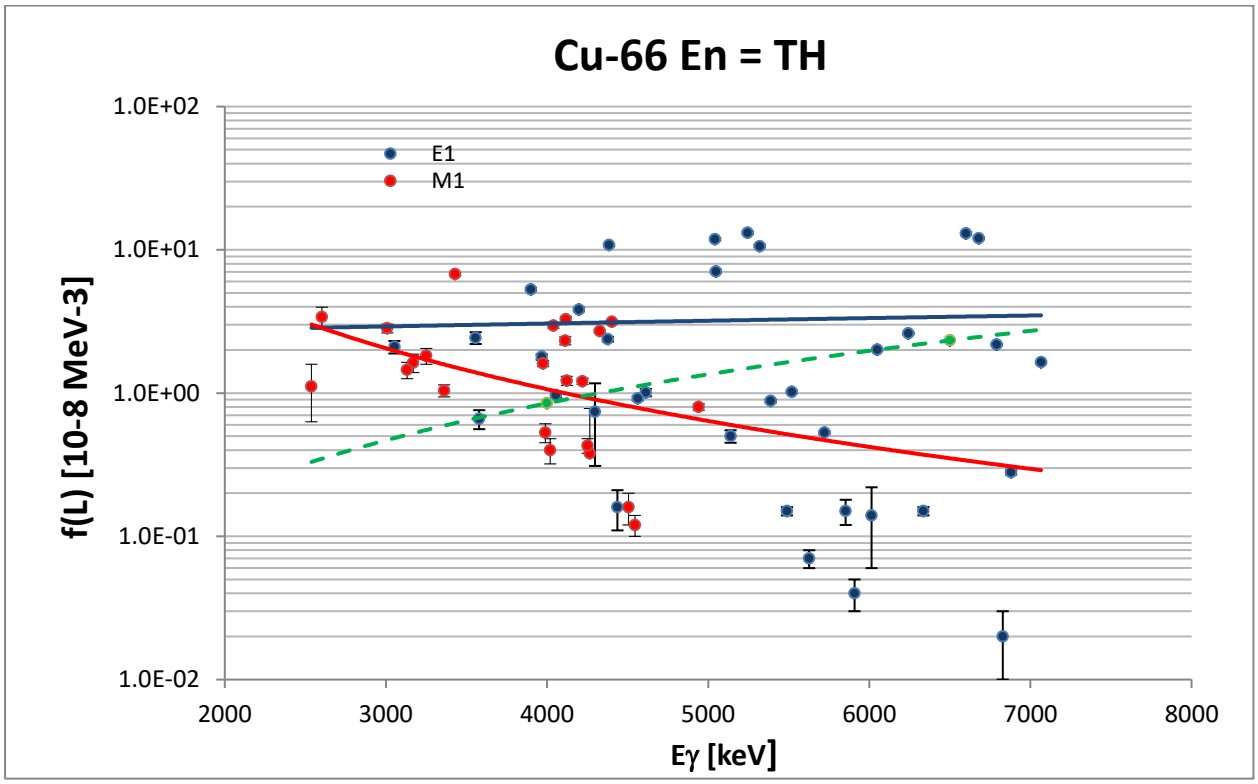

FIG. A.24 *f(E1) and f(M1) data points (blue and red) are plotted with unweighted power trend lines. The dotted green line is the <f(E1)> systematics with the assumed* E_γ^2 *dependence.*

—Nb-94—

Nb-94 TH MacMaster

Ig/10**5 captures from T.J. Kennet et al., Can. J. Phys. 66 (1988) 947
D0 = 95.6 eV Gg0 = 0.173 eV
Sum Ig = 125%
α = 0.52;

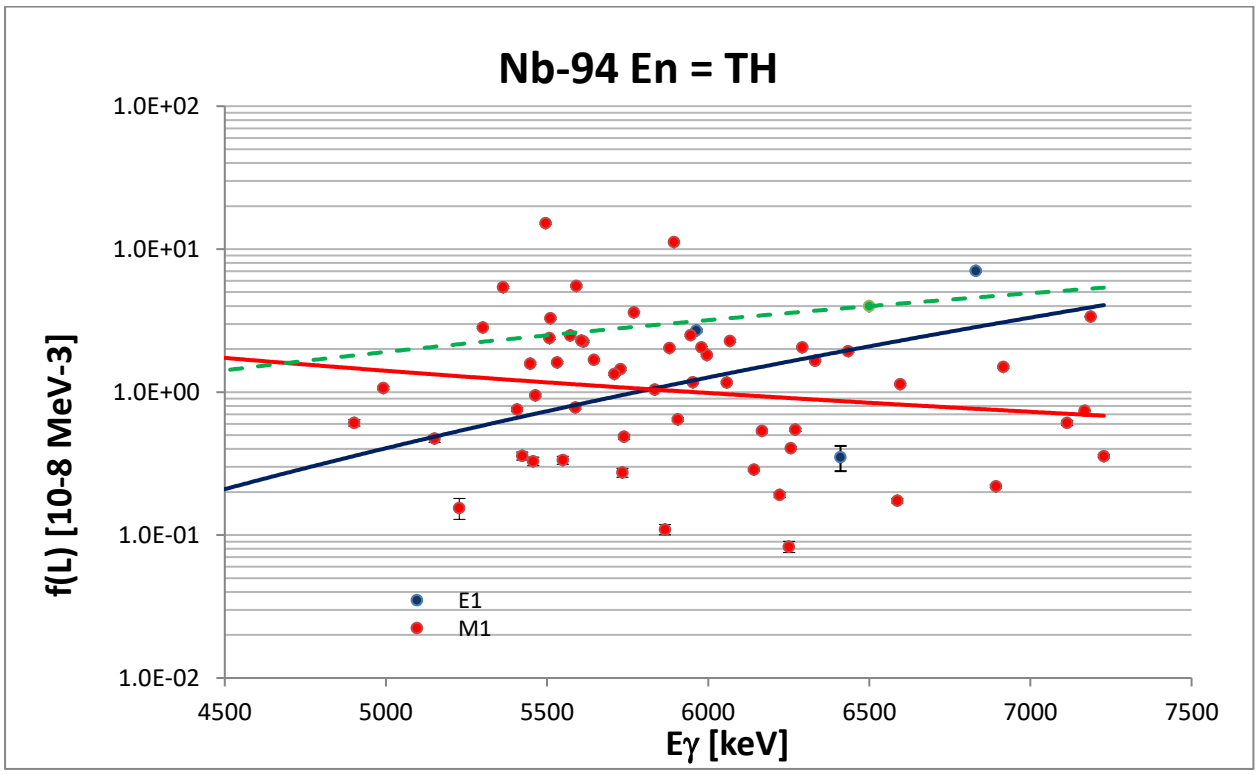

FIG. A.25 *f(E1) and f(M1) data points (blue and red) are plotted with unweighted trend lines. The dotted green line is the <f(E1)> systematics with the assumed E_γ^2 dependence.*

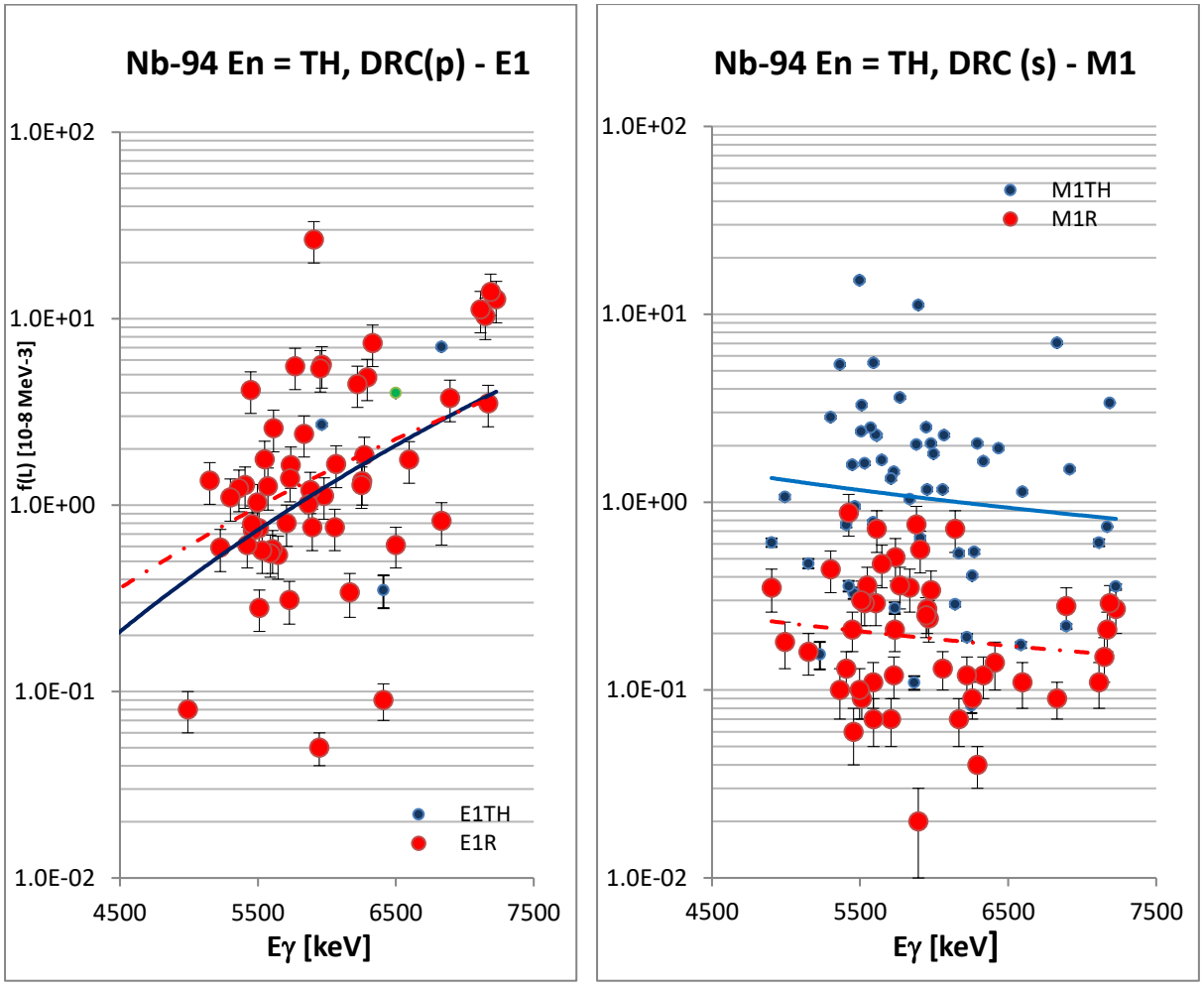

FIG. A.26 *f(E1) and f(M1) DRC) data (red points) from 3 s-wave and 4 – p wave resonances are plotted separately in two plots with unweighted trend lines (dash-dotted red curves). Note that for s – resonances Ji = 4+ and for p -resonances Ji = 4–,5–.*

—Rh-104—

Rh-104 McMaster

Ig/1000 captures from T.J. Kennet et al. Z.Phys. A 299(1981) 323

Gg0 = 0.120 eV D0 = 40 eV

Sum Ig = 48%

α = 1;

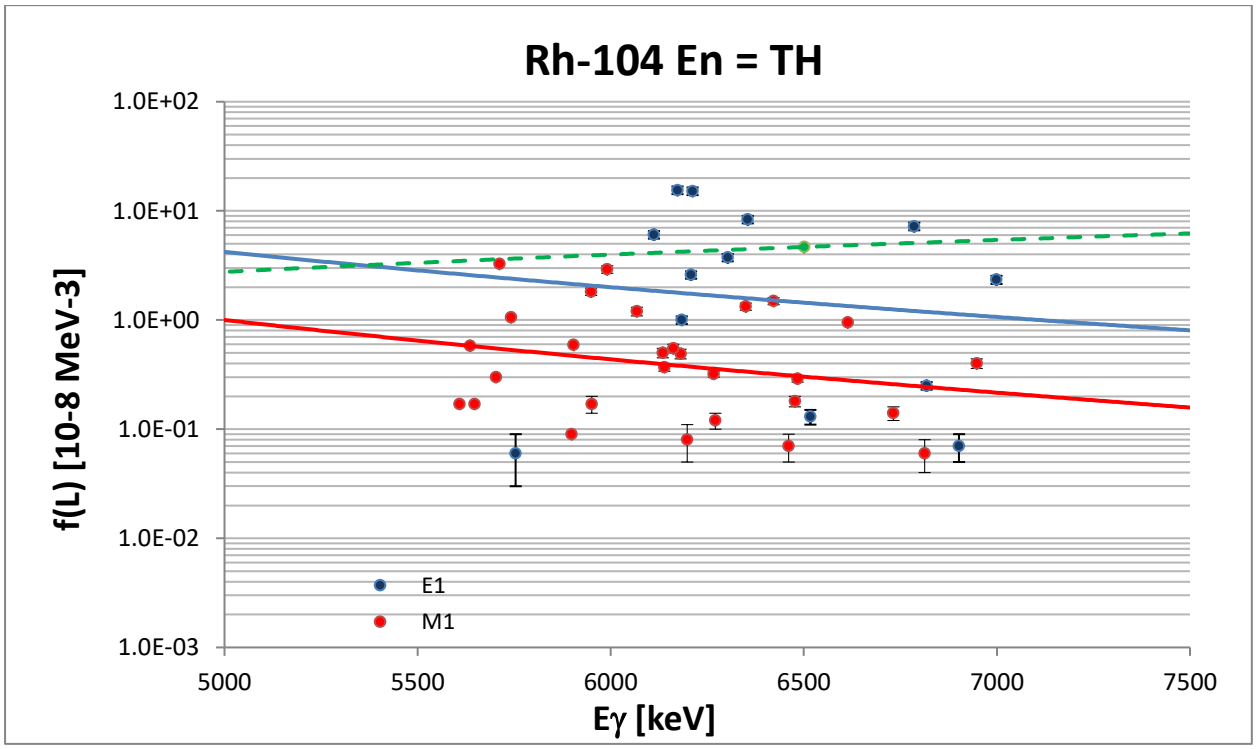

FIG. A.27 *f(E1) and f(M1) data points (blue and red) are plotted with unweighted trend lines. The dotted green line is the <f(E1)> systematics with the assumed E_γ^2 dependence.*

—Pd-106—

Pd-106 BNL
Ig/1000 captures from
Gg0 = 0.140 eV D0 = 10.9 eV
Sum Ig = 62% arbitrary units
α =0.48;

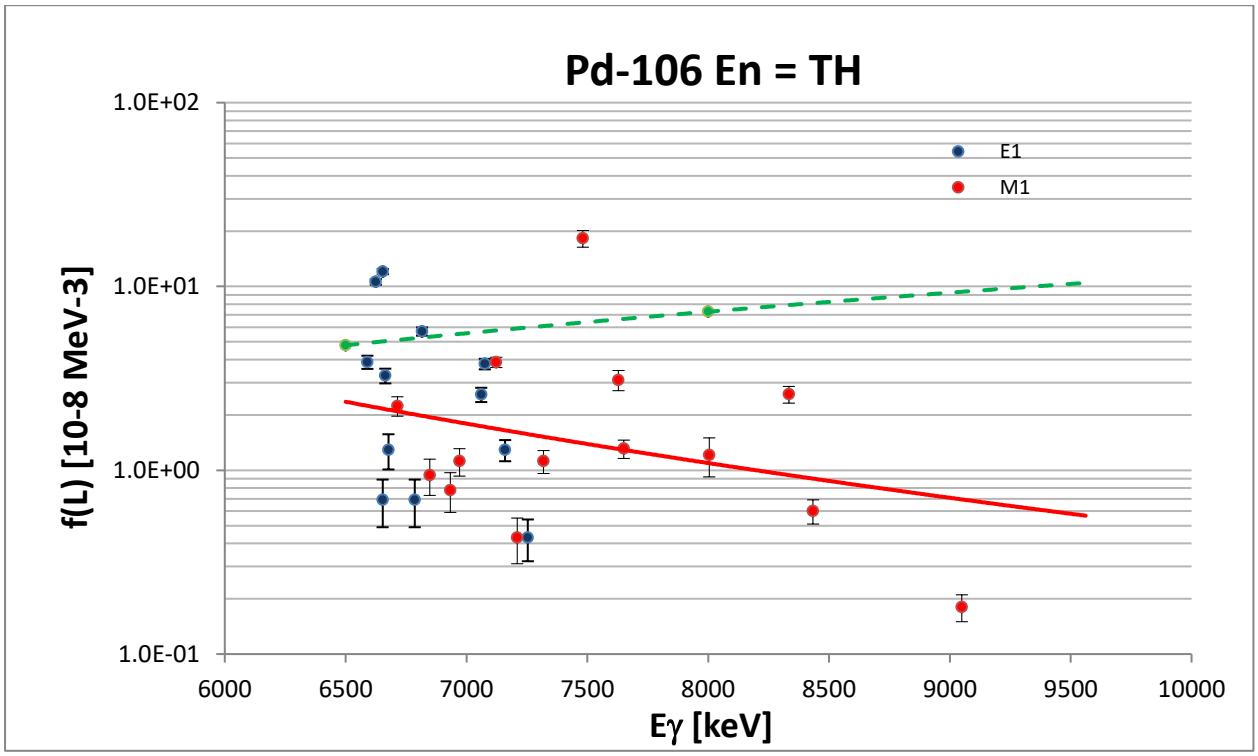

FIG. A.28 *f(E1) and f(M1) data points (blue and red) are plotted with unweighted trend lines. The dotted green line is the <f(E1)> systematics with the assumed E_γ^2 dependence.*

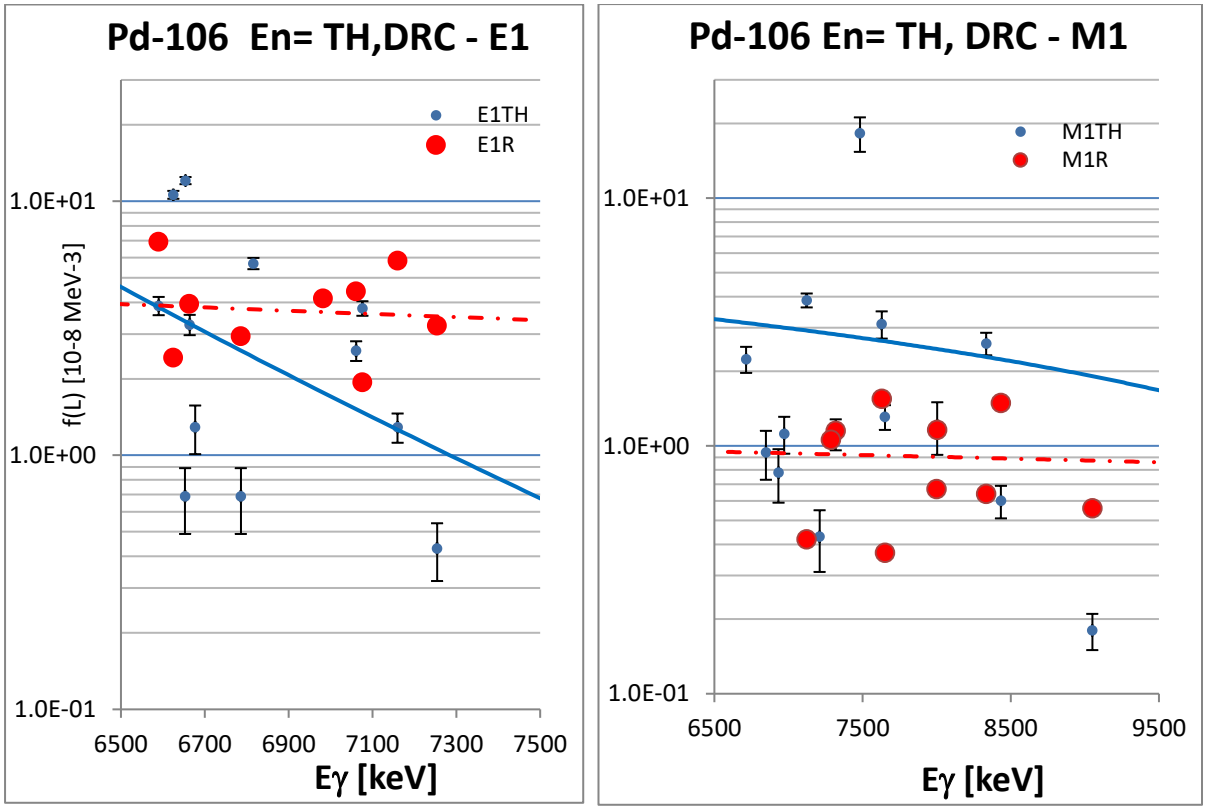

FIG. A.29 *f(E1) and f(M1) DRC) data (red points) from 9 s-wave resonances are plotted separately in two plots with unweighted trend lines (dash-dotted red curves).*

—I-128—

I-128 McMaster

Ig/10**5 captures from M.A. Islam et al., Z.Phys. A 335 (1990) 173
Ggi = 0.11 eV (negative res.) Gg0 = 0.12 (8 positive resonances)
D0 = 12.5 eV
Sum Ig = 111%
α = 0.42;

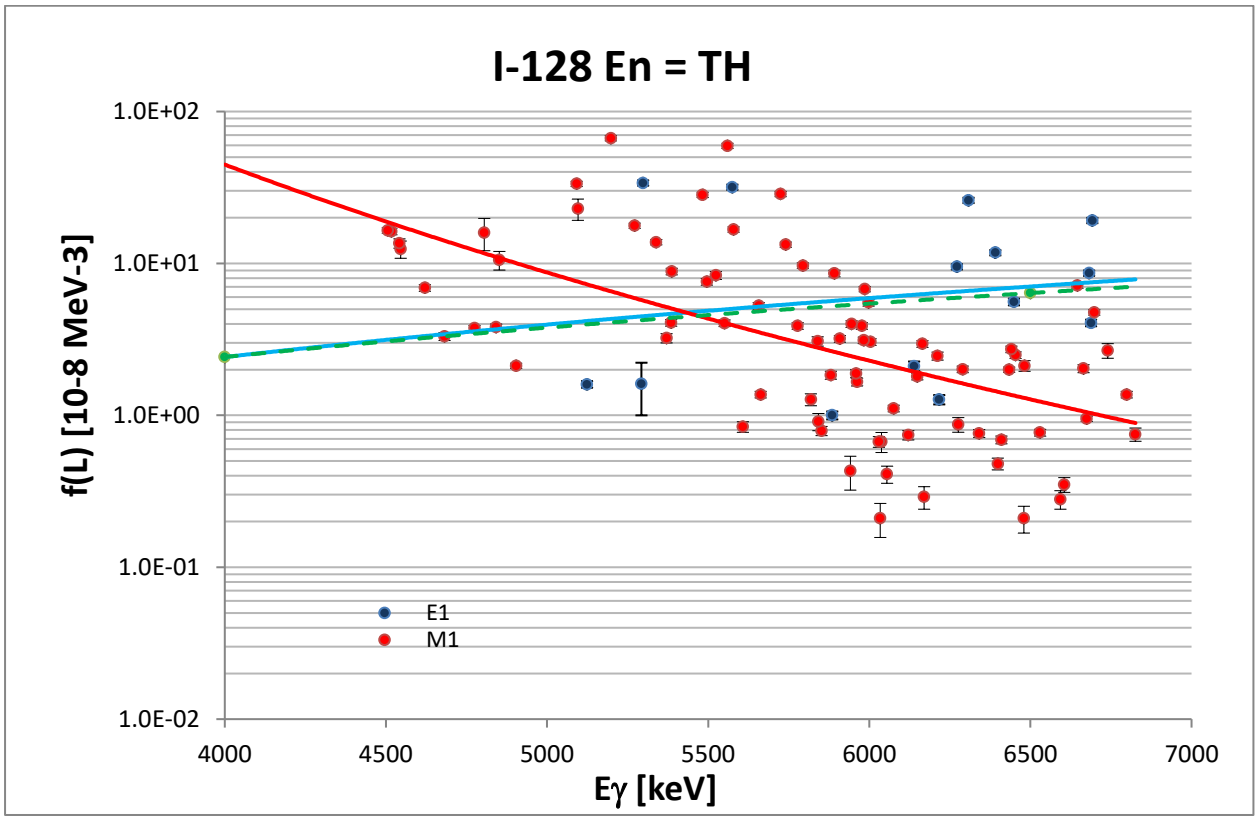

FIG. A.30 *f(E1) and f(M1) data points (blue and red) are plotted with unweighted power trend lines. The dotted green line is the <f(E1)> systematics with the assumed E_γ^2 dependence.*

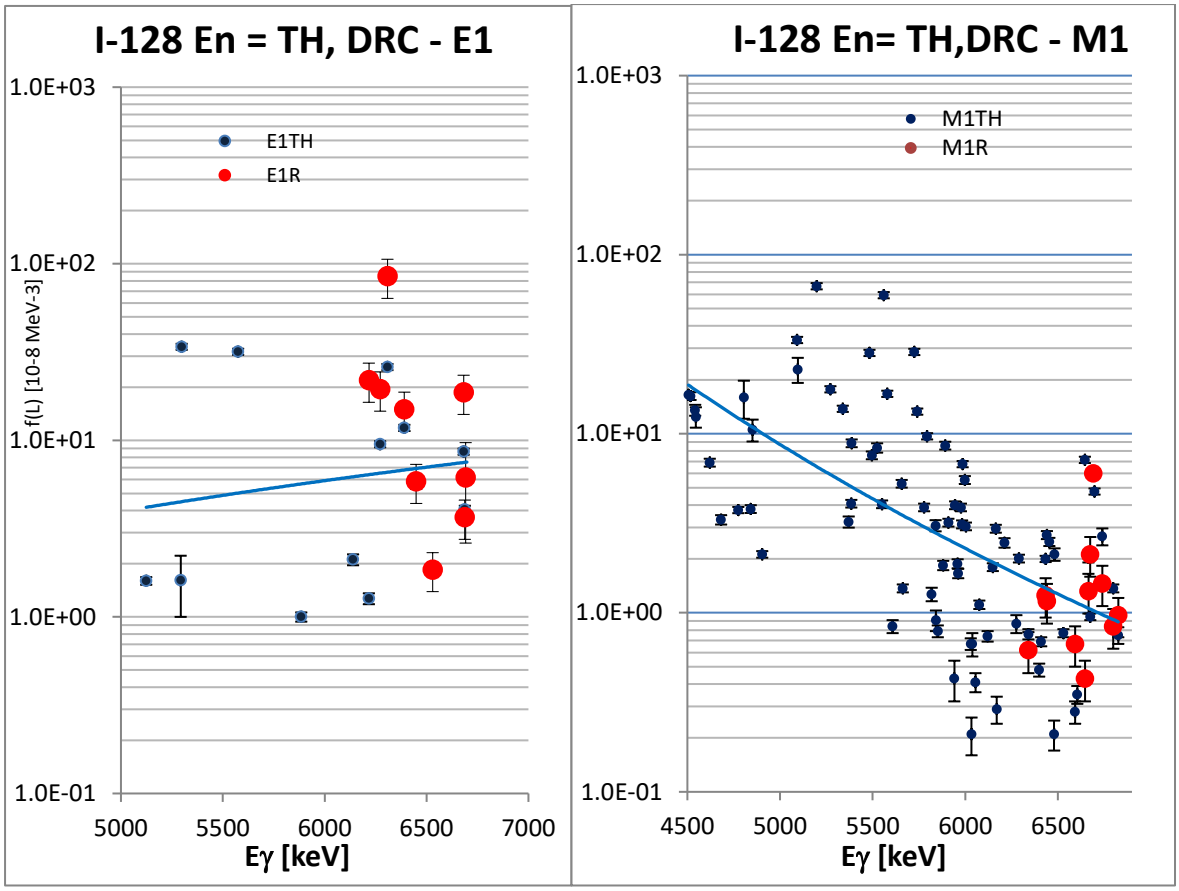

FIG. A.31 *f(E1) and f(M1) DRC) data (red points) from 8 s-wave resonances are plotted separately in two plots with no trend lines (too narrow energy range of DRC data points).*

—Cs-134—

Cs-134 McMaster

Ig/100 captures from T.J. Kennet et al. Can.J.Phys. 62(1984) 861
Gg0 = 0.120 eV D0 = 40 eV
Sum Ig = 69%
α = 0.17;

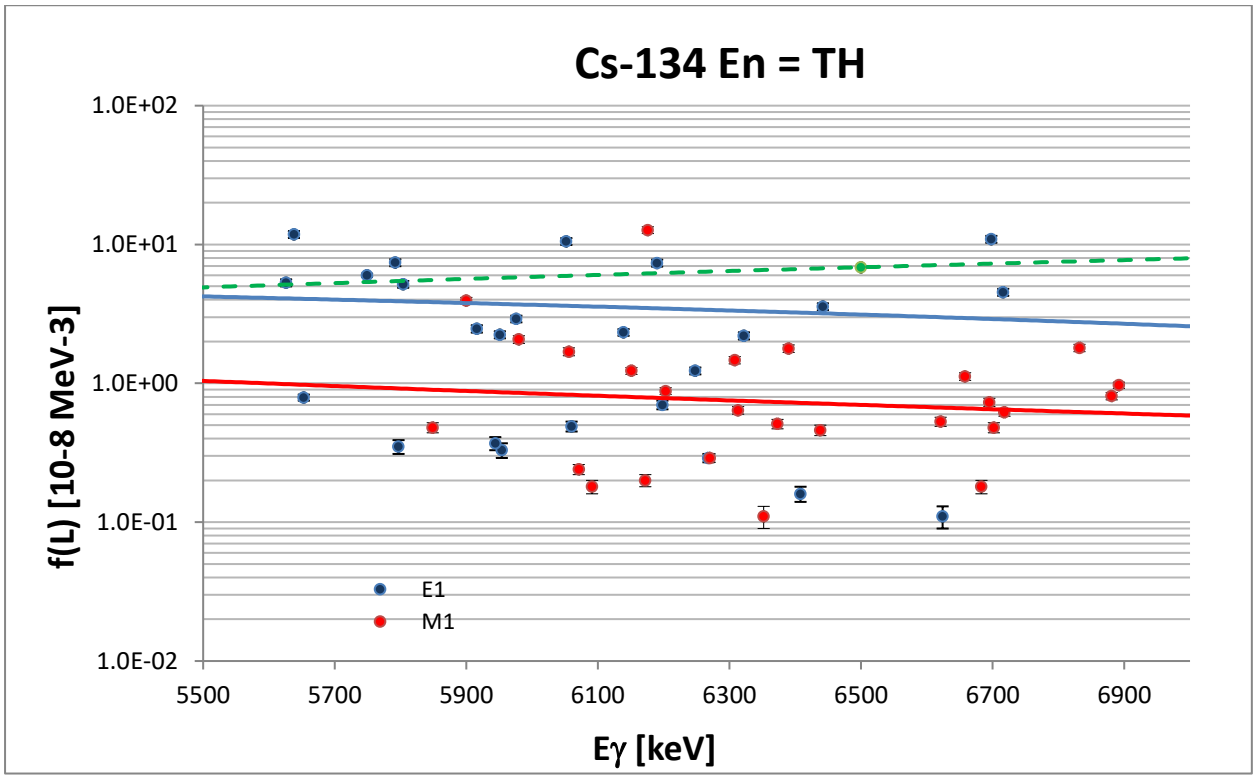

FIG. A.32 *f(E1) and f(M1) data points (blue and red) are plotted with unweighted trend lines. The dotted green line is the <f(E1)> systematics with the assumed E_γ^2 dependence.*

—Ba-136—

Ba-136 McMaster

Ig/1000 captures from M.A. Islam et al., Phys.Rev.C42 (1990) 207
Gg0 = 0.121 D0 = 40 eV
Sum Ig = 153%
α = 0.81;

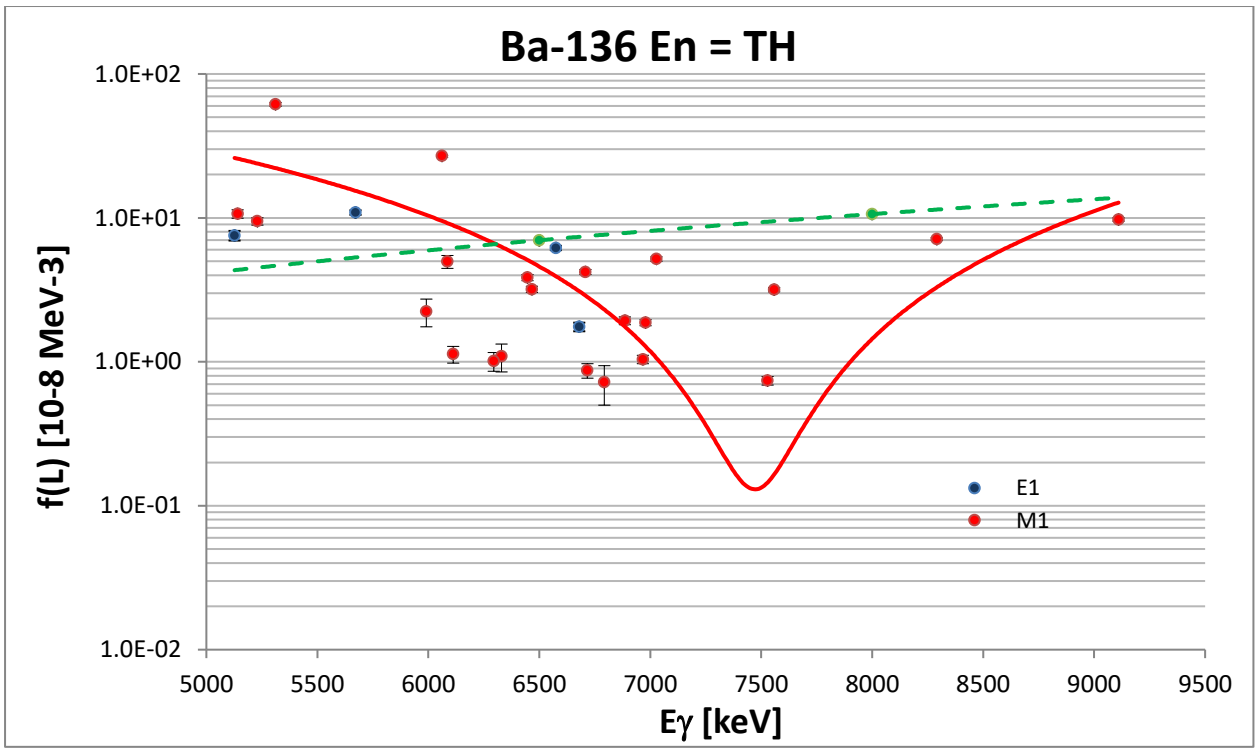

FIG. A.33 *f(E1) and f(M1) data points (blue and red) are plotted with unweighted trend lines. The dotted green line is the <f(E1)> systematics with the assumed E_γ^2 dependence.*

The value of ΣI_γ of assigned primary transitions is much larger than 100% which may signal an uncertainty either in the absolute calibration or in the level scheme.

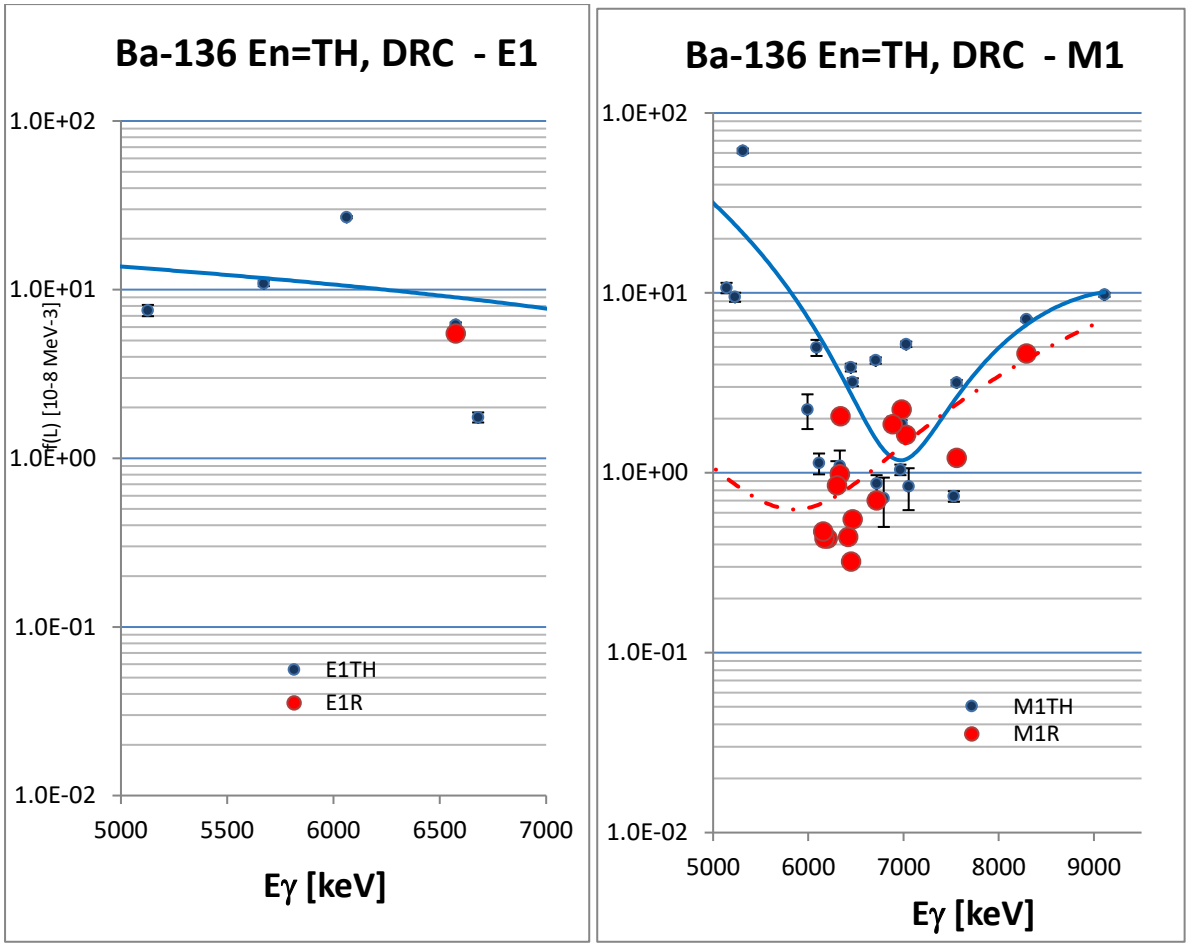

FIG. A.34 *f(E1) and f(M1) DRC) data (red points) from 10 s-wave resonances are plotted separately in two plots with no trend line for E1 data and unweighted trend line for M1 data (dash-dotted red curve).*

—Ba-138—

Ba-138 McMaster

Ig/1000 captures from M.A. Islam et al., Phys.Rev.C42 (1990) 207
Gg0 = 0.077 eV D0 =290 eV
Sum Ig = 101.4%
α = 1;

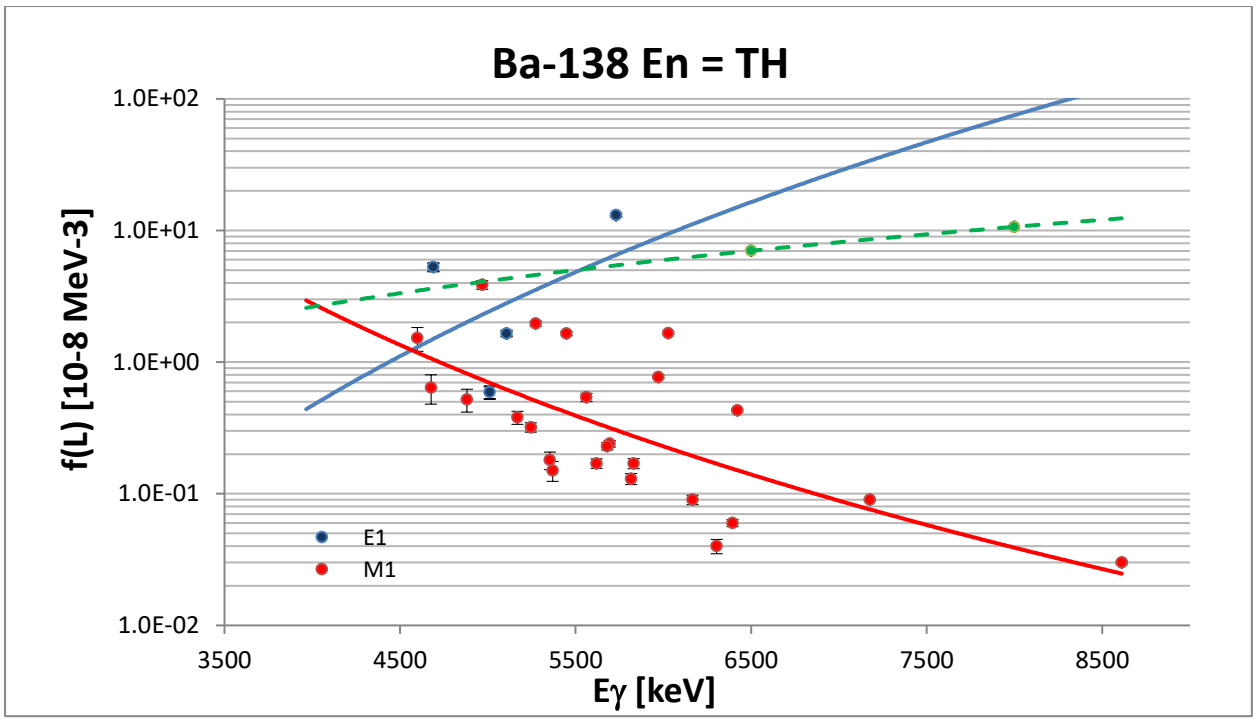

FIG. A.35 *f(E1) and f(M1) data points (blue and red) are plotted with unweighted trend lines. The dotted green line is the <f(E1)> systematics with the assumed* E_γ^2 *dependence.*

—Nd-146—

Nd-146 ANL
Ig/100 relative from D.L. Bushell et al., Phys.Rev.C14 (1976) 75
Gg0 = 0.074 eV D0 =17.8 eV
Sum Ig n.a.relative
α = 0.01

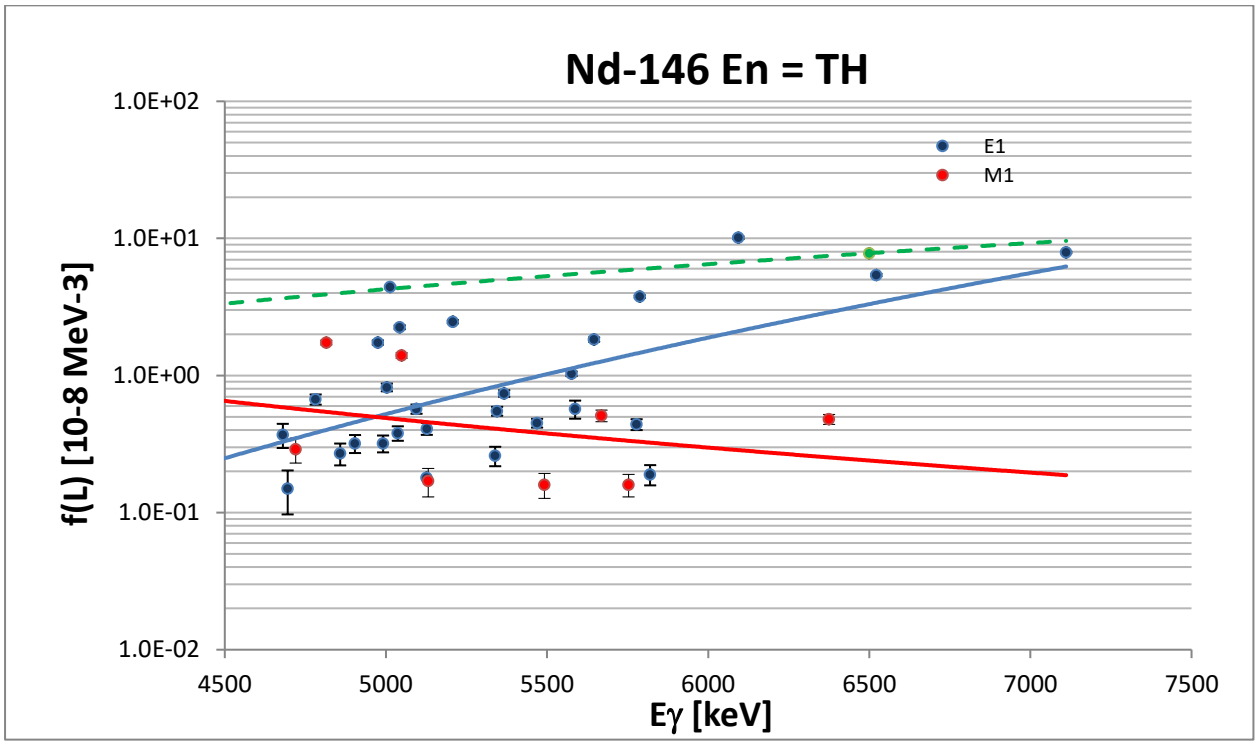

FIG. A.36 *f(E1) and f(M1) data points (blue and red) are plotted with unweighted trend lines. The dotted green line is the <f(E1)> systematics with the assumed* E_γ^2 *dependence.*

—Eu-154—

Eu-154 ILL

Ig/ relative from M.K. Baldonis et al., Nucl.Phys. A472 (1987) 445

Gg0 = 0.093 eV D0 =1.14 eV

Sum Ig n.a. arbitrary units

α = 0.92;

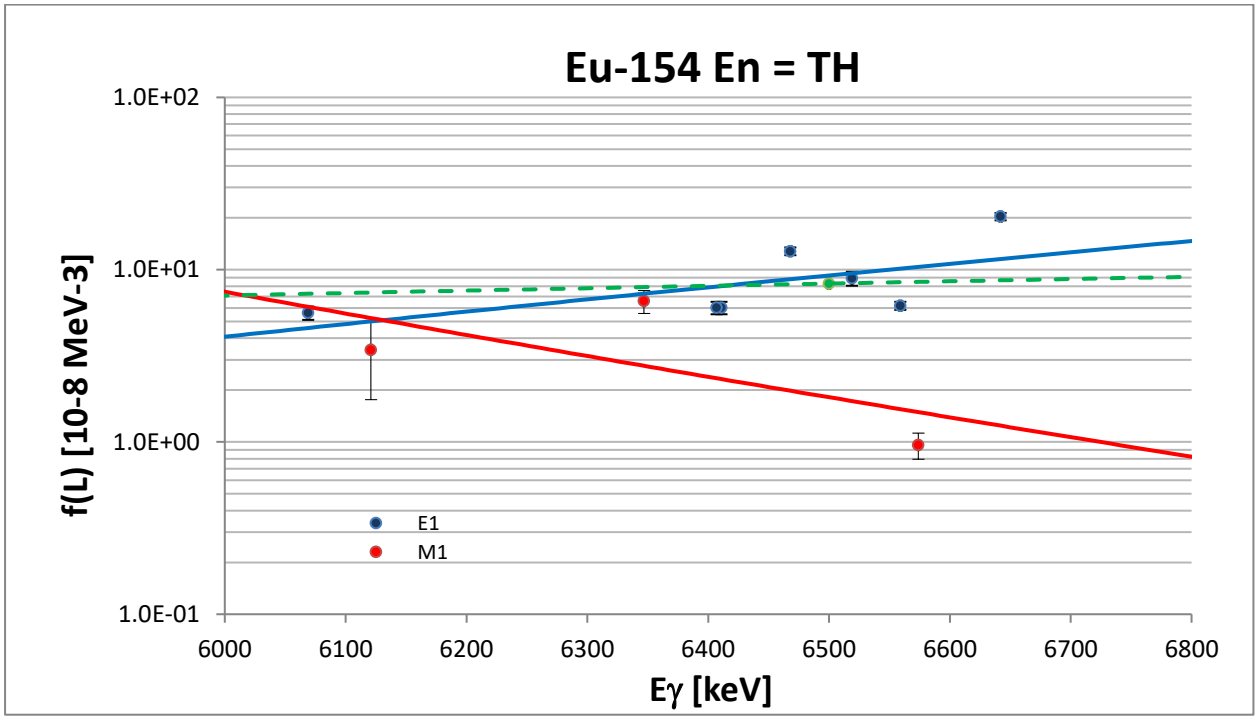

FIG. A.37 *f(E1) and f(M1) data points (blue and red) are plotted with unweighted trend lines. The dotted green line is the <f(E1)> systematics with the assumed* E_γ^2 *dependence.*

Nuclear Data Section
International Atomic Energy Agency
Vienna International Centre, P.O. Box 100
A-1400 Vienna, Austria

E-mail: nds.contact-point@iaea.org
Fax: (43-1) 26007
Telephone: (43-1) 2600 21725
Web: http://nds.iaea.org